

Dynamics of Rotors Incorporating Squeeze Film Dampers

by

ALY EL-SHAFEI

B. Mech. Eng., Cairo University (1981)
M. Eng., Cairo University (1983)

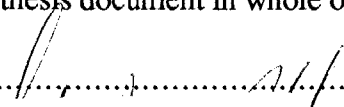
SUBMITTED TO THE DEPARTMENT OF MECHANICAL ENGINEERING IN
PARTIAL FULFILLMENT OF THE REQUIREMENTS FOR THE DEGREE OF
DOCTOR OF PHILOSOPHY

at the

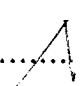
MASSACHUSETTS INSTITUTE OF TECHNOLOGY
September (1988)

© Aly El-Shafei, 1988

The author hereby grants to MIT permission to reproduce and to distribute copies of this
thesis document in whole or in part.

Signature of Author..........

Department of Mechanical Engineering
July, 1988

Certified by..........

Stephen H. Crandall
Ford Professor of Engineering
Thesis Supervisor

Accepted by..........

Ain A. Sonin, Chairman

Departmental Graduate Committee

MASSACHUSETTS INSTITUTE
OF TECHNOLOGY

SEP 06 1988

LIBRARIES
Archives



The Libraries
Massachusetts Institute of Technology
Cambridge, Massachusetts 02139

Institute Archives and Special Collections
Room 14N-118
(617) 253-5688

This is the most complete text of the
thesis available. The following page(s)
were not included in the copy of the
thesis deposited in the Institute Archives
by the author:

pg. 2

supplemented to account for the kinetic energy of the fluid particles that cross the control surface.

Using the kinetic coenergy method the fluid inertia forces acting in both long and short squeeze film dampers are determined. The inertia characteristics of the dampers are presented and are shown to be nonlinear functions of the amplitude of the journal orbit. It is also shown that the fluid inertia forces predicted by the solution of the Navier-Stokes equations for the case of a small circular-centered whirl is the same as that predicted by the kinetic coenergy method.

Finally this model of squeeze film dampers is incorporated in a dynamic analysis of a Jeffcott rotor incorporating SFDs. The steady state unbalance response of the rotor is obtained, and parametric studies of the system are presented. The nonlinear performance of the system is illustrated by the occurrence of the jump phenomenon. It is shown that fluid inertia introduces higher critical speeds and reduces the tendency of the rotors to exhibit the jump phenomenon.

Thesis Supervisor: Professor Stephen H. Crandall

Title: Ford Professor of Engineering

Acknowledgments

I am very lucky to have my thesis done under the supervision of Professor Stephen H. Crandall. Not only is he a leader in his scientific and engineering fields, but also he is a sensitive and caring person to whom I am indebted for a lot of the knowledge I gained at M.I.T. I would like to thank Professor Crandall for his guidance, encouragement and supervision.

I also would like to thank the members of my thesis committee: Professors T. R. Akylas, J. Dugundji and J. K. Hedrick. In particular I would like to thank Professors Akylas and Dugundji for several discussions that gave me further insight into the problems at hand. I had also several discussions with Professor P. Leehey, for which I am thankful.

I am indebted to the Egyptian government which provided me with financial support for my studies at M.I.T. In particular, I would like to thank Mr. Adel Abdel Hamid, of the Egyptian Cultural and Educational Bureau in Washington D. C., who administered my fellowship program.

This thesis was done within the Acoustics and Vibration Laboratory at M.I.T. Over the years, several of my fellow students contributed both to my academic and social lives, for which I would like to thank each and every one of them.

My family has been quite an inspiration. My father, mother, brother and sister provided me with love and support (financial and otherwise). My loving wife had to endure my often irregular study schedule, and she brought to life our little precious Ahmed. To all of them this thesis is dedicated.

Contents

Abstract	2
Acknowledgments	4
Contents	5
Chapter 1 Introduction	7
1.1 Background	7
1.2 Fluid inertia	11
1.3 Thesis goals and outline	13
Chapter 2 Damping forces in squeeze film dampers	17
2.1 Reynolds equation	17
2.2 Short bearing approximation	22
2.3 Long bearing approximation	26
2.4 Fluid inertia	31
Chapter 3 Fluid inertia effects in squeezing flows	35
3.1 Poiseuille flow resulting from squeezing motion	35
3.2 Kinetic coenergy method applied to Poiseuille flow	42
3.3 Squeeze flow	45
3.4 Kinetic coenergy method applied to Squeeze flow	51
3.5 Convective acceleration and moving boundary	58
Chapter 4 Fluid inertia forces in squeeze film dampers	62
4.1 Inertia coefficients for short dampers	62
4.2 Inertia coefficients for long dampers	66
4.3 Fluid inertia forces	68
4.4 Solution of the governing equations for a small circular centered whirl	81

Chapter 5	Dynamics of rotors incorporating squeeze film dampers	88
5.1	Jeffcott rotor incorporating a SFD	88
5.2	Equations of motion	91
5.3	Steady state unbalance response	94
5.4	Parametric studies of unbalance response	99
5.4.1	Short squeeze film dampers	101
5.4.2	Long squeeze film dampers	115
5.5	Conclusions	132
Chapter 6	Conclusions	138
6.1	Review of thesis contents	138
6.2	Conclusions	140
6.3	Suggestions for future research	143
Bibliography		145
Appendix	Listing of program UNBRES	153

Chapter 1

Introduction

Squeeze film dampers (SFDs) are damping devices used essentially in aircraft gas turbine engines to damp the whirling vibrations of rotors. Their ability to attenuate the amplitude of engine vibrations and to decrease the magnitude of the force transmitted to the engine frame makes them an attractive rotor support.

Figure 1.1 shows the construction of squeeze film dampers. The damper consists of an oil film in an annulus surrounding a rolling element bearing whose outer race is constrained from rotating, usually by a squirrel cage. Thus the spinning of the rotor does not reach the oil, and only when the rotor whirls does the oil film act to damp the motion. The squirrel cage serves to center the journal in the sleeve as well as to keep the outer race of the rolling element bearing from spinning.

1.1 Background

The earliest investigation of squeeze film dampers is probably that conducted by Cooper [15][†] in the early sixties, in which he concluded that squeeze film dampers are adequate for damping the whirling vibration of rotating machinery. In his experiments he observed "bistable" operation of the rotor, that is the rotor would exhibit a jump from a certain whirling orbit to another at some frequency. This is the classical jump

[†] Numbers between brackets designate references in the bibliography at the end of the thesis.

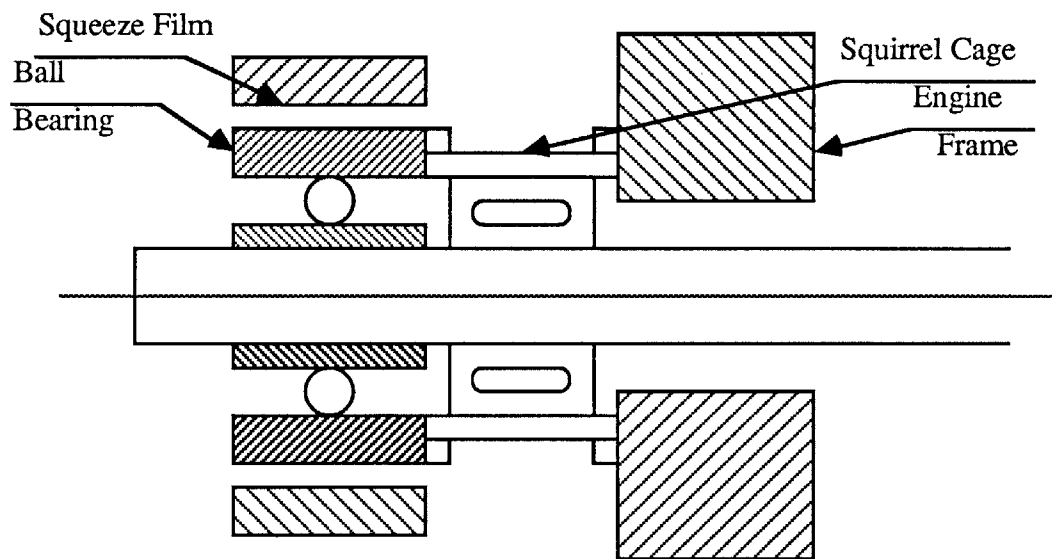
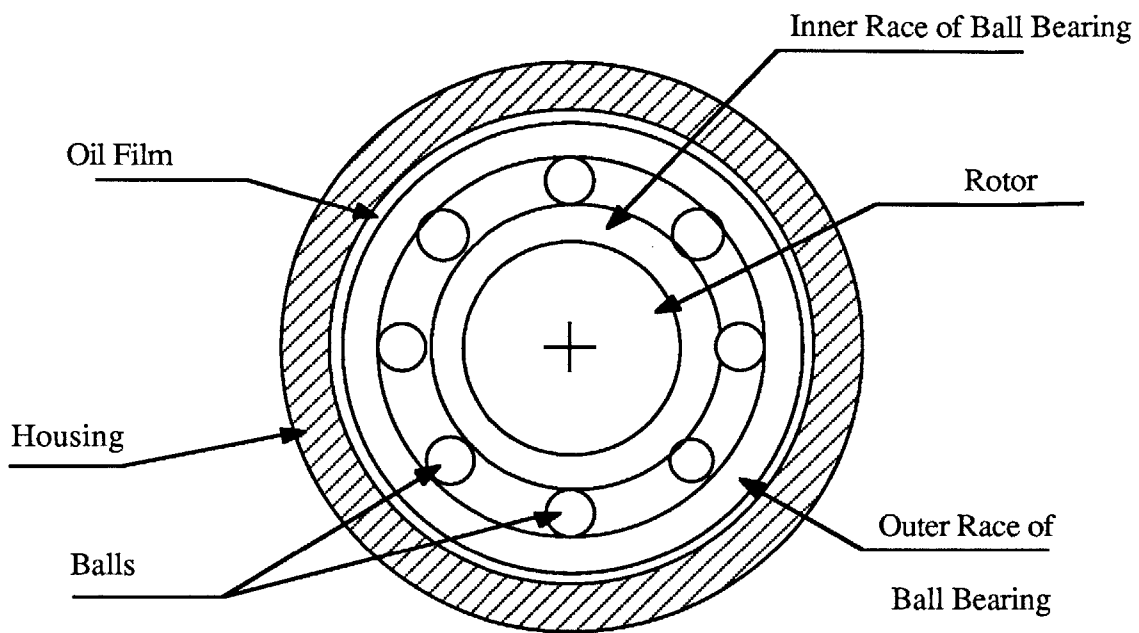


Figure 1.1 Construction of squeeze film dampers

phenomenon, and perhaps this was the first indication of the nonlinear behavior of squeeze film dampers. In the early seventies, White [101] studied theoretically and experimentally the dynamics of a rigid rotor on squeeze film dampers. He was able to calculate the forces acting in the damper based on Reynolds equation of fluid lubrication, and he calculated the so called bearing* coefficients. He predicted, both theoretically and experimentally, three steady state orbits of the rotor journal at the same frequency, but using a stability analysis he found that only two of them were stable. This confirmed Cooper's predictions for the jump phenomenon.

Since then squeeze film dampers have been widely used in aircraft gas turbine engines, and consequently the squeeze film damper (SFD) literature is quite rich. In the following we are going to highlight several of the investigations that are pertinent to this thesis, while a more complete list can be found in the bibliography. The quest of the previous investigations has been to faithfully describe the SFD theoretically, and to determine its effects on the dynamics of rotors that incorporate SFDs. These are the goals that this thesis tries to achieve. Other goals for previous investigations have been to experimentally test SFDs to determine the accuracy of the available theories and explore new configurations of SFDs.

Mohan and Hahn [57] studied the dynamics of a rigid rotor in squeeze film dampers. They obtained the steady state response by assuming a circular whirl, and they did parametric studies to determine the effect of the damper on the dynamics of the rotor, and the force transmitted to the engine frame, and also to determine the maximum rotor unbalance at which the damper is effective. They concluded that the squeeze film damper is generally an effective damping device, but for a badly designed damper, the transmitted

* In the literature the words 'damper' and 'bearing' have been used interchangeably to refer to squeeze film dampers, probably because of their similarity to journal bearings.

force can be magnified rather than attenuated, and this could lead to the failure of the engine.

Cunningham, *et. al.* [20], demonstrated the possibility of using design data for a SFD designed on the basis of single mass flexible rotor analysis, and applying it for the design of a SFD for a multi-mass flexible rotor. In an experimental parametric study, Tonnesen [97] was able to show that the forces in the damper agree with the π -bearing theory. Gunter, *et. al.* [29], numerically studied the nonlinear response of aircraft engines incorporating SFDs, and they were able to show that the rotor exhibits the jump phenomenon, and, under unidirectional loading, subharmonic whirl motion may exist. This was later verified experimentally by Sharma and Botman [77], who observed nonsynchronous whirl in their test rig, although they did not associate it with unidirectional loading.

Rabinowitz and Hahn [65] studied the steady state orbits for a flexible rotor incorporating SFDs. They did a parametric study to determine regions of unacceptable behavior of rotors due to SFDs. They also did a stability analysis of the steady state orbits they obtained [64]. Taylor and Kumar [85] did an investigation of the numerical integration techniques used to determine the response of a rigid rotor in SFDs. They were able to demonstrate the following drawbacks for numerical integration: a) only stable solutions could be found, b) false convergence, c) in regions of multiple-valued response, finding all possible solutions involves tedious trial and error, and d) the particular algorithm and convergence criteria used in the iterative approach determine the accuracy and credibility of the results. This motivated them [86] to find closed-form steady state solutions for a rigid rotor in squeeze film dampers by assuming a circular orbit. More recently, Guang and Zhong-Qing [27] used a similar technique to do a parametric study of a flexible rotor incorporating SFDs.

1.2 Fluid inertia

The above mentioned analyses are all based on Reynolds equation, which neglects the effects of fluid inertia. This has been a good assumption, since the dampers are usually operating at a very low Reynolds number. But as the speed of aircraft engines increases and as the trend of using lighter viscosity oils prevails, the values of Reynolds number for SFDs in practice have been continually increasing, and the need for a model that includes fluid inertia becomes a necessity.

Recently, in their experiments on squeeze film dampers Tecza, *et. al.* [87] showed that fluid inertia may be a significant factor in determining the dynamic characteristics of squeeze film dampers. This has prompted several investigations of the effects of fluid inertia in squeeze film dampers. Tichy [92] provided an explanation for the importance of fluid inertia in squeeze film dampers versus journal bearings. He later published experimental results to show the effect of fluid inertia [94].

Several identification techniques have evolved (especially in the United Kingdom) in the last few years, to experimentally determine the dynamic forces in SFDs, including fluid inertia. Amongst the workers in this field are Burrows *et. al.* [9] and Ramli *et. al.* [69]. For a comparison of the identification techniques used for estimating SFD coefficients see Ellis *et. al.* [22].

Perhaps one of the first attempts to study the effects of fluid inertia in hydrodynamic bearings, is the work of Smith [80] in the mid sixties. Using a unique form of Reynolds equation, he was able to obtain inertia force coefficients for journal bearings, and his conclusion was that the effect of fluid inertia in oil film bearings is to introduce an

added mass to the rotor and this may affect the dynamics of the rotor especially for short stiff rotors on wide bearings. Approximately a decade later Reinhardt and Lund [70] used a perturbation solution for small Reynolds number to obtain the force coefficients of journal bearings. They showed that fluid inertia introduces rather small corrections to the damping and stiffness coefficients of journal bearings and they also provided plots of inertia coefficients versus the eccentricity. They had to solve a set of differential equations numerically to arrive at these plots. Another notable paper, is the work of Szeri *et. al.* [84]. They used a technique based on averaging the inertia forces across the film, to obtain the force coefficients in a squeeze film damper. They also had to solve the resulting differential equations numerically. A recent paper by Ramli *et. al.* [68] compares the results of Smith, Reinhardt and Lund, and Szeri *et. al.*; and concludes that they are in good agreement, especially for short bearings. It is pointed out, however, that Smith's approach has the advantage of computational simplicity, and leads to fairly simple asymptotic analytical expressions for very short, and very long bearings.

In the literature, the methods used to handle inertia effects in hydrodynamic bearings can be divided into three categories. One method is to use a perturbation series in Reynolds number. Representative of this category are Tichy and Wiener [96], Jones and Wilson [42], and Reinhardt and Lund [70]. The solution thus obtained is valid for small values of Reynolds number. A second category is based on averaging the inertia forces across the film. Amongst those in this category are the work of Constantinescu [13], Szeri, *et. al.* [84], and San Andrés and Vance [71,72]. The third category represented by Tichy and Modest [95,56] is based on a stream function approach to the linearized momentum equation, thus convective acceleration terms are neglected. All these techniques when applied to fluid film bearings result in quite a cumbersome solution, and the first two techniques require the solution of a set of differential equations numerically ([70] and [84]).

The results of all these researchers indicate that the classical lubrication theory is in error with respect to the pressure field and the inertia forces, which can dominate at higher Reynolds numbers. On the other hand, they all seem to indicate that the velocity field predicted by the classical lubrication theory is not greatly affected by fluid inertia for Reynolds number in the range of usual application of squeeze film dampers. In fact, the method of averaged inertia is based on the assumption that the velocity profiles predicted by the classical lubrication theory are not changed much by fluid inertia.

1.3 Thesis goals and outline

The literature articles surveyed in the previous pages seem to indicate that fluid inertia is an important factor in the dynamic characteristics of SFDs. It also seems that a model of fluid inertia forces in SFDs, including forces due to convective acceleration, has yet to be developed. This model should be simple enough to be easily used in rotordynamic analyses. Also the effects of fluid inertia on the dynamics of rotors incorporating SFDs, especially on the nonlinear behavior of the system, is yet to be investigated.

The goals of this thesis are to obtain a better model of squeeze film dampers, namely to include fluid inertia effects on the forces generated in SFDs, and to incorporate this simple model in a dynamic analysis of a Jeffcott rotor incorporating squeeze film dampers.

To achieve these goals, we start in chapter 2 by deriving the damping forces acting in a squeeze film damper. Reynolds equation for fluid lubrication is first derived and both the short and the long bearing approximations are used to obtain the pressure equation in SFDs. The pressure is then integrated to obtain the damping forces. The damping forces

are sensitive to the cavitation effects in the oil. If the oil film is cavitated we use the π -bearing theory, otherwise we use the full or 2π -bearing theory.

To include fluid inertia effects in the model, we find that the simplified Navier-Stokes equations for SFDs are nearly impossible to solve, so we resort to an approximate method. It is well known[§] that if the kinetic coenergy[‡] of the fluid could be calculated, then the fluid inertia forces can be determined from the kinetic coenergy, by using Lagrange's equations. But the kinetic coenergy is not known beforehand, so we assume that the velocity profiles can be approximated by those obtained from the inertialess solution based on Reynolds equation. As discussed in the previous section this approximation is used in the method of averaged inertia. The inertia forces are then calculated using Lagrange's equations of motion.

Before applying this approximate technique to obtain the inertia forces, to squeeze film dampers, we apply it to more elementary squeezing flows. This is both to verify that the approximate method based on calculating the kinetic coenergy is sufficiently accurate, and to understand better the mechanics of squeezing flows. Chapter 3 starts by describing two elementary cases of squeezing flows, namely the Poiseuille flow due to squeezing motion and the direct squeeze flow, as limits of the flow in a SFD. The Poiseuille flow is a linear problem and is solved completely including fluid inertia. It is shown that the velocity profiles do not change much due to fluid inertia for Reynolds number in the range of usual application of SFDs. This justifies the approximation of the kinetic coenergy based on the velocity profiles of the inertialess solution. The fluid inertia force in Poiseuille flow predicted by the approximate method, is shown to be the limit of the fluid inertia force as

[§] See for instance Milne-Thomson [55].

[‡] We are going to use this more accurate terminology for reasons that will become apparent later.

Reynolds number goes to zero, and is also shown to be a good approximation for Reynolds number in the range of usual application of SFDs.

The squeeze flow is more complicated since it is nonlinear because of the presence of convective acceleration. Also the moving boundary results in time dependent boundary conditions. The problem is linearized and the inertia force due to temporal acceleration only is predicted and is shown to be in excellent agreement with that predicted by the approximate method based on the kinetic coenergy, hereinafter called the kinetic coenergy method, for Reynolds number in the range of usual application of SFDs. In this case Lagrange's equations have to be supplemented to include the effects of the fluid particles that leave the control volume carrying kinetic energy, as described in the appendix. Also the kinetic coenergy method predicts an additional term, which is shown to be due to convective acceleration, by an approximate solution of the nonlinear squeeze flow problem by the method of averaged inertia. The conclusion of this chapter is that the kinetic coenergy method adequately predicts the fluid inertia forces in squeezing flows for Reynolds number in the range of usual application of SFDs.

In Chapter 4 the kinetic coenergy method is applied to both the short and long squeeze film dampers. The dampers' inertia coefficients are derived and are shown to be nonlinear functions of the eccentricity of the journal in the bearing. These inertia coefficients represent the added mass to the journal. The fluid inertia forces are then obtained by using Lagrange's equations of motion. For the short squeeze film dampers, as in the squeeze flow case, Lagrange's equations have to be supplemented to include the effects of the fluid particles that leave the control volume carrying kinetic energy. Finally, the solution of the Navier-Stokes equations for the case of a small circular-centered whirl orbit is presented, and it is shown that the fluid inertia forces predicted by the kinetic

coenergy method is a good approximation to the forces in the damper for Reynolds number in the range of usual application of SFDs.

Chapter 5 discusses the dynamics of a Jeffcott rotor incorporating squeeze film dampers. The equations of motion are derived and it is shown that the steady state unbalance response can be obtained by assuming circular-centered whirling motions. Thus the resulting nonlinear algebraic equations are solved to obtain the unbalance response of the rotor. The simple solution for the steady state allows for parametric studies of the system to be made, and the effect of fluid inertia on the steady state dynamics of a rotor incorporating SFDs is explored.

Chapter 6 is the conclusion of the thesis. The problems attacked in this thesis are reviewed and the contributions and conclusions of the thesis are presented. Suggested topics for further research are also discussed.

Chapter 2

Damping Forces In Squeeze Film Dampers

In this chapter, we present the basic analytical tools required for the analysis of squeeze film dampers (SFDs). We first derive Reynolds equation for fluid lubrication from basic principles, then we derive the damping forces obtained by both the long and short bearing approximations of Reynolds equation. We also consider the effects of cavitation on the damping forces.

To include fluid inertia in the analysis, we find that the simplified Navier-Stokes equations for SFDs are nearly impossible to solve. To overcome this problem, we present an approximate method based on calculating the kinetic coenergy of the fluid, and using Lagrange's equations of motion to obtain the inertia forces in the damper. This method is outlined here, and will be discussed in detail in subsequent chapters.

2.1 Reynolds equation

Reynolds equation for fluid lubrication is an equation that the pressure in the damper has to satisfy. It is based on the solution of the continuity equation and the simplified Navier-Stokes equations subject to the boundary conditions in the damper.

In a squeeze film damper (SFD), the ratio of the clearance c to the radius R is very small, $c/R = O(10^{-3})$, thus we can assume that the effects of curvature on the damper are

negligible and we can use a cartesian coordinate system in analyzing the flow in the damper. In addition, the following assumptions are going to be made [82]:

- 1- The variation of the pressure across the film is small and can be neglected.
- 2- The flow is predominantly two-dimensional (circumferential and axial).
- 3- The flow is laminar, and incompressible.
- 4- The flow is fully developed and steady.
- 5- The rate of change of any one velocity component along the film is small compared to the rate of change of the same velocity component across the film.
- 6- Fluid inertia can be neglected.

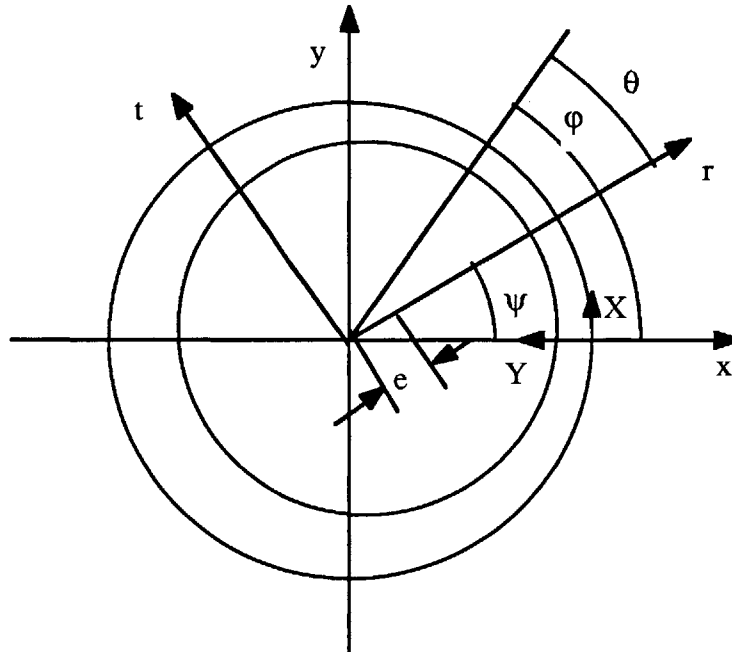


Figure 2.1 Squeeze film damper

Figure 2.1 shows a SFD, and the coordinate system used. The film thickness h at any given location is given by

$$h = c - e \cos \theta$$

where e is the eccentricity of the journal and θ is measured from the positive r -axis of the whirling coordinate system (r, t, z). The z -axis is perpendicular to the plane of the paper.

Also shown in Figure 2.1, the stationary coordinate system (x, y, z) and the angle ϕ which is measured from the positive x -axis, and $\theta = \phi - \psi$. For a steady circular whirl $\psi = \omega t$, where ω is the whirling frequency of the journal and t is time.

Since we assumed that the effects of curvature can be neglected, we can use the stationary cartesian (X, Y, Z) coordinate system shown in Figure 2.1, (with the Z -axis perpendicular to the plane of the paper), to describe the flow. To an observer in this coordinate system, because c/R is small, it appears as if the damper is unwrapped, as shown in Figure 2.2. The upper surface in Figure 2.2 represents the journal, while the lower surface represents the bearing. The motion of the journal, i.e. the upper surface in Figure 2.2, results in the motion of the fluid in the clearance between the two surfaces. Due to the motion of the journal, the upper surface in Figure 2.2 travels in a wave-like fashion, and also changes its shape if the journal is moving radially. It should be noted that since the flow in the damper is cyclic, i.e. the conditions at $\phi = 0$ are the same as those at $\phi = 2\pi$, then the model of Figure 2.2 is repeated every $2\pi R$ in the X -direction.

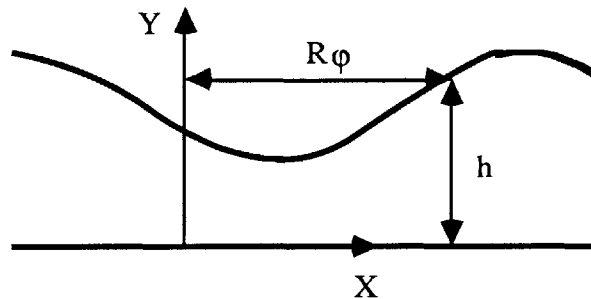


Figure 2.2 Unwrapped squeeze film damper

Using the coordinate system and the assumptions described above, the Navier-Stokes equations reduce to

$$\frac{\partial p}{\partial X} = \mu \frac{\partial^2 u}{\partial Y^2} \quad (2.1)$$

$$\frac{\partial p}{\partial Y} = 0 \quad (2.2)$$

$$\frac{\partial p}{\partial Z} = \mu \frac{\partial^2 w}{\partial Y^2} \quad (2.3)$$

where p is the pressure, u is the velocity of the fluid in the X -direction, w is the velocity of the fluid in the Z -direction and μ is its viscosity .

Since p is independent of Y (equation (2.2)) thus we can integrate equations (2.1) and (2.3) with respect to Y using the boundary conditions

$$\text{At } Y = 0 \quad u = 0 \quad w = 0$$

$$\text{At } Y = h \quad u = U \quad w = 0$$

Thus we get

$$u = \frac{1}{2\mu} \frac{\partial p}{\partial X} (Y^2 - Yh) + \frac{Y}{h} U \quad (2.4)$$

$$w = \frac{1}{2\mu} \frac{\partial p}{\partial Z} (Y^2 - Yh) \quad (2.5)$$

For the continuity of flow

$$\frac{\partial u}{\partial X} + \frac{\partial v}{\partial Y} + \frac{\partial w}{\partial Z} = 0 \quad (2.6)$$

where v is the velocity of the fluid in the Y -direction. Instead of integrating equation (2.6) over Y from 0 to h [62,82], to obtain Reynolds equation, (with the implication that the continuity of flow is satisfied on the average), we are going to determine v from equation (2.6). Thus

$$v = - \int \frac{\partial u}{\partial X} dY - \int \frac{\partial w}{\partial Z} dY + C$$

where $C = C(X,Z)$ is yet to be determined. Substituting for u and w from (2.4) and (2.5), we get

$$v = - \frac{1}{2\mu} \left\{ \frac{\partial}{\partial X} \left[\left(\frac{Y^3}{3} - \frac{Y^2 h}{2} \right) \frac{\partial p}{\partial X} \right] + \frac{\partial}{\partial Z} \left[\left(\frac{Y^3}{3} - \frac{Y^2 h}{2} \right) \frac{\partial p}{\partial Z} \right] \right\} - \frac{\partial}{\partial X} \left(\frac{Y^2}{2h} U \right) + C$$

for the v velocity profile. The above equation has to satisfy the following boundary conditions

$$\begin{aligned} \text{At } Y = 0 & \quad v = 0 \\ \text{At } Y = h & \quad v = V \end{aligned}$$

The first boundary condition implies that $C = 0$, while the second gives us Reynolds equation for fluid lubrication

$$\frac{\partial}{\partial X} \left(\frac{h^3}{\mu} \frac{\partial p}{\partial X} \right) + \frac{\partial}{\partial Z} \left(\frac{h^3}{\mu} \frac{\partial p}{\partial Z} \right) = 12 V + 6 U \frac{\partial h}{\partial X} + 6 h \frac{\partial U}{\partial X} \quad (2.7)$$

If the journal has a radial velocity \dot{e} in the r -direction of Figure 2.1 and a tangential velocity $e\dot{\psi}$ in the t -direction, then U and V , the velocities of the journal surface at any θ , become (see Figure 2.3)

$$\begin{aligned} U &= e \dot{\psi} \cos \theta - \dot{e} \sin \theta \\ V &= -e \dot{\psi} \sin \theta - \dot{e} \cos \theta \end{aligned} \quad (2.8)$$

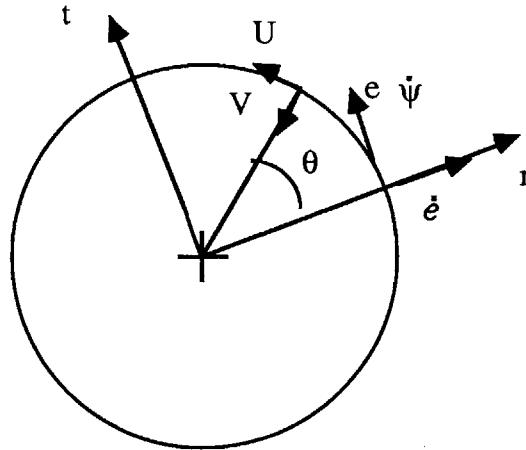


Figure 2.3 Journal velocities

Since $X = R\phi$ and $Z = z$, then Reynolds equation for a squeeze film damper, in the (r, t) coordinate system, becomes

$$\frac{1}{R} \frac{\partial}{\partial \phi} \left(\frac{h^3}{\mu R} \frac{\partial p}{\partial \phi} \right) + \frac{\partial}{\partial z} \left(\frac{h^3}{\mu} \frac{\partial p}{\partial z} \right) = -12 (e \dot{\psi} \sin \theta + \dot{e} \cos \theta) \quad (2.9)$$

after neglecting terms of order c/R in the right hand side of equation (2.9).

Equation (2.9) is quite difficult to solve in closed form. Infinite series solutions for equation (2.9) exist [100], and it can be solved numerically [62]. Yet, for rotordynamic applications, it is beneficial to have a closed form solution for the forces acting on the journal, both to gain a better understanding of the dynamics of the rotors due to the oil film, and to reduce computation time for more involved rotordynamic analyses. Fortunately, two mathematical approximations to Reynolds equation exist that rely on the physical dimensions of the damper. These are the short and long bearing approximations to Reynolds equation and are presented in the following sections.

2.2 Short bearing approximation

For dampers with a length to diameter ratio up to 0.25, the short bearing approximation is a good approximation to Reynolds equations [62]. In the short bearing approximation, it is assumed that the damper is so short in the z -direction that the pressure gradient in the ϕ -direction is much smaller than that in the z -direction, and thus the flow is essentially in the axial direction. The above statement is true even for sealed dampers, if the dampers are short. The dynamic pressures that are present in the damper are so large (of the order of a thousand psi) that no simple seal can stop the axial flow.

Using the short bearing approximation, Reynolds equation, equation (2.9) reduces to

$$\frac{\partial}{\partial z} \left(\frac{h^3}{\mu} \frac{\partial p}{\partial z} \right) = -12 (e \dot{\psi} \sin \theta + \dot{e} \cos \theta)$$

Integrating twice with respect to z with the boundary conditions

$$p = 0 \quad \text{at} \quad z = \pm L/2$$

where L is the length of the damper, we get for the pressure

$$p = \frac{6\mu}{h^3} \left(\frac{L^2}{4} - z^2 \right) (e \dot{\psi} \sin \theta + \dot{e} \cos \theta) \quad (2.10)$$

and the flow velocities u and w can be obtained by substituting from (2.10) into (2.4) and (2.5) respectively. For future reference the w velocity profile is given by

$$w = \frac{6z}{h} \left(\frac{Y}{h} - \frac{Y^2}{h^2} \right) (e \dot{\psi} \sin \theta + \dot{e} \cos \theta) \quad (2.11)$$

The damping forces can be obtained by integrating the pressure, equation (2.10). Thus the radial and tangential forces F_{rc} and F_{tc} acting on the journal are given by (see Figure 2.4)

$$F_{rc} = - \int_{-\frac{L}{2}}^{\frac{L}{2}} \int_{\theta_1}^{\theta_2} p \cos \theta R d\theta dz \quad (2.12)$$

$$F_{tc} = - \int_{-\frac{L}{2}}^{\frac{L}{2}} \int_{\theta_1}^{\theta_2} p \sin \theta R d\theta dz \quad (2.13)$$

Substituting for the pressure from equation (2.10) and integrating over z we get

$$F_{rc} = - \frac{\mu R L^3}{c^3} \int_{\theta_1}^{\theta_2} \frac{\cos^2 \theta}{(1 - \epsilon \cos \theta)^3} d\theta \dot{e} - \frac{\mu R L^3}{c^3} \int_{\theta_1}^{\theta_2} \frac{\cos \theta \sin \theta}{(1 - \epsilon \cos \theta)^3} d\theta e \dot{\psi} \quad (2.14)$$

$$F_{tc} = - \frac{\mu R L^3}{c^3} \int_{\theta_1}^{\theta_2} \frac{\cos \theta \sin \theta}{(1 - \epsilon \cos \theta)^3} d\theta \dot{e} - \frac{\mu R L^3}{c^3} \int_{\theta_1}^{\theta_2} \frac{\sin^2 \theta}{(1 - \epsilon \cos \theta)^3} d\theta e \dot{\psi} \quad (2.15)$$

where $\epsilon = e/c$ is the eccentricity ratio. The limits of integration θ_1 and θ_2 represent the extent of the fluid film.

If there is no cavitation in the damper the limits of the integration are $\theta_1 = 0$ and $\theta_2 = 2\pi$. This would be the case if we had a highly pressurized damper. For a cavitated damper, we are going to use the π -bearing theory. Cavitation is not a well understood

phenomenon, and there is a lot of research going into cavitation in fluid film bearings [59, 99] and more involved analytical models for cavitation exist, but the π -bearing theory is the most acceptable theory in the literature of oil film bearings probably because of its simplicity.

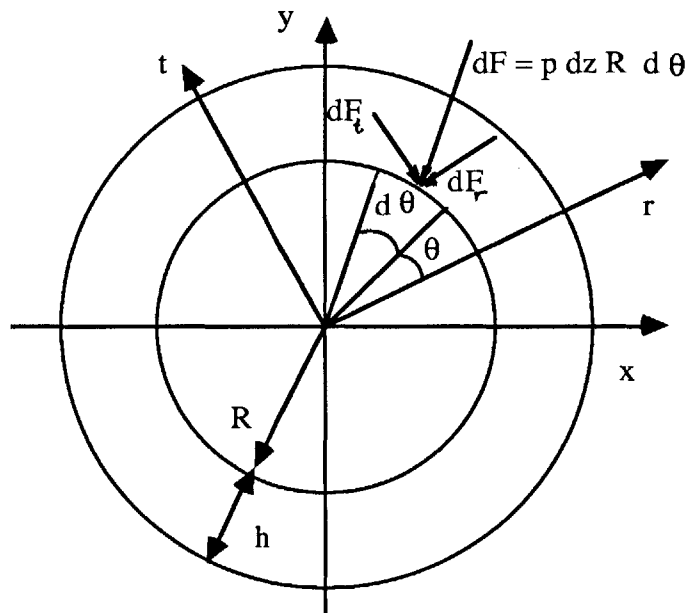


Figure 2.4 Forces on element in the damper

For a π -bearing, the oil film is assumed to extend in the region of positive pressure. Since the fluid cannot sustain tension, the region of negative pressure is assumed to be at zero pressure. The region of positive pressure is determined from equation (2.10), that is it extends from θ_1 such that

$$\theta_1 = \tan^{-1} \left(-\frac{\dot{e}}{e \dot{\psi}} \right) \quad (2.16)$$

to θ_2 such that

$$\theta_2 = \theta_1 + \pi \quad (2.17)$$

Thus the oil film boundaries are moving such that the journal velocity vector acts in the direction of the center of the film. For a nearly circular whirl, the limits of integration can be taken to be $\theta_1 = 0$ and $\theta_2 = \pi$ for a counter-clockwise whirl. For a circular clockwise whirl the limits of integration can be taken to be $\theta_1 = \pi$ and $\theta_2 = 2\pi$. If the journal is travelling radially outwards then the limits of integration are $\theta_1 = -\pi/2$, and $\theta_2 = \pi/2$.

Returning to the forces F_{rc} and F_{lc} of equations (2.14) and (2.15), which may be written in the form

$$F_{rc} = -C_{rr} \dot{e} - C_{rt} e \dot{\psi} \quad (2.18)$$

$$F_{lc} = -C_{tt} \dot{e} - C_{tr} e \dot{\psi} \quad (2.19)$$

where the coefficients C_{rr} , C_{tt} , C_{tr} and C_{rt} are the damper's damping coefficients, and are given by

$$C_{rr} = \frac{\mu R L^3}{c^3} \int_{\theta_1}^{\theta_2} \frac{\cos^2 \theta}{(1 - \epsilon \cos \theta)^3} d\theta$$

$$C_{tt} = \frac{\mu R L^3}{c^3} \int_{\theta_1}^{\theta_2} \frac{\sin^2 \theta}{(1 - \epsilon \cos \theta)^3} d\theta$$

$$C_{rt} = \frac{\mu R L^3}{c^3} \int_{\theta_1}^{\theta_2} \frac{\cos \theta \sin \theta}{(1 - \epsilon \cos \theta)^3} d\theta$$

and $C_{tr} = C_{rt}$

It can be seen from equations (2.18) and (2.19) that the damping coefficients represent a symmetric tensor relating the force vector to the velocity vector. This means that the oil film is not isotropic, we get different damping forces when the journal moves in different directions. Also the cross-coupling damping coefficients C_{rt} and C_{tr} imply that we get both radial and tangential damping forces even if the journal is moving in the tangential direction only, for instance.

For a π -bearing, with a journal executing a nearly circular counter-clockwise whirl, the coefficients C_{rr} , C_{tt} , C_{tr} and C_{rt} take the form

$$C_{rr} = \frac{\mu R L^3}{c^3} C_{rr}^*, C_{tt} = \frac{\mu R L^3}{c^3} C_{tt}^*, C_{rt} = C_{tr} = \frac{\mu R L^3}{c^3} C_{rt}^*$$

$$C_{rr}^* = \frac{\pi}{2} \frac{(1 + 2\varepsilon^2)}{(1 - \varepsilon^2)^{5/2}} \quad (2.20)$$

$$C_{tt}^* = \frac{\pi}{2} \frac{1}{(1 - \varepsilon^2)^{3/2}} \quad (2.21)$$

$$C_{rt}^* = \frac{2\varepsilon}{(1 - \varepsilon^2)^2} \quad (2.22)$$

These coefficients are plotted in Figure 2.5, versus the eccentricity ratio, from which it can be seen that the damping coefficients increase drastically with the increase of the radius of the orbit, and become infinite as ε approaches 1. Thus as the journal executes a larger orbit the fluid exerts a larger resisting force. For a 2π -bearing the coefficients C_{rr} and C_{tt} are double those for a π -bearing and C_{rt} and C_{tr} are zero.

2.3 Long bearing approximation

The long bearing approximation is based on the assumption that the damper is infinitely long in the z -direction such that the pressure gradient in the θ -direction is much larger than that in the z -direction, and thus the flow is essentially in the circumferential direction. The long bearing approximation is valid for dampers with $L/D > 4$, or for tightly sealed dampers.

For long bearings, Reynolds equation, equation (2.9) reduces to

$$\frac{1}{R} \frac{\partial}{\partial \theta} \left(\frac{h^3}{\mu R} \frac{\partial p}{\partial \theta} \right) = -12 (e \dot{\psi} \sin \theta + \dot{e} \cos \theta)$$

Integrating twice with respect to θ , we get

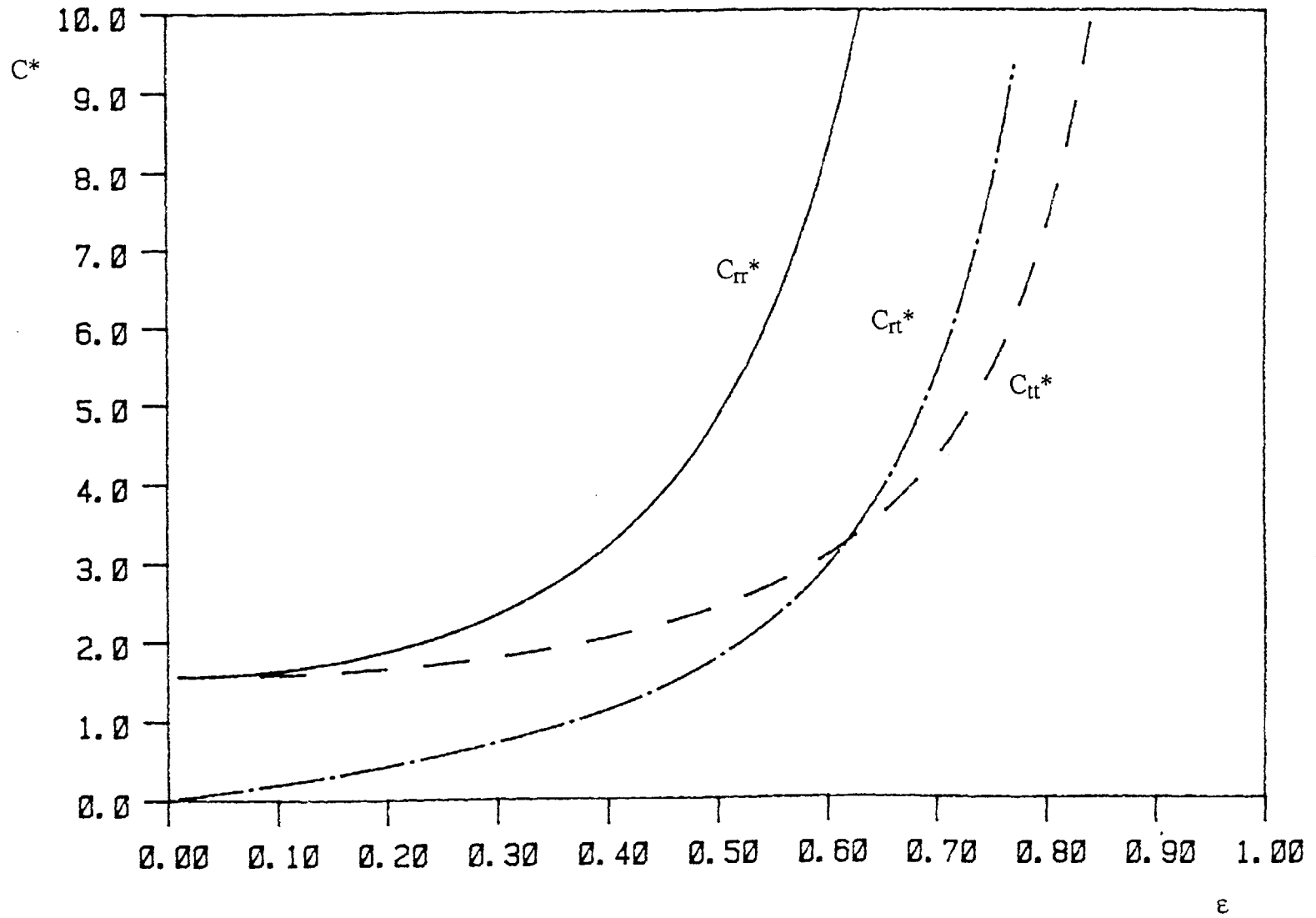


Figure 2.5 Nondimensional damping coefficients for the short damper

$$p = -\frac{12 \mu R^2}{c^3} \int \frac{\sin \theta}{(1 - \epsilon \cos \theta)^3} d\theta \dot{e} + \frac{12 \mu R^2}{c^3} \int \frac{\cos \theta}{(1 - \epsilon \cos \theta)^3} d\theta e \dot{\psi} \\ + \int \frac{d\theta}{(1 - \epsilon \cos \theta)^3} C_1 + C_2$$

where C_1 and C_2 are constants of integration. With the aid of a table of integrals [4], the above integrations can be performed, thus the pressure becomes

$$p = \frac{6 \mu R^2}{c^3} \frac{1}{(1 - \epsilon \cos \theta)^2} \dot{e} \\ + \frac{12 \mu R^2}{c^3} e \dot{\psi} \left[\frac{\sin \theta}{2(1 - \epsilon^2)(1 - \epsilon \cos \theta)^2} + \frac{(1 + 2\epsilon^2) \sin \theta}{2(1 - \epsilon^2)^2(1 - \epsilon \cos \theta)} + \right. \\ \left. + \frac{3\epsilon \delta}{2(1 - \epsilon^2)^{5/2}} \cos^{-1} \left(\frac{-\epsilon + \cos \theta}{1 - \epsilon \cos \theta} \right) \right] \\ + C_1 \left[\frac{\epsilon \sin \theta}{2(1 - \epsilon^2)(1 - \epsilon \cos \theta)^2} + \frac{3\epsilon \sin \theta}{2(1 - \epsilon^2)^2(1 - \epsilon \cos \theta)} + \right. \\ \left. + \frac{(2 + \epsilon^2) \delta}{2(1 - \epsilon^2)^{5/2}} \cos^{-1} \left(\frac{-\epsilon + \cos \theta}{1 - \epsilon \cos \theta} \right) \right] + C_2 \quad (2.23)$$

where δ is defined as

$$\delta = \begin{cases} 1 & \sin \theta \geq 0 \\ -1 & \sin \theta \leq 0 \end{cases}$$

The pressure has to satisfy the condition of periodicity, i.e. $p(\theta = -\pi) = p(\theta = \pi)$. At $\theta = \pi$ the film thickness is at its maximum and thus the lowest pressure occurs at this section. Since we are interested in the dynamic pressures only, we can assume without any loss of generality that the pressure at $\theta = \pi$ is equal to zero. Thus the boundary conditions that equation (2.23) has to satisfy are

$$\begin{array}{lll} \text{at} & \theta = -\pi & p = 0 \\ \text{and} & \text{at} & \theta = \pi & p = 0 \end{array}$$

Using these boundary conditions C_1 and C_2 are evaluated to be

$$C_1 = -\frac{12 \mu R^2}{c^3} e \dot{\psi} \frac{3 \epsilon}{(2 + \epsilon^2)}$$

and
$$C_2 = -\frac{6 \mu R^2}{c^3} \frac{1}{\epsilon (1 + \epsilon)^2} \dot{e}$$

Finally the pressure is given by

$$p = \frac{6 \mu R^2}{c^3} \left\{ \left[\frac{1}{\epsilon (1 - \epsilon \cos \theta)^2} - \frac{1}{\epsilon (1 + \epsilon)^2} \right] \dot{e} + \left[\frac{2 \sin \theta (2 - \epsilon \cos \theta)}{(2 + \epsilon^2) (1 - \epsilon \cos \theta)^2} \right] e \dot{\psi} \right\} \quad (2.24)$$

The flow velocities u and w can be obtained by substituting from (2.24) into (2.4) and (2.5) respectively. For future reference the u velocity profile (neglecting terms of $O(c/R)$) is given by

$$u = \frac{6 R}{h} \left(\frac{Y}{h} - \frac{Y^2}{h^2} \right) \left[\sin \theta \dot{e} - \cos \theta e \dot{\psi} + \frac{3 \epsilon}{(2 + \epsilon^2)} e \dot{\psi} \right] \quad (2.25)$$

The damping forces, as in the short bearing case, are obtained by substituting the pressure from equation (2.24) into equations (2.12) and (2.13). Thus the radial and tangential damping forces acting on the journal are

$$F_{rc} = -\frac{6 \mu R^3 L}{c^3} \int_{\theta_1}^{\theta_2} \left[\frac{\cos \theta}{\epsilon (1 - \epsilon \cos \theta)^2} - \frac{\cos \theta}{\epsilon (1 + \epsilon)^2} \right] d\theta \dot{e} \\ - \frac{12 \mu R^3 L}{c^3} \int_{\theta_1}^{\theta_2} \frac{\sin \theta \cos \theta (2 - \epsilon \cos \theta)}{(2 + \epsilon^2) (1 - \epsilon \cos \theta)^2} d\theta e \dot{\psi} \quad (2.26)$$

and

$$F_{tc} = -\frac{6 \mu R^3 L}{c^3} \int_{\theta_1}^{\theta_2} \left[\frac{\sin \theta}{\epsilon (1 - \epsilon \cos \theta)^2} - \frac{\sin \theta}{\epsilon (1 + \epsilon)^2} \right] d\theta \dot{e} \\ - \frac{12 \mu R^3 L}{c^3} \int_{\theta_1}^{\theta_2} \frac{\sin^2 \theta (2 - \epsilon \cos \theta)}{(2 + \epsilon^2) (1 - \epsilon \cos \theta)^2} d\theta e \dot{\psi} \quad (2.27)$$

Equations (2.26) and (2.27) can be written in the form of equations (2.18) and (2.19)

$$F_{rc} = -C_{rr} \dot{e} - C_{rt} e \dot{\psi} \quad (2.18)$$

$$F_{tc} = -C_{tr} \dot{e} - C_{tt} e \dot{\psi} \quad (2.19)$$

where C_{rr} , C_{tt} , C_{rt} and C_{tr} are the damping coefficients and are given by

$$C_{rr} = \frac{6 \mu R^3 L}{c^3} \int_{\theta_1}^{\theta_2} \left[\frac{\cos \theta}{\epsilon (1 - \epsilon \cos \theta)^2} - \frac{\cos \theta}{\epsilon (1 + \epsilon)^2} \right] d\theta$$

$$C_{tt} = \frac{12 \mu R^3 L}{c^3} \int_{\theta_1}^{\theta_2} \frac{\sin^2 \theta (2 - \epsilon \cos \theta)}{(2 + \epsilon^2) (1 - \epsilon \cos \theta)^2} d\theta$$

$$C_{rt} = \frac{12 \mu R^3 L}{c^3} \int_{\theta_1}^{\theta_2} \frac{\sin \theta \cos \theta (2 - \epsilon \cos \theta)}{(2 + \epsilon^2) (1 - \epsilon \cos \theta)^2} d\theta$$

$$C_{tr} = \frac{6 \mu R^3 L}{c^3} \int_{\theta_1}^{\theta_2} \left[\frac{\sin \theta}{\epsilon (1 - \epsilon \cos \theta)^2} - \frac{\sin \theta}{\epsilon (1 + \epsilon)^2} \right] d\theta$$

It can be seen from equations (2.18) and (2.19) that the damping coefficients represent an unsymmetric tensor relating the force vector to the velocity vector. As for the short bearing, this means that the oil film is not isotropic.

Also here we are going to adopt the π -bearing theory for the cavitated damper and the 2π -bearing for the uncavitated damper. For a cavitated damper executing a nearly circular whirl, the limits of integration are $\theta_1 = 0$ and $\theta_2 = \pi$. Thus the damping coefficients become

$$C_{rr} = \frac{\mu R^3 L}{c^3} C_{rr}^*, \quad C_{tt} = \frac{\mu R^3 L}{c^3} C_{tt}^*, \quad C_{rt} = \frac{\mu R^3 L}{c^3} C_{rt}^*, \quad C_{tr} = \frac{\mu R^3 L}{c^3} C_{tr}^* \quad (2.28)$$

$$C_{rr}^* = \frac{6 \pi}{(1 - \epsilon^2)^{3/2}} \quad (2.28)$$

$$C_{tt}^* = \frac{12 \pi}{(2 + \epsilon^2) (1 - \epsilon^2)^{1/2}} \quad (2.29)$$

$$C_{rt}^* = \frac{24 \epsilon}{(2 + \epsilon^2) (1 - \epsilon^2)} \quad (2.30)$$

$$C_{tr}^* = \frac{24}{(1 + \epsilon)(1 - \epsilon^2)} \quad (2.31)$$

These coefficients are plotted in Figure 2.6, versus the eccentricity ratio, from which it can be seen that, as in the short bearing, the damping coefficients increase drastically with the increase of the radius of the orbit, and become infinite as ϵ approaches 1. Thus as the journal executes a larger orbit the fluid exerts a larger resisting force. For a 2π -bearing the coefficients C_{rr} and C_{tt} are double those for a π -bearing and C_{rt} and C_{tr} are zero.

Comparing the damping coefficients of the short damper with those of the long damper, we find that the damping coefficients of the long damper are relatively larger than those of the short damper, i.e.

$$\frac{C_{long}}{C_{short}} = O\left(12 \frac{R_{long}^2}{L_{short}^2}\right)$$

Thus for example, if $R_{long} = L_{short}$, then $C_{long} = 12 C_{short}$. This is to be expected since the oil in the short damper flows axially, and thus is squeezed out of the damper, while for the long damper the oil flows circumferentially and is forced to resist the motion. Also the damping coefficients of the short damper form a symmetric tensor, i.e. $C_{rt} = C_{tr}$, while those for the long damper form an unsymmetric tensor.

2.4 Fluid inertia

Historically, as mentioned in the introduction, fluid inertia was neglected in the analysis of squeeze film dampers until it was demonstrated experimentally that fluid inertia does affect the performance of the dampers [87].

To include fluid inertia in the analysis and assuming an unsteady flow, but still retaining the rest of the assumptions, the Navier-Stokes equations become

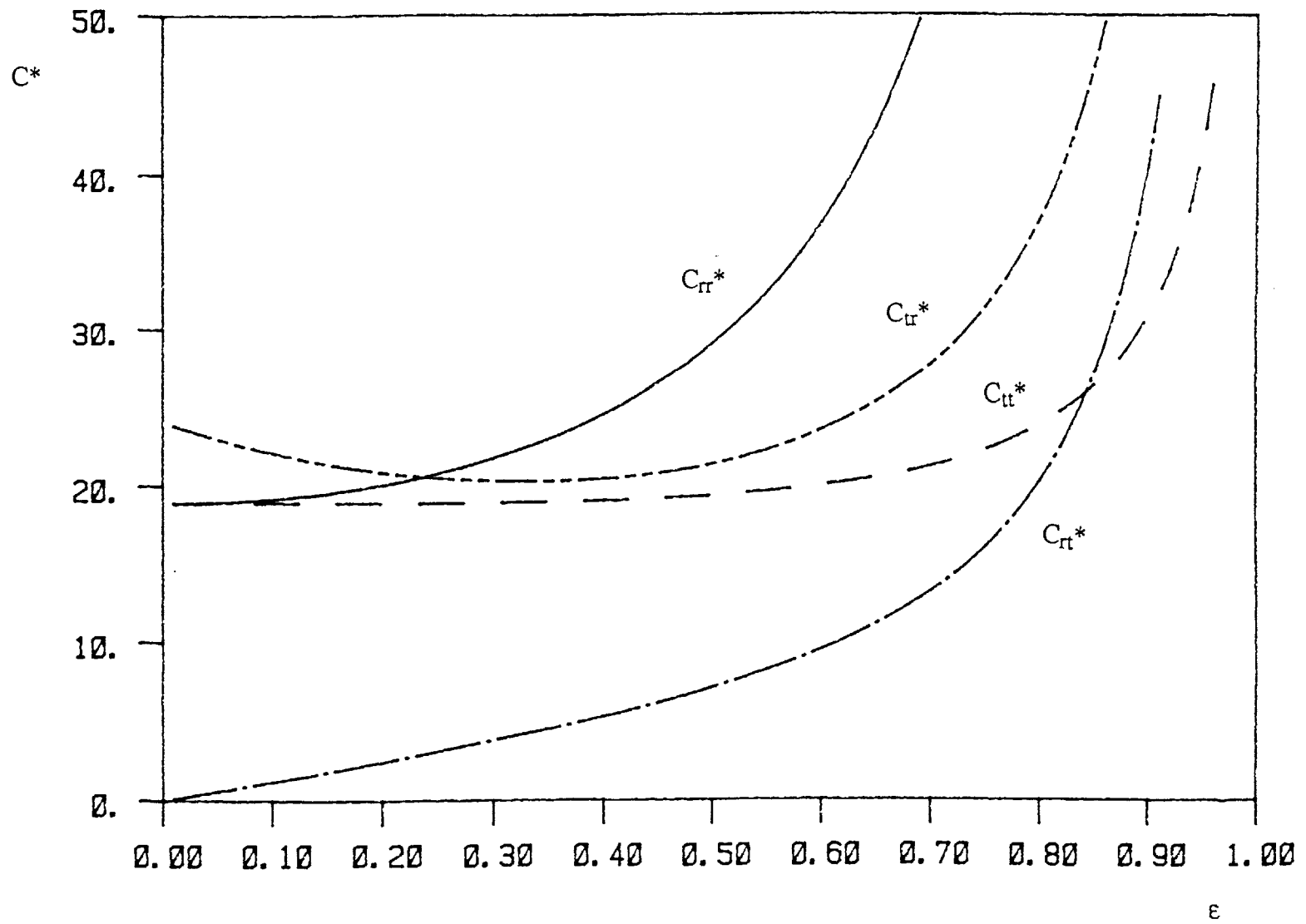


Figure 2.6 Nondimensional damping coefficients for the long damper

$$\frac{\partial u}{\partial t} + u \frac{\partial u}{\partial X} + v \frac{\partial u}{\partial Y} + w \frac{\partial u}{\partial Z} = -\frac{1}{\rho} \frac{\partial p}{\partial X} + \mu \frac{\partial^2 u}{\partial Y^2} \quad (2.32)$$

$$\frac{\partial p}{\partial Y} = 0 \quad (2.33)$$

$$\frac{\partial w}{\partial t} + u \frac{\partial w}{\partial X} + v \frac{\partial w}{\partial Y} + w \frac{\partial w}{\partial Z} = -\frac{1}{\rho} \frac{\partial p}{\partial Z} + \mu \frac{\partial^2 w}{\partial Y^2} \quad (2.34)$$

The above equations have to satisfy the following boundary conditions

$$\text{At } y = 0 \quad u = 0 \quad v = 0 \quad w = 0$$

$$\text{At } y = h \quad u = U \quad v = V \quad w = 0$$

where U and V are given by equation (2.8). The above system of partial differential equations, together with the continuity equation, equation (2.6), is nearly impossible to solve analytically except in very special cases.

To circumvent this handicap, we resort to an approximate method to calculate the fluid inertia forces in a squeeze film damper. Since the fluid in the damper moves only due to the motion of the journal, then if we were able to calculate the kinetic coenergy of the fluid, we can use Lagrange's equations of motion, with the velocities of the journal taken as the generalized velocities [55], to predict the inertia forces in the damper.

The kinetic coenergy of the fluid is defined as

$$T^* = \frac{1}{2} \int_V \rho (u^2 + v^2 + w^2) dV \quad (2.35)$$

where V is the volume of the fluid in the damper. Thus to calculate the kinetic coenergy we have to know the velocities of the fluid. But since we do not know the velocities of the fluid beforehand, we are going to assume that the velocity profiles predicted by the classical lubrication theory are a good approximation of the actual velocity profiles, even at relatively high squeeze Reynolds numbers. This approximation has been used before in conjunction with the method of averaged inertia [13], and is justified by the results of previous

researchers[†] that indicate that the velocity field predicted by the classical lubrication theory is not greatly affected by fluid inertia for Reynolds number in the range of usual application of squeeze film dampers.

In the next chapter, it is going to be shown that this assumption is reasonable in simple squeezing flows for Reynolds numbers in the range of usual application of squeeze film dampers. The application of this technique, hereinafter called the kinetic coenergy method, to obtain fluid inertia forces in squeeze film dampers is illustrated in chapter 4.

[†] See discussion in the introduction.

Chapter 3

Fluid Inertia Effects In Squeezing Flows

As mentioned in the introduction, the results of previous researchers indicate that the classical lubrication theory is in error with respect to the pressure field and the inertia forces, which can dominate at higher Reynolds numbers. On the other hand, they all seem to indicate that the velocity field predicted by the classical lubrication theory is not greatly affected by fluid inertia for Reynolds number in the range of usual application of squeeze film dampers.

The aim of this chapter is to study the basic constituents of the flow in a squeeze film damper, namely, the Poiseuille flow produced because of squeezing motion, and the direct Squeeze flow, both to understand the mechanics of squeezing flows and to illustrate the effectiveness of the kinetic coenergy method introduced in the previous chapter. It will be shown that this approximate method agrees favorably with the full solution, including convective acceleration.

3.1 Poiseuille flow resulting from squeezing motion

Consider a block of a rigid material having length L , width D and thickness b moving with a velocity \dot{e} in a chamber filled with an incompressible fluid, as shown in Figure 3.1. This can be considered as a simplified squeeze film damper (SFD). Figure 3.2 shows a SFD moving radially outwards with a velocity \dot{e} . Comparing Figures 3.1 and 3.2,

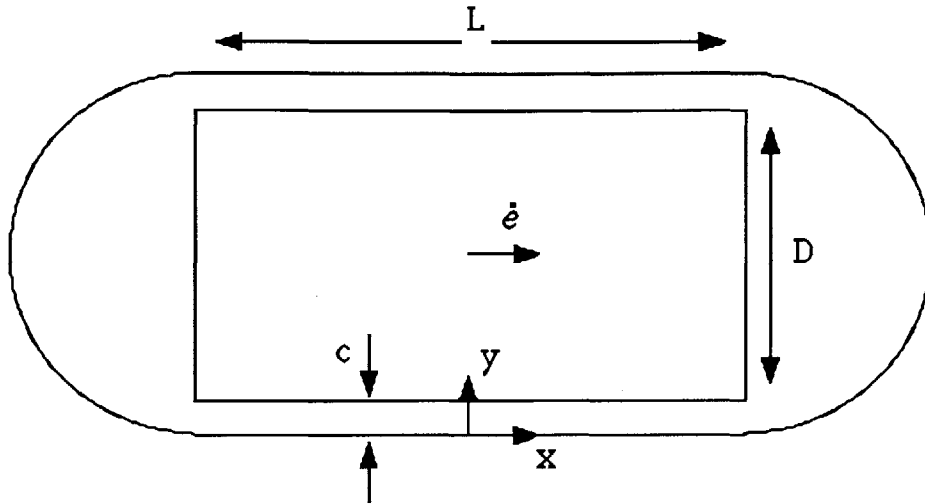


Figure 3.1 Schematic of a block moving in a fluid-filled chamber.

we can see that the block in Figure 3.1 represents the journal in Figure 3.2, but is simpler in the sense that the flow past the block in the clearances moves in a straight channel, while the flow past the journal in the damper clearance moves in a curved channel. We assume that, in the Poiseuille flow of Figure 3.1, the side chambers are large, such that the pressure is uniform in these side chambers.

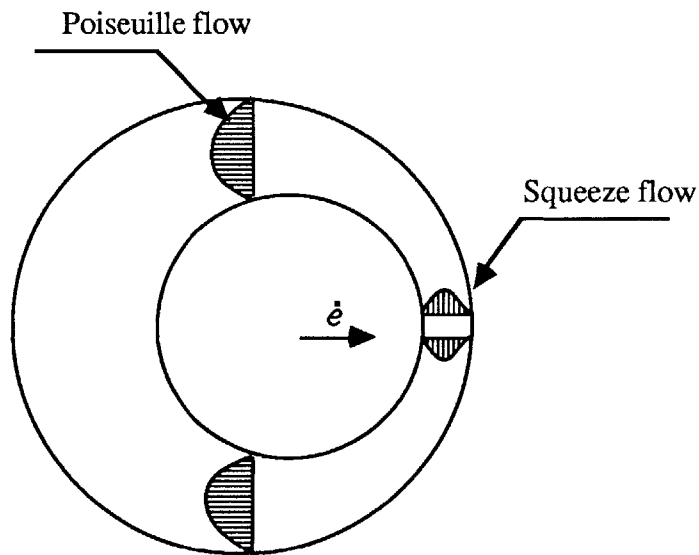


Figure 3.2 Radial motion of SFD

Let c be the clearance between the block and the chamber, with $D/c \gg 1$, and consider a stationary reference frame (x,y) attached to the chamber with the x -axis coinciding with the lower surface of the chamber. Since the problem is symmetric the flow in the upper and lower clearances is the same, and only the flow in the lower clearance will be obtained. The classical lubrication theory solution (inertialess solution) will be presented first, followed by the solution of the problem including the inertia of the fluid.

In the classical lubrication theory, i.e. neglecting fluid inertia, the x -momentum equation reduces to

$$\mu \frac{d^2 u}{dy^2} - \frac{dp}{dx} = 0 \quad (3.1)$$

where μ is the viscosity of the fluid, u is the velocity of the fluid in the x -direction and dp/dx is the pressure gradient. The y -momentum equation is

$$\frac{dp}{dy} = 0 \quad (3.2)$$

thus the pressure gradient dp/dx is independent of y . Equation (3.1) can be integrated twice with respect to y , with the boundary conditions

$$\begin{aligned} \text{at } y = 0 & \quad u = 0 \\ \text{at } y = c & \quad u = \dot{e} \end{aligned} \quad (3.3)$$

thus the velocity u is given by

$$u = \frac{y}{c} \dot{e} - \frac{c^2}{2\mu} \frac{dp}{dx} \left(\frac{y}{c} - \frac{y^2}{c^2} \right) \quad (3.4)$$

To determine the pressure gradient recourse has to be made to the continuity of the flow in the chamber. The fluid squeezed by the block has to flow through the clearances.

Therefore

$$-D b \dot{e} = 2 b \int_0^c u dy \quad (3.5)$$

Note that the negative sign in the left hand side of equation (3.5) is because the fluid and the block are moving in opposite directions. Substituting (3.4) into (3.5), the pressure gradient becomes (neglecting terms of order c/D)

$$\frac{dp}{dx} = 6 \frac{\mu D}{c^3} \dot{e} \quad (3.6)$$

and the velocity u becomes

$$u = \frac{y}{c} \dot{e} - \frac{3D}{c} \left(\frac{y}{c} - \frac{y^2}{c^2} \right) \dot{e} \quad (3.7)$$

Also, the force F resisting the motion is

$$F = - (p_1 - p_2) D b$$

where p_1 and p_2 are the pressures in front of the block and behind it, respectively. The negative sign is because the force F opposes the motion. By using (3.6), the force F becomes

$$F = - 6 \frac{\mu D^2 b L}{c^3} \dot{e} \quad (3.8)$$

The force F in equation (3.8) is proportional to the velocity of the block and is due to viscous effects.

The above analysis was for the case when fluid inertia is neglected. If the effect of fluid inertia is introduced equation (3.1) becomes

$$\frac{\partial u}{\partial t} = - \frac{1}{\rho} \frac{\partial p}{\partial x} + \nu \frac{\partial^2 u}{\partial y^2} \quad (3.9)$$

where ρ is the fluid density, ν is its kinematic viscosity, and t is time. To solve equation (3.9), for an oscillating block, assume u , p and \dot{e} to have an $e^{i\omega t}$ time behavior. Thus, let $u = U e^{i\omega t}$, $p = P e^{i\omega t}$, and $\dot{e} = U_0 e^{i\omega t}$, and equation (3.9) becomes

$$i \omega U = - \frac{1}{\rho} \frac{dP}{dx} + \nu \frac{d^2 U}{dy^2} \quad (3.10)$$

The pressure gradient is still independent of y , and we can solve the differential equation (3.10) for U , using the boundary conditions (3.3)

$$U = -\frac{i}{\omega \rho} \frac{dP}{dx} \frac{\sinh (s y) - \sinh (s(y-c)) - \sinh (s c)}{\sinh (s c)} + \frac{\sinh (s y)}{\sinh (s c)} U_0 \quad (3.11)$$

where

$$s = \frac{1}{c} (1+i) \sqrt{\frac{Re}{2}} \quad (3.12)$$

and

$$Re = \frac{\omega c^2}{\nu} \quad (3.13)$$

is the Reynolds number. It can be shown that as $Re \rightarrow 0$, equation (3.11) reduces to equation (3.4). Substituting equation (3.11) into equation (3.5), the pressure gradient becomes

$$\frac{dP}{dx} = \frac{i U_0 \omega \rho \left[\frac{1}{2} \frac{D}{c} s c \sinh (s c) + \cosh (s c) - 1 \right]}{[2 - 2 \cosh (s c) + s c \sinh (s c)]} \quad (3.14)$$

and the force F is

$$F = -L D b \frac{dP}{dx}$$

and thus the nondimensional force

$$F^* = \frac{F c^3}{L b U_0 \mu D^2} \quad (3.15)$$

becomes

$$F^* = -\frac{i Re \left[\frac{1}{2} s c \sinh (s c) + \frac{c}{D} \cosh (s c) - \frac{c}{D} \right]}{[2 - 2 \cosh (s c) + s c \sinh (s c)]} \quad (3.16)$$

It can be shown that as $Re \rightarrow 0$, F^* has the form (neglecting terms of $O(c/D)$)

$$\lim_{Re \rightarrow 0} F^* = -6 [1 + i 0.1 Re] \quad (3.17)$$

which shows that as $Re \rightarrow 0$, F^* has a real part equal to that of equation (3.8) predicted by the classical lubrication theory. The real part of F^* represents the viscous force, while the imaginary part represents the force due to the inertia of the fluid. Equation (3.17) shows that the inertia force, as $Re \rightarrow 0$, is linear with Re , which is also nondimensional frequency. Figure 3.3 shows the nondimensional force F^* plotted versus Re , using equation (3.16), for $D/c = 1000$. On the same figure the classical lubrication solution,

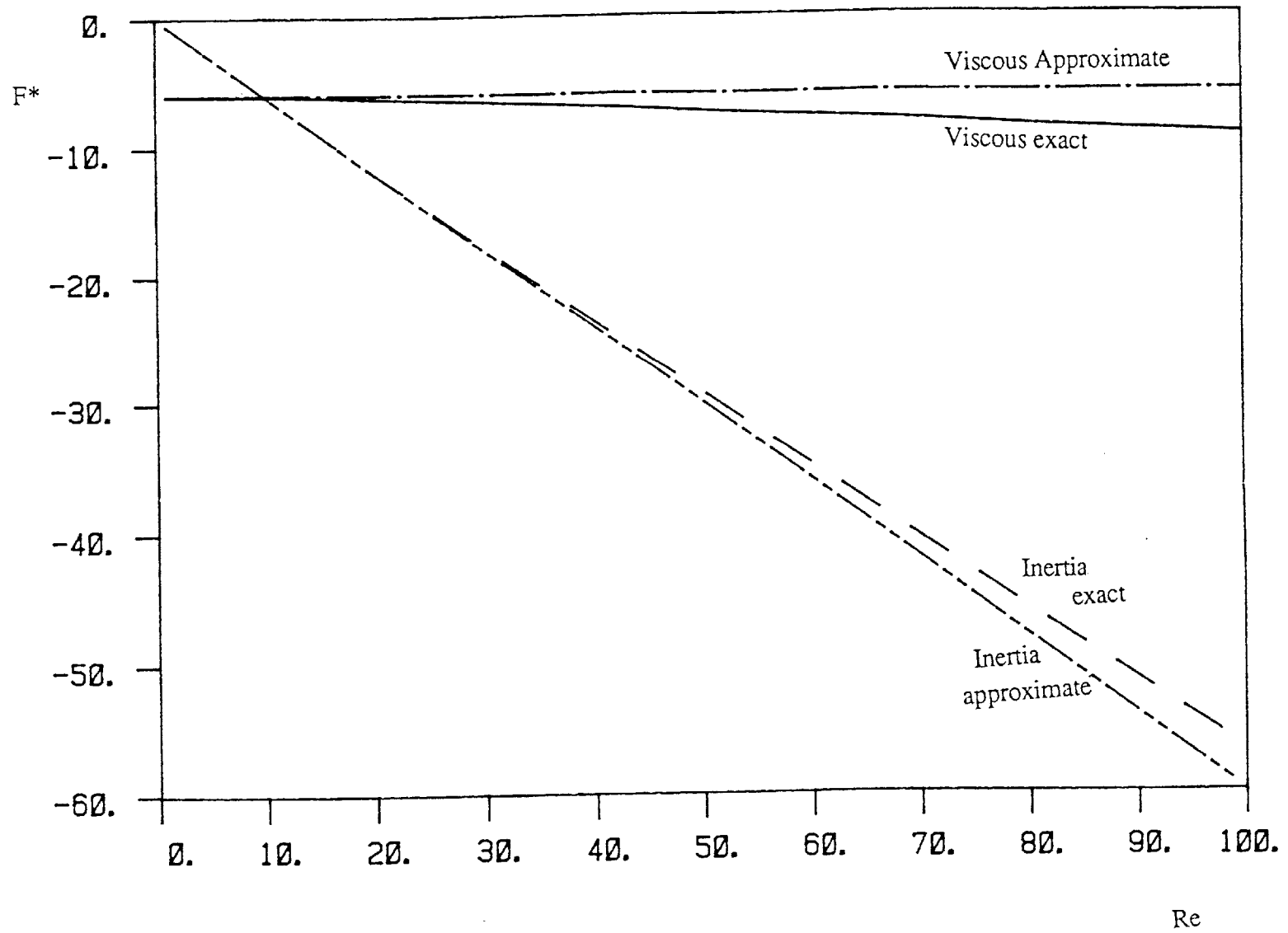


Figure 3.3 Nondimensional forces acting on block in Poiseuille flow

equation (3.8), is plotted for a sinusoidal velocity. It can be seen that the real part of the full solution deviates by only a few percent from the inertialess solution equation (3.8), for Re up to 50, which is the range of Reynolds numbers found in practice for squeeze film dampers [84]. The deviation increases to up to 50 per cent at $Re = 100$, but at that point the flow is totally dominated by inertia rather than viscous effects. In fact, the viscous force is equal to the inertia force at $Re = 10$, and for higher Reynolds numbers the inertia force is larger. The imaginary part of the force in equation (3.16), which represents the inertia force, is shown in Figure 3.3 to be nearly linear with Re . Also shown is the solution predicted by the approximate method, discussed in the next section, for the inertia forces.

It should be noted that the total force F_s acting on the block is the real part of $F^* e^{i\omega t}$, that is, from equation (3.17), the force acting on the block as $Re \rightarrow 0$, is given by

$$F_s = -6 \frac{\mu L b D^2}{c^3} [\cos \omega t - 0.1 Re \sin \omega t] \quad (3.18)$$

As an example of the effect of fluid inertia, it can be seen from equation (3.17) that the amplitude of the inertia force (for small Re) is given by

$$|F_i| = 0.6 Re \frac{\mu U_0 L b D^2}{c^3} = 0.6 \frac{\rho L b D^2}{c} (\omega U_0)$$

Thus the mass added to the block is

$$m = 0.6 \frac{\rho L b D^2}{c} \quad (3.19)$$

while the mass of the block is

$$M = \rho_b L b D$$

where ρ_b is the density of the block. Thus the ratio of the mass added to the block due to fluid inertia to the mass of the block is

$$\frac{m}{M} = 0.6 \frac{D}{c} \frac{\rho}{\rho_b}$$

If the block is made of steel, its density would be about $\rho_b = 7800 \text{ kg/m}^3$ and typically the density of oil would be about $\rho = 800 \text{ kg/m}^3$, and for squeeze film damper applications D/c is in the order of 1000, then m/M would be of the order of 60. This means that due to the huge velocities and accelerations in the clearances the mass of the block, which is made of steel, can be neglected with respect to the added mass due to the inertia of the oil. Also it can be seen from the above relationship that m/M increases as the clearance c decreases, this is because for smaller clearances the velocity and acceleration of the fluid in the clearance increases, and thus the added mass increases, even though the actual mass of the fluid film has decreased.

3.2 Kinetic coenergy method applied to Poiseuille flow

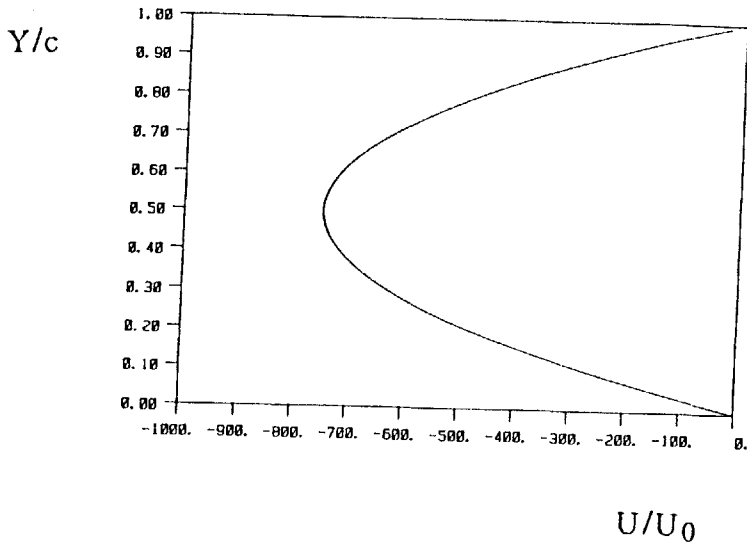
The flow velocity U in the full inertial solution can be obtained by substituting equation (3.14) into (3.11). The velocity profile thus obtained is plotted in Fig. 3.4 for $D/c = 1000$, and $Re = 1, 10, 30$, and 100 . Plotted also is the inertialess velocity profile, equation (3.7), and it can be seen that they match nearly identically for low Re . This was expected, as discussed in the introduction, from the previous literature.

The approximate method is based on the assumption that the velocity profile is not changed much by the inertia of the fluid. Thus the flow can be assumed to be that of the classical lubrication theory, and the kinetic coenergy of the fluid can be calculated. The inertia forces acting on the block can thus be obtained by the use of Lagrange's equations.

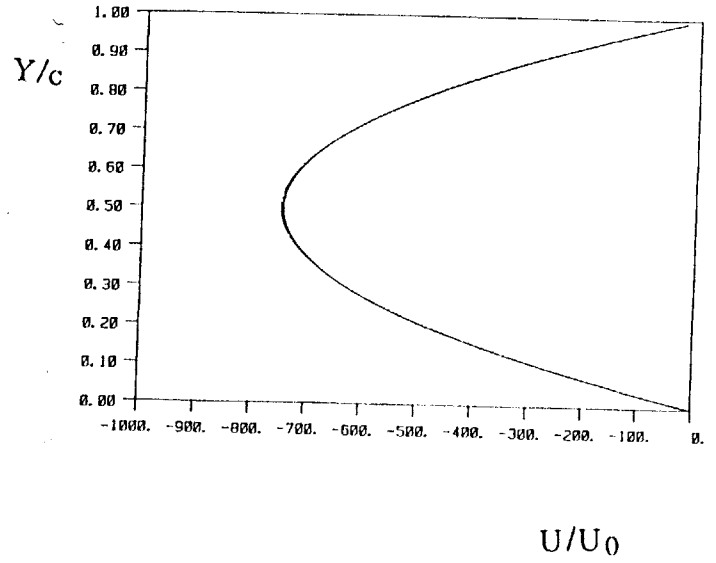
Assuming that the fluid velocity is given by the inertialess solution equation (3.7), the kinetic coenergy stored in the fluid is then

$$T^* = \frac{1}{2} \left[2 \int u^2 dm \right]$$

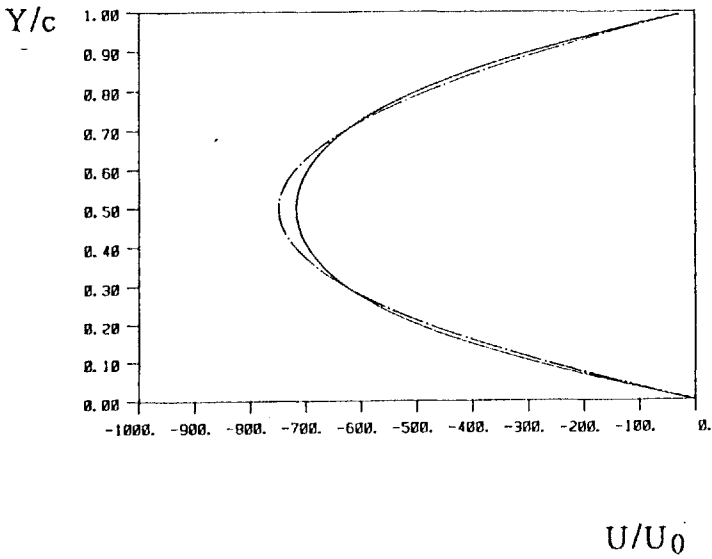
Re=1.0



Re=10.0



Re=30.0



Re=100.0

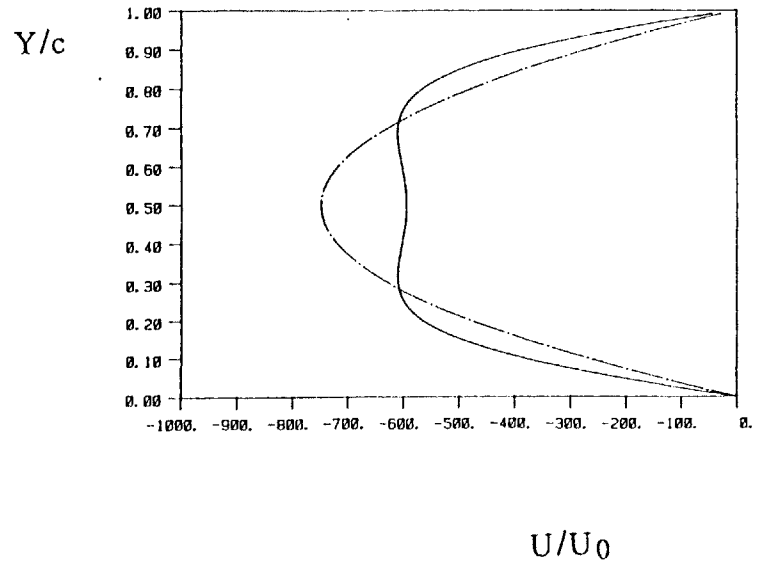


Figure 3.4 Velocity profiles for Poiseuille flow for $D/c=1000$

where dm is the mass of an infinitesimal volume of fluid flowing in the clearance.

Therefore

$$T^* = \frac{1}{2} \left[2 \rho L b \int_0^c u^2 dy \right]$$

Substituting for u from equation (3.7), we get (neglecting terms of order c/D)

$$T^* = \frac{1}{2} \left[0.6 \frac{\rho L b D^2}{c} \right] \dot{e}^2 \quad (3.20)$$

The added mass to the block is represented by the quantity between brackets in equation (3.20), which is exactly equal to the added mass predicted by equation (3.19). Equation (3.20) represents the kinetic coenergy stored in the fluid, but it is only a function of the velocity of the block \dot{e} . The added mass to the block due to fluid inertia, means that we are representing the fluid particles with a point mass at the center of the block. Thus we can obtain the forces acting on the block due to fluid inertia by calculating the inertia force due to the point mass. If we take the velocity of the block \dot{e} as our generalized velocity, then the generalized momentum in the direction of \dot{e} is given by

$$\frac{\partial T^*}{\partial \dot{e}} = 0.6 \frac{\rho L b D^2}{c} \dot{e}$$

Note that this generalized momentum acts in the opposite direction of the fluid velocity.

Using Lagrange's equation of motion, the force due to the inertia of the fluid is

$$F_i = - \frac{d}{dt} \left(\frac{\partial T^*}{\partial \dot{e}} \right) + \frac{\partial T^*}{\partial e} = - 0.6 \frac{\rho L b D^2}{c} \ddot{e}$$

For $\dot{e} = U_0 \cos \omega t$, then $\ddot{e} = - \omega U_0 \sin \omega t$ and

$$F_i = 0.6 \frac{\rho L b D^2}{c} \omega U_0 \sin \omega t \quad (3.21)$$

which is exactly the same as that predicted by equation (3.18), for the full solution as $Re \rightarrow 0$. Equation (3.21) (in complex form) is plotted on Fig. 3.3 which shows the close agreement, especially at low Re , between the exact solution equation (3.16) and the approximate solution equation (3.21). The approximate solution has the advantage of simplicity, since it only requires the knowledge of the velocity profile predicted by the classical lubrication theory, without having to solve the partial differential equations of

motion including the inertia terms. It should be noted that we did not have to consider the kinetic energy of the fluid particles that leave and enter the system, since the fluid particles that enter the system at one side have the same velocity distribution as the fluid particles that leave the system from the other side. Thus there is no net gain or loss of kinetic energy. We will have to consider the flux of the kinetic energy from the system when we obtain the inertia force in the squeeze flow case.

3.3 Squeeze flow

The second constituent of the flow in a squeeze film damper is the direct Squeeze flow. Consider a flat surface moving downwards towards a stationary flat surface, and squeezing an

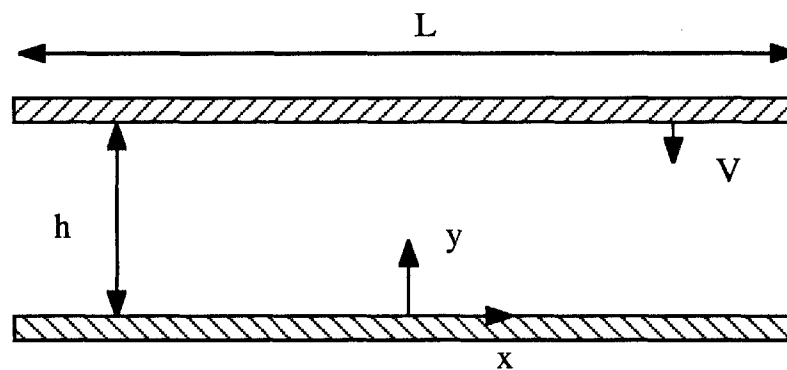


Figure 3.5 Squeeze flow between two flat surfaces

incompressible fluid, as shown in Figure 3.5. Let the distance between the two surfaces be h and the length and width of the surfaces be L and b , respectively, and let $h/L \ll 1$. Consider an (x,y) frame attached to the lower surface at its center. Let u and v be the velocities of the fluid in the x - and y -directions, respectively, and p be the pressure. This can also be considered as a simplified squeeze film damper, by comparing Figures 3.5 and 3.2. At the point of minimum thickness of the oil film in Figure 3.2, the oil flow divides, and the oil flows in two opposing directions. This is very similar to the squeeze flow of

Figure 3.5. As the plate moves downwards, it squeezes the oil, which divides and flows in two opposing directions. Thus, the squeeze flow can be considered as a simplified model of the squeeze film damper. This becomes clearer if we compare Figures 3.5 and 2.2. The upper flat surface of Figure 3.5 approximates the upper curved surface of the unwrapped SFD of Figure 2.2, but it simplifies the analysis because the flat surface simplifies the boundary conditions and also because it moves vertically only, while the upper curved surface of Figure 2.2 moves both vertically and horizontally.

Here also the inertialess solution is presented first, followed by the full inertial solution. In classical lubrication theory fluid inertia is neglected. The momentum equation in the x- direction becomes

$$\mu \frac{d^2 u}{dy^2} - \frac{dp}{dx} = 0 \quad (3.22)$$

where μ is the viscosity of the fluid. The momentum equation in the y-direction reduces to

$$\frac{dp}{dy} = 0$$

Thus, the pressure is independent of y, and also the pressure gradient dp/dx is independent of y. Integrating equation (3.22) twice with respect to y, with the boundary conditions

$$u = 0 \quad \text{at} \quad y = 0 \quad (3.23)$$

$$u = 0 \quad \text{at} \quad y = h$$

we get for the velocity u

$$u = -\frac{h^2}{2\mu} \frac{dp}{dx} \left(\frac{y}{h} - \frac{y^2}{h^2} \right) \quad (3.24)$$

Notice that h is varying with time.

The continuity equation for a two dimensional flow is

$$\frac{\partial u}{\partial x} + \frac{\partial v}{\partial y} = 0 \quad (3.25)$$

Integrating the continuity equation over y

$$v = - \int \frac{\partial u}{\partial x} dy + C$$

where $C=C(x)$ is yet to be determined. Substituting for u from (3.24) we get

$$v = \frac{h^2}{2\mu} \frac{d^2 p}{dx^2} \left(\frac{y^2}{2h} - \frac{y^3}{3h^2} \right) + C \quad (3.26)$$

The boundary conditions that (3.26) have to satisfy are

$$\text{at } y = 0 \quad v = 0 \quad (3.27)$$

and at $y = h \quad v = dh/dt = \dot{h}$

The first boundary condition implies that $C = 0$, while the second gives us the following equation that the pressure has to satisfy

$$\frac{d^2 p}{dx^2} = 12 \frac{\mu}{h^3} \dot{h}$$

Integrating twice with respect to x , with the boundary conditions

$$\text{at } x = \pm L/2, \quad p = 0$$

assuming atmospheric pressure on the sides, the pressure becomes

$$p = -6 \frac{\mu}{h^3} \left[\frac{L^2}{4} - x^2 \right] \dot{h} \quad (3.28)$$

and the force F is

$$F = b \int_{-L/2}^{L/2} p dx = - \frac{\mu b L^3}{h^3} \dot{h} \quad (3.29)$$

and from equation (3.24) the velocity u becomes

$$u = -6 \frac{x}{h} \left(\frac{y}{h} - \frac{y^2}{h^2} \right) \dot{h} \quad (3.30)$$

Notice that the velocity profile u for Squeeze flow is parabolic as that of the Poiseuille flow due to squeeze motion, equation (3.7).

To include the fluid inertia effects, the momentum equation in the x -direction becomes

$$\frac{\partial u}{\partial t} + u \frac{\partial u}{\partial x} + v \frac{\partial u}{\partial y} = - \frac{1}{\rho} \frac{\partial p}{\partial x} + \nu \frac{\partial^2 u}{\partial y^2}$$

where ρ is the density of the fluid and ν is its kinematic viscosity. For a sinusoidal motion with a small amplitude, h has the form

$$h = c - e \cos \omega t$$

or in complex form

$$h = (c - e e^{i\omega t})$$

where c is the mean distance and e is the amplitude of the sinusoidal motion, and $e/c \ll 1$, and thus $\dot{h} = V_0 e^{i\omega t}$, where $V_0 = -i \omega e$. For these conditions Tichy and Modest [95] show that the convective acceleration terms can be neglected and the momentum equation can be reduced to

$$\frac{\partial u}{\partial t} = -\frac{1}{\rho} \frac{\partial p}{\partial x} + \nu \frac{\partial^2 u}{\partial y^2} \quad (3.31)$$

which is a linear equation. If we assume $u = U e^{i\omega t}$, $p = P e^{i\omega t}$ and $v = V e^{i\omega t}$, equation (3.31) becomes

$$i \omega U = -\frac{1}{\rho} \frac{dP}{dx} + \nu \frac{d^2 U}{dy^2} \quad (3.32)$$

where dP/dx is still independent of y . The boundary conditions that equation (3.32) has to satisfy are given by (3.23) and (3.27). We cannot satisfy the boundary conditions (3.23), (3.27) and still use the conventional techniques for solving linear differential equations, because h is time dependent. But we can satisfy these boundary conditions "on the average", by replacing h by its average value c , and we can still use these conventional techniques. Thus, U becomes

$$U = -\frac{i}{\omega \rho} \frac{dP}{dx} \frac{\sinh(sy) - \sinh(s(y-c)) - \sinh(sc)}{\sinh(sc)} \quad (3.33)$$

where s and Re are the same as those of the Poiseuille flow. It can be shown that as $Re \rightarrow 0$, equation (3.33) reduces to equation (3.24) of the inertialess solution with h replaced by c . Following the same procedure as in the inertialess case, we substitute (3.33) into the continuity equation (3.25) and integrate over y , to get

$$V = \frac{i}{\omega \rho} \frac{d^2 P}{dx^2} \frac{[\cosh(sy) - \cosh(s(y-c)) - sy \sinh(sc)]}{s \sinh(sc)} + C$$

where $C=C(x)$ is yet to be determined. The first boundary condition in (3.27) implies that

$$C = -\frac{i}{\omega \rho} \frac{d^2 P}{dx^2} \frac{[1 - \cosh(sc)]}{s \sinh(sc)}$$

while the second boundary condition in (3.27) when satisfied at the average position $y = c$ implies that

$$\frac{d^2 P}{dx^2} = \frac{i V_0 \omega \rho s \sinh(sc)}{[2 - 2 \cosh(sc) + sc \sinh(sc)]}$$

Integrating twice with respect to x with the boundary conditions

at $x = \pm L/2$, $p = 0$, then

$$P = -\frac{1}{2} \frac{i V_0 \omega \rho s \sinh(sc)}{[2 - 2 \cosh(sc) + sc \sinh(sc)]} \left[\frac{L^2}{4} - x^2 \right] \quad (3.34)$$

and the force acting on the surface is

$$F = b \int_{-\frac{L}{2}}^{\frac{L}{2}} p \, dx$$

Therefore the non-dimensional force

$$F^* = \frac{F c^3}{V_0 \mu b L^3} \quad (3.35)$$

becomes

$$F^* = -\frac{i \operatorname{Re} sc \sinh(sc)}{12 [2 - 2 \cosh(sc) + sc \sinh(sc)]} \quad (3.36)$$

As $\operatorname{Re} \rightarrow 0$, F^* reduces to

$$\lim_{\operatorname{Re} \rightarrow 0} F^* = -[1 + i 0.1 \operatorname{Re}] \quad (3.37)$$

which shows that real part of F^* reduces to that predicted by the inertialess solution equation (3.29) (if h is replaced by c). The real and imaginary parts of F^* from equation (3.36) are plotted on Figure 3.6 versus Re . It can be seen that the inertia force (imaginary part of F^*) is equal in magnitude to the viscous force (real part of F^*) at $\operatorname{Re} = 10$, and is larger thereafter. Also shown are the results for the inertialess solution equation (3.29) and the inertia force predicted by the kinetic coenergy method, which will be shown to coincide

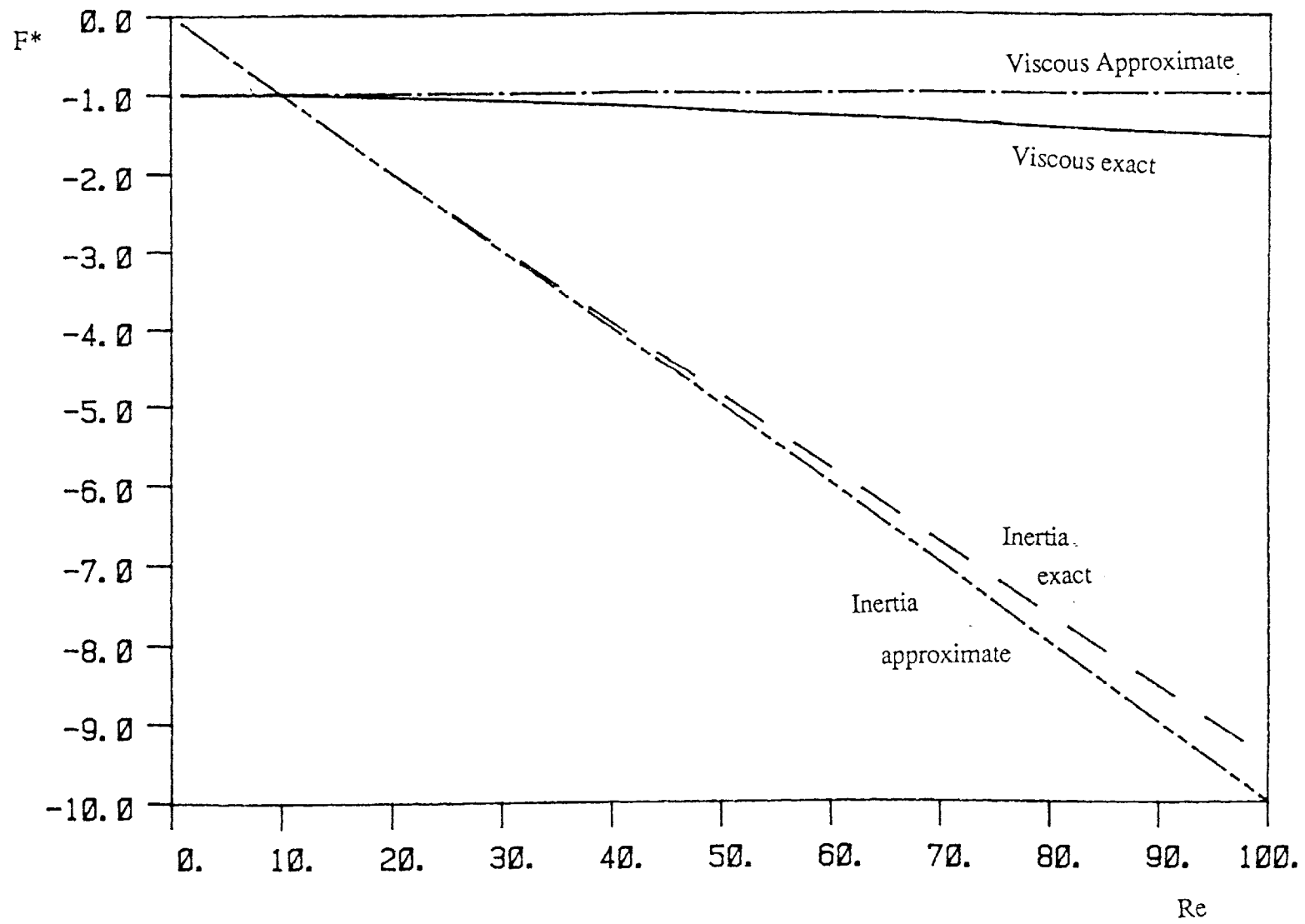


Figure 3.6 Nondimensional forces acting on moving surface in Squeeze flow

with the imaginary part of equation (3.37). These results are in close agreement with the full solution for Re in the range of application of squeeze film dampers.

It should be noted that the total force F_s acting on the surface is the real part of $F^* e^{i\omega t}$, that is, from equation (3.37), the force acting on the block as $Re \rightarrow 0$, is given by

$$F_s = - \frac{\mu b L^3}{c^3} [0.1 Re \cos \omega t + \sin \omega t] e \omega \quad (3.38)$$

or as a function of the moving surface velocity and acceleration

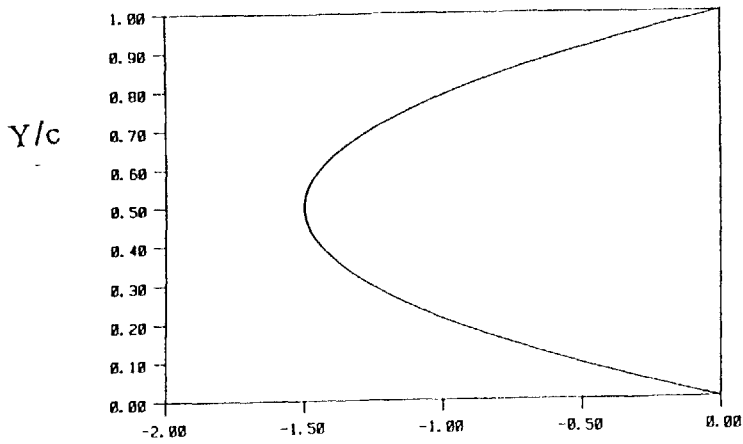
$$F_s = - \frac{\rho b L^3}{10} \left[\frac{\dot{h}}{c} + \frac{10 \nu}{c^3} \ddot{h} \right]$$

It is worth mentioning that the force predicted in the Poiseuille flow problem is 6 D/L times greater than that of the Squeeze flow (if we take L and c to be the same for each case). If D=L, then the force in the Poiseuille flow problem, would be 6 times larger than that of the Squeeze flow problem. This is because in the Poiseuille flow case all the fluid in the clearances is trying to resist the motion in the same way, while in the case of the Squeeze flow the fluid on the sides is resisting the motion harder than the fluid in the middle. Also, as a consequence, the added mass in the Poiseuille flow case is 6 times the added mass in the Squeeze flow case.

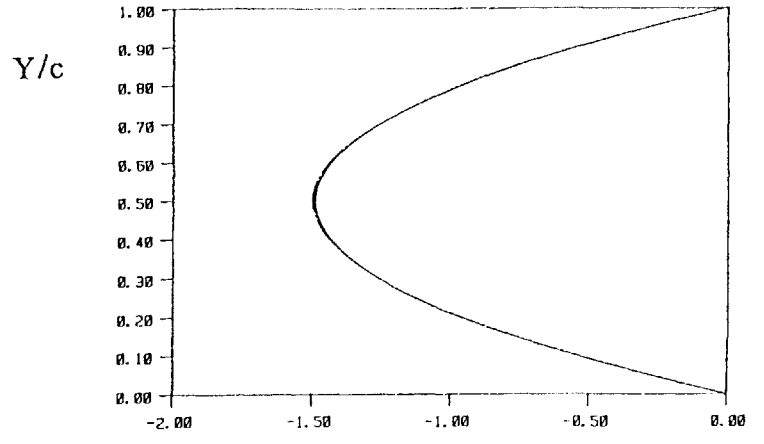
3.4 Kinetic coenergy method applied to Squeeze flow

In Figure 3.7, the velocity profiles of the inertialess solution, equation (3.30), and that of the full solution obtained from equation (3.33) are plotted for Re=1, 10, 30, 100, and $x/h = 1$. It can be seen that the profiles match, nearly identically, for small Re. The kinetic coenergy method is based on the assumption that fluid inertia does not change the velocity profile much.

Re=1.0



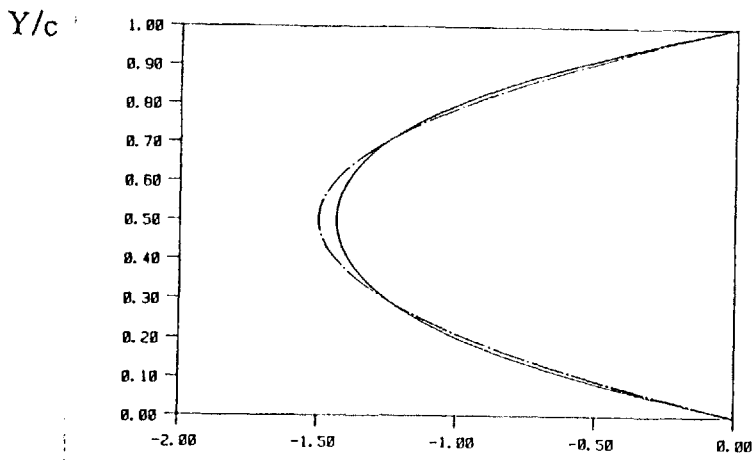
Re=10.0



V/V_0

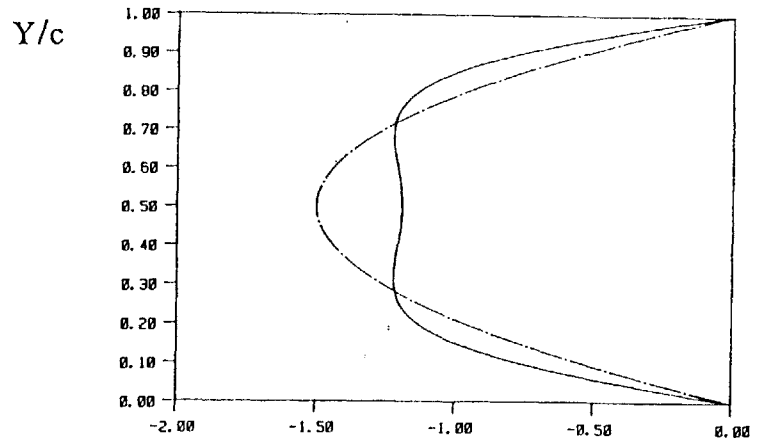
V/V_0

Re=30.0



V/V_0

Re=100.0



V/V_0

Figure 3.7 Velocity profiles for Squeeze flow for $x/h=1$

The kinetic coenergy stored in the fluid is

$$T^* = \frac{1}{2} \int u^2 dm$$

where $dm = \rho b dx dy$ is an infinitesimal mass of the fluid, thus

$$T^* = \frac{1}{2} \rho b \int_0^h \int_{-\frac{L}{2}}^{\frac{L}{2}} u^2 dx dy$$

and if we assume that u is given by the inertialess solution, equation (3.30), then

$$T^* = \frac{1}{2} \left[0.1 \frac{\rho b L^3}{h} \right] \dot{h}^2 \quad (3.39)$$

Equation (3.39) represents the kinetic coenergy stored in the fluid, but it is only a function of the position and velocity of the surface h and \dot{h} , respectively. The quantity between the brackets represents the "added mass" to the surface, that is we are representing the fluid particles with a point mass located at the center of the surface. Thus, here also, we can obtain the forces acting on the surface due to fluid inertia by calculating the inertia force due to the point mass. If we take the velocity of the surface \dot{h} as our generalized velocity, then the generalized momentum in the direction of \dot{h} is given by

$$\frac{\partial T^*}{\partial \dot{h}} = \left(0.1 \frac{\rho b L^3}{h} \right) \dot{h} \quad (3.40)$$

Note that this generalized momentum acts in the perpendicular direction to the fluid velocity. In obtaining the full solution, we were not able to satisfy the boundary conditions (3.23), (3.27) as discussed earlier, and we had to replace h by its mean value c . To be able to compare the approximate solution with the full solution, replace h by c in equation (3.40). This is an approximation for small $\epsilon=e/c$. Thus in this case, we can neglect the effect of the kinetic energy of the fluid particles that leave the system. Using Lagrange's equation of motion, we find that the inertia force is given by

$$F_i = - \frac{d}{dt} \left(\frac{\partial T^*}{\partial \dot{h}} \right) + \frac{\partial T^*}{\partial h} = - \left(0.1 \frac{\rho b L^3}{c} \right) \dot{h}$$

For $\dot{h} = e \omega \sin \omega t$, then $\ddot{h} = e \omega^2 \cos \omega t$ and

$$F_i = - \left(0.1 \frac{\rho b L^3}{c} \right) e \omega^2 \cos \omega t \quad (3.41)$$

which is exactly the same as that predicted by equation (3.38). This result is plotted in Figure 3.6 (in complex form) and it can be seen that we obtain excellent agreement with the imaginary part of equation (3.36), especially at values of Re less than 50. Thus one may conclude that the approximate kinetic coenergy method gives a reliable prediction of the inertia force.

If we retain h in equation (3.39), then using Lagrange's equations the inertia force becomes

$$F_i = - \frac{d}{dt} \left(\frac{\partial T^*}{\partial \dot{h}} \right) + \frac{\partial T^*}{\partial h} = - (0.1 \rho b L^3) \left[\frac{\dot{h}}{h} - \frac{1}{2} \frac{\dot{h}^2}{h^2} \right] \quad (3.42)$$

but in this case it is necessary to consider the effect of the kinetic energy that leaves or enters the control volume, which is defined to be the volume between the two surfaces. One possible approach is to use the transformation between a system of fixed identity and a control volume with fixed boundaries[102]. This transformation for any extensive property of the fluid N , is given by [102]

$$\frac{DN}{Dt} = \frac{d}{dt} \int_{cv} \rho \eta dV + \int_{cs} \eta \rho \mathbf{V} \cdot \hat{\mathbf{n}} dS \quad (3.43)$$

where η is the extensive property per unit mass, V is the volume of the control volume, S is the area of the control surface, \mathbf{V} is the vector velocity distribution on the control surface, and $\hat{\mathbf{n}}$ is the unit normal on the control surface. The first term on the right hand side of the above equation represents the rate of change of the extensive property within the control volume, and the second term on the right hand side of the above equation represents the flux of the extensive property through the control surface. If we consider our extensive property to be the inertia force predicted by Lagrange's equations, and defining t^* to be the kinetic coenergy per unit volume within the control volume, such that

$$T^* = \int_{cv} t^* dV \quad (3.44)$$

then applying equation (3.43), we get

$$F_{i,j} = \left[-\frac{d}{dt} \left(\frac{\partial T^*}{\partial \xi_j} \right) + \frac{\partial T^*}{\partial \xi_j} \right] - \left[\int_{cs} \frac{\partial t^*}{\partial \xi_j} \mathbf{V} \cdot \hat{\mathbf{n}} \, dS + \int_{cs} t^* \frac{\partial (\mathbf{V} \cdot \hat{\mathbf{n}})}{\partial \xi_j} \, dS \right] \quad (3.45)$$

where ξ_j is our generalized coordinate. The first term on the right hand side of the above equation represents the inertia force within the control volume, and the second term on the right hand side of the above equation represents the inertia force due to flux of the kinetic coenergy through the control surface.

Evaluating the terms in equation (3.45), using h as our generalized coordinate, we get

$$F_i = - (0.1 \rho b L^3) \left[\frac{\ddot{h}}{h} - \frac{17}{7} \frac{\dot{h}^2}{h^2} \right] \quad (3.46)$$

which is the inertia force, including the effect of the flux of kinetic energy through the control surface.

Another approach to obtain the full inertia force is to perform an energy balance on our system. Thus the rate of work done by the inertia force is equal to the rate of change of kinetic energy within the control volume plus the flux of energy crossing the control surface. For this system the kinetic energy T is equal to the kinetic coenergy T^* (see appendix), and we can write the following:

$$\text{Rate of work done by the inertia force} = - F_i \dot{h}$$

$$\text{Rate of change of kinetic energy within the control volume} = \partial T / \partial t$$

$$\text{Flux of energy crossing the control surface} = 2 \int_0^h \frac{1}{2} \rho u_{L/2}^2 b u_{L/2} \, dy$$

where $u_{L/2}$ is the velocity distribution at $x=L/2$.

Thus

$$- F_i \dot{h} = \frac{\partial T}{\partial t} + 2 \int_0^h \frac{1}{2} \rho u_{L/2}^2 b u_{L/2} \, dy$$

or

$$- F_i \dot{h} = (0.1 \rho b L^3) \left[\frac{\ddot{h}}{h} - \frac{1}{2} \frac{\dot{h}^2}{h^2} \right] \dot{h} - \frac{27}{140} \rho b L^3 \frac{\dot{h}^2}{h^2} \dot{h} \quad (3.47)$$

Therefore

$$F_i = - (0.1 \rho b L^3) \left[\frac{\ddot{h}}{h} - \frac{17}{7} \frac{\dot{h}^2}{h^2} \right] \quad (3.48)$$

which is the final form for the inertia force. That is the inertia force of equation (3.42) has to be corrected to take into account the kinetic energy that leaves or enters the control volume, to arrive at the inertia force of equation (3.48). But it is instructive to see the process of obtaining the inertia force. It can be seen from equation (3.47) that the rate of work done by the inertia force obtained by Lagrange's equations, equation (3.42), is equal to the negative of the rate of change of kinetic energy within the control volume $\partial T/\partial t$. Thus the correction to the inertia force predicted by Lagrange's equations can be obtained only by considering that the rate of work done by this correction to the inertia force is equal to the flux of energy crossing the control surface. It should be noted that the inertia forces predicted by equation (3.46) and equation (3.48) are the same.

Perhaps it would be a good idea to summarize the procedure for obtaining the inertia force, for systems that lose kinetic energy through the flux of particles crossing the control surface. First define the control surface and the generalized coordinates for the system. Next calculate the kinetic coenergy for the fluid within the control surface, then use Lagrange's equations to predict (part of) the inertia force. A correction to this inertia force can be obtained by considering that the rate of work done by this correction to the inertia force is equal to the flux of energy crossing the control surface. This approach is valid only for a single component of inertia force, for a multi component inertia force we should use the first approach in the last step, that is we should use the transformation between a system of fixed identity and a control volume with fixed boundaries.

For $\ddot{h} = e \omega^2 \cos \omega t$, $\dot{h} = e \omega \sin \omega t$ and $h = c - e \cos \omega t$, then (3.48) becomes

$$F_i = - \frac{\rho b L^3}{10 c} \left[\frac{\cos \omega t}{(1 - \epsilon \cos \omega t)} - \frac{17}{7} \frac{\epsilon \sin^2 \omega t}{(1 - \epsilon \cos \omega t)^2} \right] e \omega^2 \quad (3.49)$$

where $\varepsilon = e/c$.

In order to be able to compare the inertia forces predicted by equations (3.49) and (3.38), let us first recall the assumptions upon which each is based. Equation (3.38) represents the force obtained from the solution of the differential equations governing the fluid flow, and assuming

- a) $\varepsilon = e/c \ll 1$,
- b) convective acceleration is neglected,
- c) the boundary conditions at the moving boundary are satisfied at an average position.

While equation (3.49) represents the inertia force calculated from the kinetic coenergy of the fluid assuming that the velocity profiles predicted by the classical lubrication theory are a good enough approximation, even with the presence of fluid inertia. The restrictions a) and c) above are not assumed.

Because of the assumptions made in obtaining equation (3.38) (outlined above), the effects of convective acceleration and the moving boundary cannot be estimated from this kind of formal solution of the differential equations of motion using the techniques of linear theory.

On the other hand, the kinetic coenergy method should, in principle, be able to determine the effects of convective acceleration on the total inertia force as well as the temporal acceleration. Comparing equations (3.38) and (3.41) it is clear that the kinetic coenergy method determines the effects of temporal acceleration quite accurately. But this was done by adding the restriction that h is replaced by c . Leaving in h , as was done in obtaining (3.49), should at least account for the time varying nature of the boundary conditions.

The first term inside the brackets in equation (3.49), as $\epsilon \rightarrow 0$, is the same as the inertia force predicted by equation (3.38), so it may be considered to be a correction to equation (3.38) for large ϵ . The second term inside the brackets in equation (3.49) is of the same order of magnitude as the first term if ϵ is large, but can be neglected for small ϵ . This second term is not present at all in equation (3.38). In the next section we are going to show that this term is due to the combined effect of the moving boundary and convective acceleration.

3.5 Convective acceleration and moving boundary

An alternative approximation to the solution of the Squeeze flow problem that will enable us to estimate the effects of convective acceleration and the moving boundary is described below. An assumed velocity profile is inserted into the momentum equations which are then integrated to obtain the forces. Let us consider the full x-momentum equation

$$\frac{\partial u}{\partial t} + u \frac{\partial u}{\partial x} + v \frac{\partial u}{\partial y} = -\frac{1}{\rho} \frac{\partial p}{\partial x} + \nu \frac{\partial^2 u}{\partial y^2} \quad (3.50)$$

while the y-momentum still implies that the pressure gradient $\partial p / \partial x$ is independent of y.

Also the continuity equation is still

$$\frac{\partial u}{\partial x} + \frac{\partial v}{\partial y} = 0 \quad (3.51)$$

Let us assume that the x and y dependence of the u velocity is similar to that of the classical lubrication theory. That is let

$$u = U(x, y) \left(1 - \frac{y}{h} \right) \quad (3.52)$$

where U is a still undetermined function of time. This assumption will facilitate the solution of the problem.

Substituting (3.52) in the continuity equation (3.51) and integrating over y from 0 to h , we get

$$U \int_0^h y \left(1 - \frac{y}{h} \right) dy + \dot{h} = 0$$

from which we can determine U to be

$$U = - \frac{6}{h^2} \dot{h}$$

and substituting in (3.52), u becomes

$$u = - \frac{6}{h^2} \dot{h} x y \left(1 - \frac{y}{h} \right) \quad (3.53)$$

Substituting (3.53) into the continuity equation (3.51) and integrating over y , we find that

$$v = \frac{6}{h^2} \dot{h} \left(\frac{y^2}{2} - \frac{y^3}{3h} \right) + C$$

where $C=C(x,t)$ is yet to be determined. The above equation has to satisfy the following boundary conditions

$$\text{at } y = 0 \quad v = 0$$

$$\text{and at } y = h \quad v = \dot{h}$$

we find that a value of $C = 0$ satisfies both boundary conditions, thus v becomes

$$v = \frac{6}{h^2} \dot{h} \left(\frac{y^2}{2} - \frac{y^3}{3h} \right) \quad (3.54)$$

Integrating the x -momentum equation (3.50) over y from 0 to h and substituting for u and v from equations (3.53) and (3.54) respectively, we get

$$\frac{\partial p}{\partial x} = \rho x \left[\frac{1}{h} \ddot{h} - \frac{2.4}{h^2} \dot{h}^2 + \frac{12 v}{h^3} \dot{h} \right]$$

The above equation can be integrated over x , with the boundary conditions

$$p = 0 \quad \text{at } x = \pm L/2$$

Thus

$$p = \frac{\rho}{2} \left[\frac{1}{h} \ddot{h} - \frac{2.4}{h^2} \dot{h}^2 + \frac{12 v}{h^3} \dot{h} \right] \left(x^2 - \frac{L^2}{4} \right)$$

The force F acting on the surfaces is

$$\begin{aligned}
F &= b \int_{-\frac{L}{2}}^{\frac{L}{2}} p \, dx \\
&= -\frac{\rho b L^3}{12} \left[\frac{1}{h} \dot{h} - \frac{2.4}{h^2} \dot{h}^2 + \frac{12 v}{h^3} \dot{h} \right] \quad (3.55)
\end{aligned}$$

If we let $h = c - \epsilon \cos \omega t$, then F becomes

$$F = -\frac{\mu b L^3}{c^3} \left[\frac{\sin \omega t}{(1 - \epsilon \cos \omega t)^3} + \frac{Re}{12} \frac{\cos \omega t}{(1 - \epsilon \cos \omega t)} - \frac{2.4 Re}{12} \frac{\epsilon \sin^2 \omega t}{(1 - \epsilon \cos \omega t)^2} \right] \quad (3.56)$$

where Re is given by equation (3.13).

Equation (3.56) represents the force acting on the moving surface, including the effects of the moving boundary. The first term represents the contribution of the viscous force, the second term is the force due to temporal acceleration, and the third term is the force due to convective acceleration. The $(1 - \epsilon \cos \omega t)$ terms in the denominators of each of these three terms represent the effect of the moving boundary. The denominators all tend to a value of 1 as the amplitude of oscillations tends to zero.

Comparing equation (3.56) with equation (3.38), we find that, apart from the effect of the moving boundary described in the previous paragraph, the viscous terms are the same (which are also the same as the viscous force predicted by the classical lubrication theory solution, equation (3.29)), and the terms due to temporal acceleration differ only by a factor of 1.2. This is because we assumed that the velocity profile, equation (3.52), is that of the classical lubrication theory, and thus the effect of larger Reynolds numbers is not taken into account. Equation (3.38) does not contain the term due to convective acceleration present in equation (3.56) as it was neglected.

Comparing equation (3.56) with the kinetic coenergy method result equation (3.49), we find that both the temporal and convective acceleration terms differ

approximately by a factor of 1.2, (the $17/7$ term in (3.49) is equal to 2.43 versus 2.4 in (3.52)). In fact the difference between (3.49) and (3.56) is 16.67% in temporal acceleration terms, and 17.65% in convective acceleration terms. Now we have to keep in mind that both of the techniques that led to equations (3.49) and (3.56) are approximate, thus these differences should be expected, and we cannot determine if one of them is more accurate, but one can say that both techniques account for the convective acceleration terms and they both show the nature of the effect of convective acceleration on the inertia force approximately.

It was shown earlier that the temporal acceleration term predicted by the kinetic coenergy method is the limit as $Re \rightarrow 0$ of the temporal inertia force acting on the surfaces, in the case that $\epsilon \ll 1$, and it was also shown that this limit is quite accurate for Re up to about 50. This seems to give the inertia force predicted by the kinetic coenergy, equation (3.49), an edge over that predicted by equation (3.56), since equation (3.56) will not predict the temporal acceleration term correctly (there is a factor of 1.2) as $\epsilon \ll 1$.

Thus it may be concluded that the kinetic coenergy method is capable of finding the forces due to the inertia of the fluid, due to both temporal and convective accelerations, rather simply and accurately.

Chapter 4

Fluid Inertia Forces In Squeeze Film Dampers

In the previous chapters we introduced the kinetic coenergy method as a simple and effective tool for calculating the fluid inertia forces in squeezing flows. In this chapter we use the kinetic coenergy method to calculate the inertia coefficients of squeeze film dampers. Both the long and short bearing approximations are considered.

The fluid inertia forces acting on the journal for both the long and the short dampers are calculated by using Lagrange's equations, which should be supplemented to account for the effects of the fluid particles that leave (and enter) the control surface carrying kinetic energy.

Finally, the fluid inertia forces are calculated by solving the governing equations for a squeeze film damper executing a small circular centered whirl. It is shown that in this case, the kinetic coenergy method correctly predicts the fluid inertia forces.

4.1 Inertia coefficients for short dampers

The kinetic coenergy of the fluid was defined in chapter 2 as

$$T^* = \frac{1}{2} \int_V \rho (u^2 + v^2 + w^2) dV \quad (2.35)$$

where V is the volume of the fluid in the damper. Thus to calculate the kinetic coenergy we have to know the velocities of the fluid. But since we do not know the velocities of the

fluid beforehand, we are going to assume that the velocity profiles predicted by the classical lubrication theory are a good approximation of the actual velocity profiles, even at relatively high Reynolds numbers, as we did in the previous chapter.

For dampers described by the short bearing approximation, the circumferential (u) and radial (v) velocity profiles are $O(c/R)$ smaller than the axial (w) velocity profile, thus u and v can be neglected with respect to w, and the kinetic coenergy becomes

$$T^* = \frac{1}{2} \int_{\theta_1}^{\theta_2} \int_0^h \int_{-\frac{L}{2}}^{\frac{L}{2}} \rho w^2 R d\theta dY dZ \quad (4.1)$$

The axial velocity, w, was calculated in chapter 2 to be

$$w = \frac{6z}{h} \left(\frac{Y}{h} - \frac{Y^2}{h^2} \right) (e\dot{\psi} \sin \theta + \dot{e} \cos \theta) \quad (2.11)$$

Substituting in (4.1), and integrating over Y and Z, the kinetic coenergy becomes

$$\begin{aligned} T^* = & \frac{1}{2} \frac{\rho R L^3}{10c} \int_{\theta_1}^{\theta_2} \frac{\cos^2 \theta}{(1 - \epsilon \cos \theta)} d\theta \dot{e}^2 + \frac{1}{2} \frac{\rho R L^3}{10c} \int_{\theta_1}^{\theta_2} \frac{\sin^2 \theta}{(1 - \epsilon \cos \theta)} d\theta (e\dot{\psi})^2 \\ & + \frac{\rho R L^3}{10c} \int_{\theta_1}^{\theta_2} \frac{\sin \theta \cos \theta}{(1 - \epsilon \cos \theta)} d\theta \dot{e} e\dot{\psi} \end{aligned} \quad (4.2)$$

Equation (4.2) can be written in the form

$$T^* = \frac{1}{2} m_{rr} \dot{e}^2 + \frac{1}{2} m_{tt} (e\dot{\psi})^2 + m_{rt} \dot{e} e\dot{\psi} \quad (4.3)$$

where m_{rr} , m_{tt} and m_{rt} represent the inertia coefficients of the short damper and are given by

$$\begin{aligned} m_{rr} &= \frac{\rho R L^3}{10c} \int_{\theta_1}^{\theta_2} \frac{\cos^2 \theta}{(1 - \epsilon \cos \theta)} d\theta \\ m_{tt} &= \frac{\rho R L^3}{10c} \int_{\theta_1}^{\theta_2} \frac{\sin^2 \theta}{(1 - \epsilon \cos \theta)} d\theta \\ m_{rt} &= \frac{\rho R L^3}{10c} \int_{\theta_1}^{\theta_2} \frac{\sin \theta \cos \theta}{(1 - \epsilon \cos \theta)} d\theta \end{aligned}$$

The limits of integration θ_1 and θ_2 represent the extent of the fluid film in the damper. Thus for a full film $\theta_1 = 0$ and $\theta_2 = 2\pi$. For a cavitated damper we are going to assume the π -film theory, which we discussed in chapter 2. Although the π -film theory does not describe accurately the conditions in the damper, we have used it in obtaining the damping coefficients for lack of a better theory. Including inertia in the analysis, we anticipate that the extent of the positive pressure in the film should be different from π , yet because we do not fully understand cavitation, and to have results compatible with the damping analysis in chapter 2, we are going to use the π -film theory here also. The discussion in chapter 2 about the limits of integration for the damping coefficients apply here also for the inertia coefficients. Thus for a general motion the inertia coefficients of a π -bearing will depend on the velocity of the journal, as well as its position.

For a π -bearing, with a journal executing a nearly circular counter-clockwise whirl, the limits of integration can be taken to be $\theta_1 = 0$ and $\theta_2 = \pi$, and the coefficients m_{rr} , m_{tt} and m_{rt} take the form

$$m_{rr} = \frac{\rho R L^3}{c} m_{rr}^*, \quad m_{tt} = \frac{\rho R L^3}{c} m_{tt}^*, \quad m_{rt} = \frac{\rho R L^3}{c} m_{rt}^*$$

where

$$m_{rr}^* = \frac{1}{10} \frac{\pi}{\epsilon^2} \left[\frac{1}{(1 - \epsilon^2)^{1/2}} - 1 \right] \quad (4.4)$$

$$m_{tt}^* = \frac{1}{10} \frac{\pi}{\epsilon^2} [1 - (1 - \epsilon^2)^{1/2}] \quad (4.5)$$

$$m_{rt}^* = -\frac{1}{10} \frac{1}{\epsilon} \left[\frac{1}{\epsilon} \log \left(\left| \frac{1 - \epsilon}{1 + \epsilon} \right| \right) + 2 \right] \quad (4.6)$$

These coefficients are plotted in Figure 4.1, versus the eccentricity ratio, from which it can be seen that the inertia coefficients increase with the increase of the radius of the orbit, and m_{rr} and m_{rt} become infinite as ϵ approaches 1. Thus as the journal executes a larger orbit a larger amount of kinetic coenergy is stored in the fluid. For a 2π -bearing the coefficients m_{rr} and m_{tt} are double those for a π -bearing and m_{rt} is zero.

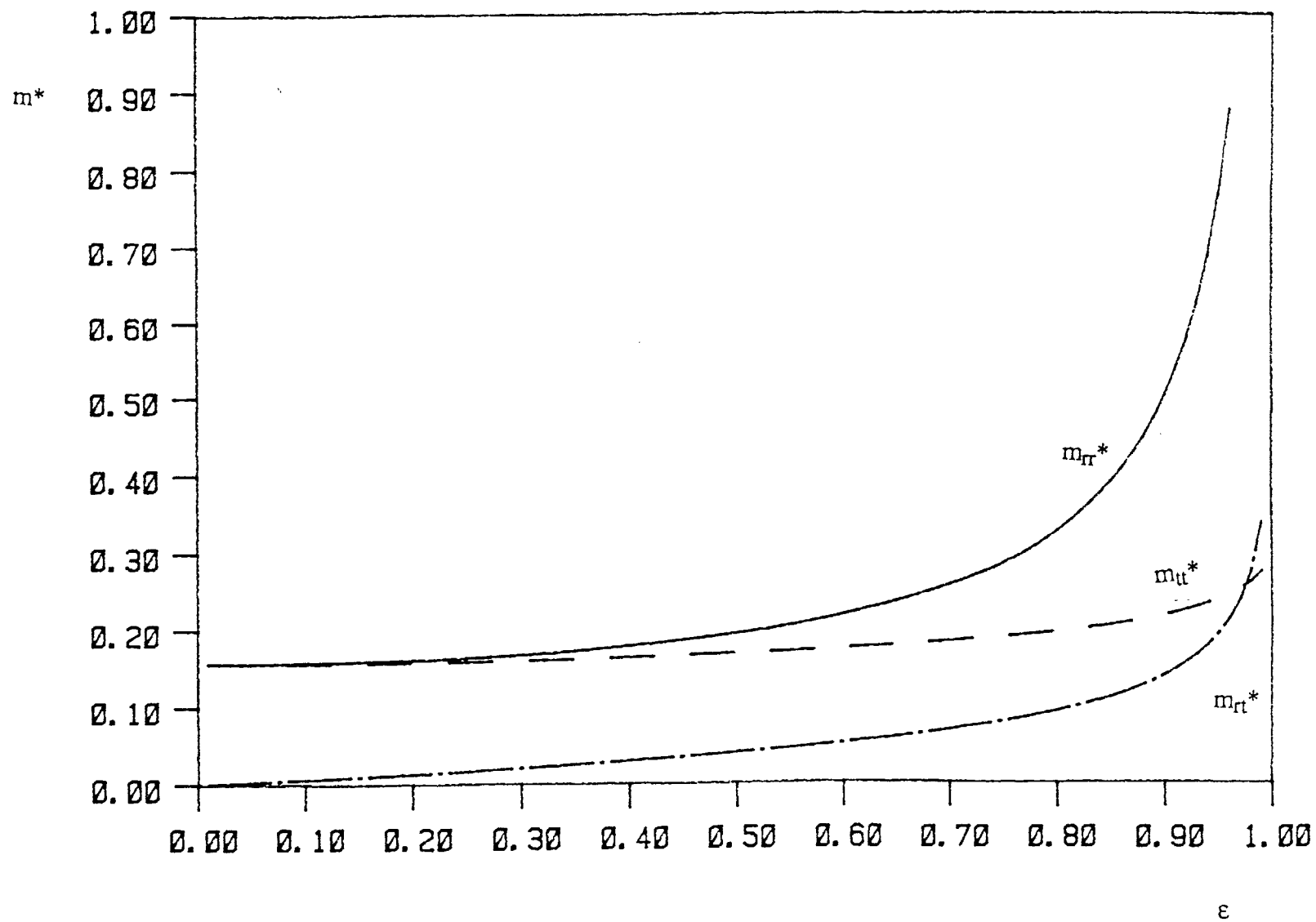


Figure 4.1 Nondimensional inertia coefficients for the short damper

The inertia coefficients m_{rr} , m_{tt} and m_{rt} are quite similar to those obtained by Smith [80]. In fact they are only 20% larger than the coefficients he derived through a heuristic argument [70]. In section 4.4, we are going to show that the inertia coefficients derived here provide the correct inertia forces in some limiting cases.

Equation (4.3) implies that we are modeling the fluid particles by a point tensor mass (whose components are m_{rr} , m_{tt} and m_{rt}) at the center of the journal. This tensor mass represents the inertia coefficients in the control volume which contains the fluid in the damper. To see that the added mass has the characteristics of a tensor, let us calculate the momentum vector \vec{P} of the point mass

$$\vec{P} = p_r \vec{u}_r + p_t \vec{u}_t$$

where p_r and p_t are the radial and tangential components of the momentum vector and \vec{u}_r and \vec{u}_t are unit vectors in the radial and tangential directions respectively, and

$$p_r = \frac{\partial T^*}{\partial \dot{e}} \quad \text{and} \quad p_t = \frac{1}{e} \frac{\partial T^*}{\partial \dot{\psi}}$$

On calculating the above quantities, assuming that m_{rr} , m_{tt} and m_{rt} are velocity independent, we find that

$$\begin{Bmatrix} p_r \\ p_t \end{Bmatrix} = \begin{pmatrix} m_{rr} & m_{rt} \\ m_{rt} & m_{tt} \end{pmatrix} \begin{Bmatrix} \dot{e} \\ e\dot{\psi} \end{Bmatrix}$$

from which it can be seen that the point mass is a tensor relating the momentum vector to the velocity vector. Having a mass tensor representation of a particle implies that the particle has different inertia characteristics in different directions, that is it is non-isotropic. We had seen earlier that the damping characteristics of the damper are non-isotropic too.

4.2 Inertia coefficients for long dampers

For dampers described by the long bearing approximation, the radial (v) and the axial (w) velocity profiles are $O(c/R)$ smaller than the circumferential (u) velocity profile,

thus v and w can be neglected with respect to u , and the kinetic coenergy, equation (2.35) becomes

$$T^* = \frac{1}{2} \int_{\theta_1}^{\theta_2} \int_0^h \int_{-\frac{L}{2}}^{\frac{L}{2}} \rho u^2 R d\theta dY dZ \quad (4.7)$$

The circumferential velocity, u , was calculated in chapter 2 to be

$$u = \frac{6R}{h} \left(\frac{Y}{h} - \frac{Y^2}{h^2} \right) \left[\sin \theta \dot{e} - \cos \theta e \dot{\psi} + \frac{3\epsilon}{(2+\epsilon^2)} e \dot{\psi} \right] \quad (2.25)$$

Substituting in (4.6), and integrating over Y and Z , the kinetic coenergy becomes

$$\begin{aligned} T^* = & \frac{1}{2} \frac{12 \rho R^3 L}{10 c} \int_{\theta_1}^{\theta_2} \frac{\sin^2 \theta}{(1 - \epsilon \cos \theta)} d\theta \dot{e}^2 + \frac{1}{2} \frac{12 \rho R^3 L}{10 c} \int_{\theta_1}^{\theta_2} \frac{\left(\frac{3\epsilon}{2+\epsilon^2} - \cos \theta \right)^2}{(1 - \epsilon \cos \theta)} d\theta (e \dot{\psi})^2 \\ & + \frac{12 \rho R^3 L}{10 c} \int_{\theta_1}^{\theta_2} \frac{\sin \theta \left(\frac{3\epsilon}{2+\epsilon^2} - \cos \theta \right)}{(1 - \epsilon \cos \theta)} d\theta \dot{e} e \dot{\psi} \end{aligned} \quad (4.8)$$

Equation (4.8) can be written in the form of equation (4.3) where in this case m_{rr} , m_{tt} and m_{rt} represent the inertia coefficients of the long damper and are given by

$$\begin{aligned} m_{rr} &= \frac{12 \rho R^3 L}{10 c} \int_{\theta_1}^{\theta_2} \frac{\sin^2 \theta}{(1 - \epsilon \cos \theta)} d\theta \\ m_{tt} &= \frac{12 \rho R^3 L}{10 c} \int_{\theta_1}^{\theta_2} \frac{\left(\frac{3\epsilon}{2+\epsilon^2} - \cos \theta \right)^2}{(1 - \epsilon \cos \theta)} d\theta \\ m_{rt} &= \frac{12 \rho R^3 L}{10 c} \int_{\theta_1}^{\theta_2} \frac{\sin \theta \left(\frac{3\epsilon}{2+\epsilon^2} - \cos \theta \right)}{(1 - \epsilon \cos \theta)} d\theta \end{aligned}$$

As discussed in the previous section, the limits of integration θ_1 and θ_2 represent the extent of the fluid film in the damper. Thus for a full film $\theta_1 = 0$ and $\theta_2 = 2\pi$. For a cavitated damper we are going to use the π -film theory, and in general the limits of integration will depend on the velocity of the journal.

For a π -bearing, with a journal executing a nearly circular counter-clockwise whirl, the limits of integration can be taken to be $\theta_1 = 0$ and $\theta_2 = \pi$, and the coefficients m_{rr} , m_{tt} and m_{rt} take the form

$$m_{rr} = \frac{\rho R^3 L}{c} m_{rr}^*, \quad m_{tt} = \frac{\rho R^3 L}{c} m_{tt}^*, \quad m_{rt} = \frac{\rho R^3 L}{c} m_{rt}^*$$

where

$$m_{rr}^* = \frac{12}{10} \frac{\pi}{\epsilon^2} [1 - (1 - \epsilon^2)^{1/2}] \quad (4.9)$$

$$m_{tt}^* = \frac{12}{10} \left\{ \frac{\pi}{\epsilon^2 (2 + \epsilon^2)} \left[\frac{4(1 - \epsilon^2)^{3/2}}{(2 + \epsilon^2)} + (5\epsilon^2 - 2) \right] \right\} \quad (4.10)$$

$$m_{rt}^* = \frac{12}{10} \left[\frac{2}{\epsilon} + \frac{2(1 - \epsilon^2)}{\epsilon^2 (2 + \epsilon^2)} \log \left(\left| \frac{1 - \epsilon}{1 + \epsilon} \right| \right) \right] \quad (4.11)$$

These coefficients are plotted in Figure 4.2, versus the eccentricity ratio, from which it can be seen that the inertia coefficients increase with the increase of the radius of the orbit. For a 2π -bearing the coefficients m_{rr} and m_{tt} are double those for a π -bearing and m_{rt} is zero.

It should be noted that, unlike for the short damper, the inertia coefficients for the long damper presented here, are different from those of Smith's [80], but the coefficients derived here provide the correct inertia forces in some limiting cases (see section 4.4).

4.3 Fluid inertia forces

In sections 4.1 and 4.2, we have calculated the kinetic coenergy of the fluid as a function of the velocity of the journal. For both the long and short dampers the kinetic coenergy takes the form of equation (4.3) which indicates that the fluid particles are modeled as a tensor mass at the center of the journal.

As discussed in chapter 3, the fluid inertia force consists of two components, one component is due to the inertia of the fluid within the control volume and the other

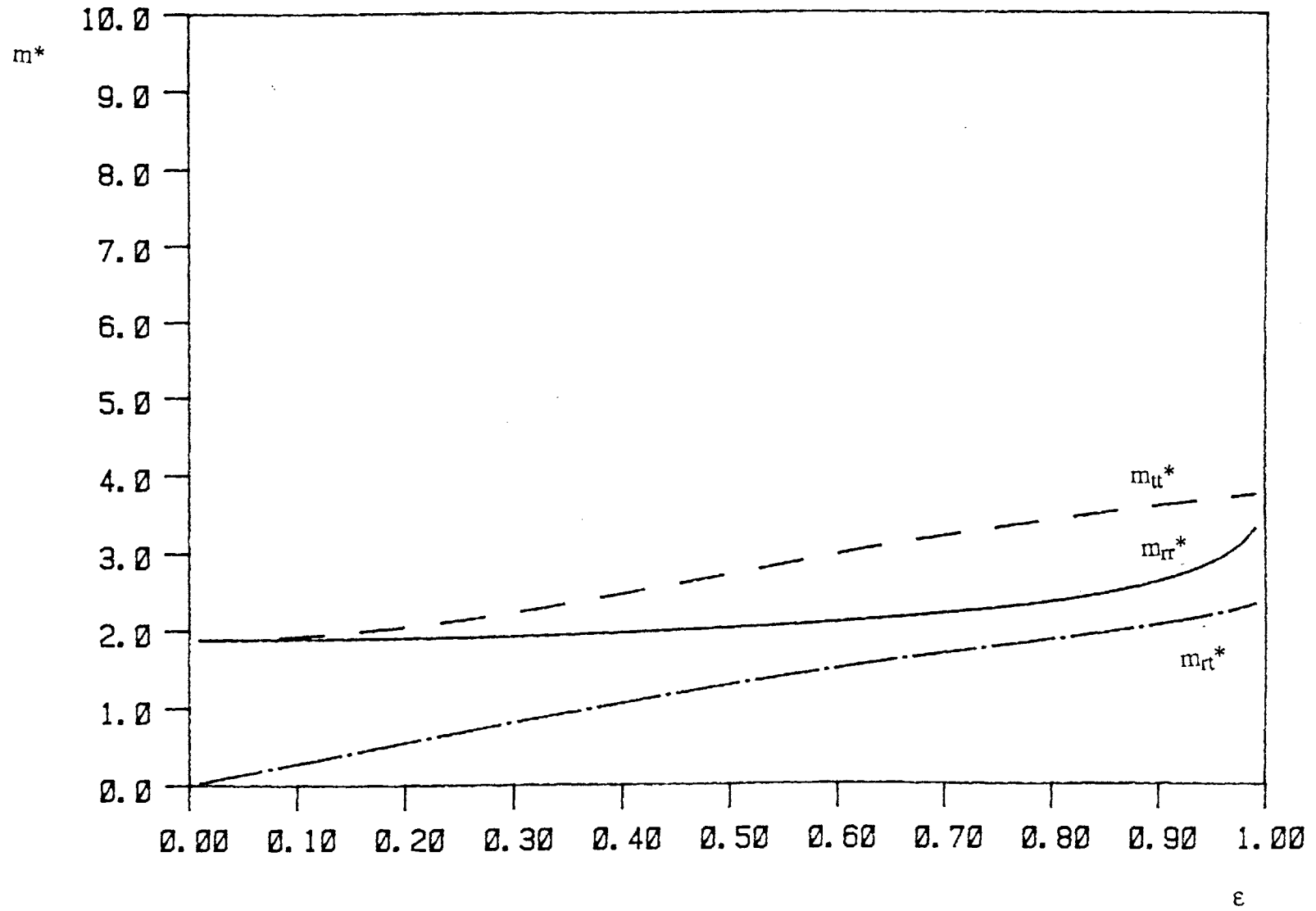


Figure 4.2 Nondimensional inertia coefficients for the long damper

component is due to the flux of the fluid at the control surface. The inertia force predicted by Lagrange's equations is the component due to the inertia of the fluid within the control volume. Thus the fluid inertia forces take the form (see equation (3.45))

$$F_{i,r} = F_{ri} - \int_{cs} \frac{\partial t^*}{\partial \dot{e}} \mathbf{V} \cdot \hat{\mathbf{n}} \, dS + \int_{cs} t^* \frac{\partial(\mathbf{V} \cdot \hat{\mathbf{n}})}{\partial \dot{e}} \, dS \quad (4.12)$$

$$\text{and} \quad F_{i,t} = F_{ti} - \frac{1}{e} \int_{cs} \frac{\partial t^*}{\partial \dot{\psi}} \mathbf{V} \cdot \hat{\mathbf{n}} \, dS + \frac{1}{e} \int_{cs} t^* \frac{\partial(\mathbf{V} \cdot \hat{\mathbf{n}})}{\partial \dot{\psi}} \, dS \quad (4.13)$$

where $F_{i,r}$ is the radial inertia force and $F_{i,t}$ is the tangential inertia force, t^* is the kinetic coenergy per unit volume, \mathbf{V} is the velocity of the fluid with respect to the control surface S , $\hat{\mathbf{n}}$ is the outward normal vector on the control surface, and F_{ri} and F_{ti} are obtained by Lagrange's equations and are given by

$$F_{ri} = - \frac{d}{dt} \left(\frac{\partial T^*}{\partial \dot{e}} \right) + \frac{\partial T^*}{\partial e} \quad (4.14)$$

$$\text{and} \quad F_{ti} = - \frac{1}{e} \frac{d}{dt} \left(\frac{\partial T^*}{\partial \dot{\psi}} \right) + \frac{1}{e} \frac{\partial T^*}{\partial \psi} \quad (4.15)$$

Before calculating the inertia forces, we note that in general cavitation has the effect of making the inertia coefficients depend on velocity as well as position. For uncavitated dampers and for cavitated dampers whose journals execute nearly circular centered whirls, the inertia coefficients are position dependent only. This is the case that we are interested in in this thesis (see chapter 5). Thus we are going to neglect the velocity dependence of the inertia coefficients when we calculate the inertia forces.

First we calculate the components of the inertia forces given by equations (4.14) and (4.15). Thus we get

$$F_{ri} = - m_{rr} \ddot{e} - \frac{1}{2} \left(e \frac{\partial m_{rr}}{\partial e} \right) \frac{\dot{e}^2}{e} - m_{rt} e \ddot{\psi} + \left(m_{tt} + \frac{1}{2} e \frac{\partial m_{tt}}{\partial e} \right) e \dot{\psi}^2 \quad (4.16)$$

$$\text{and} \quad F_{ti} = - m_{rt} \ddot{e} - \left(m_{rt} + e \frac{\partial m_{rt}}{\partial e} \right) \frac{\dot{e}^2}{e} - \left(m_{tt} + \frac{1}{2} e \frac{\partial m_{tt}}{\partial e} \right) 2 \dot{e} \dot{\psi} - m_{tt} e \ddot{\psi} \quad (4.17)$$

Equations (4.16) and (4.17) indicate that the F_{ri} and F_{ti} components of the fluid inertia forces are a function of the accelerations of the journal, namely the radial acceleration \ddot{e} , the

tangential acceleration $e \ddot{\psi}$, the centripetal acceleration $e \dot{\psi}^2$, and the coriolis acceleration $2 \dot{e} \dot{\psi}$, and a radial acceleration \dot{e}^2/e which is not an acceleration of the journal, but the journal "feels" its effects due to the inertia of the fluid. This acceleration requires more investigation, since the techniques we employ here do not give us a clear understanding of its origin.

The quantities $e \frac{\partial m_{\pi}}{\partial e}$, $e \frac{\partial m_{tt}}{\partial e}$, and $e \frac{\partial m_{rt}}{\partial e}$, which are present in equations (4.16) and (4.17) are plotted versus the eccentricity ratio ϵ (in nondimensional form), for a π -bearing, whose journal executes a nearly circular centered whirl, in Figures 4.3 and 4.4 for short and long dampers, respectively. From these plots it can be seen that these quantities are nearly zero up to $\epsilon = 0.1$ and then increase. Thus these quantities can be neglected in the analysis of dynamic systems in which ϵ is relatively small.

To calculate the flux terms in equations (4.12) and (4.13) for the short squeeze film damper, we note that the velocity vector \mathbf{V} depends on the axial velocity profile at $z=L/2$ and $z = -L/2$, termed w_L and w_{-L} respectively. Substituting $z = L/2$ in equation (2.11) for w_L then

$$w_L = \frac{3L}{h} \left(\frac{Y}{h} - \frac{Y^2}{h^2} \right) (\dot{e} \cos\theta + e \dot{\psi} \sin\theta) \quad (4.18)$$

and substituting $z = -L/2$ for w_{-L} then

$$w_{-L} = -\frac{3L}{h} \left(\frac{Y}{h} - \frac{Y^2}{h^2} \right) (\dot{e} \cos\theta + e \dot{\psi} \sin\theta) \quad (4.19)$$

and thus the kinetic coenergy per unit volume at $z=L/2$ and $z=-L/2$, termed t^*_L and t^*_{-L} respectively are given by

$$t^*_L = t^*_{-L} = \frac{9 \rho L^2}{2 h^2} \left(\frac{Y^2}{h^2} - 2 \frac{Y^3}{h^3} + \frac{Y^4}{h^4} \right) (\cos^2\theta \dot{e}^2 + 2 \sin\theta \cos\theta \dot{e} e \dot{\psi} + \sin^2\theta e^2 \dot{\psi}^2) \quad (4.20)$$

The velocity $\mathbf{V} \cdot \hat{n}$ is given by

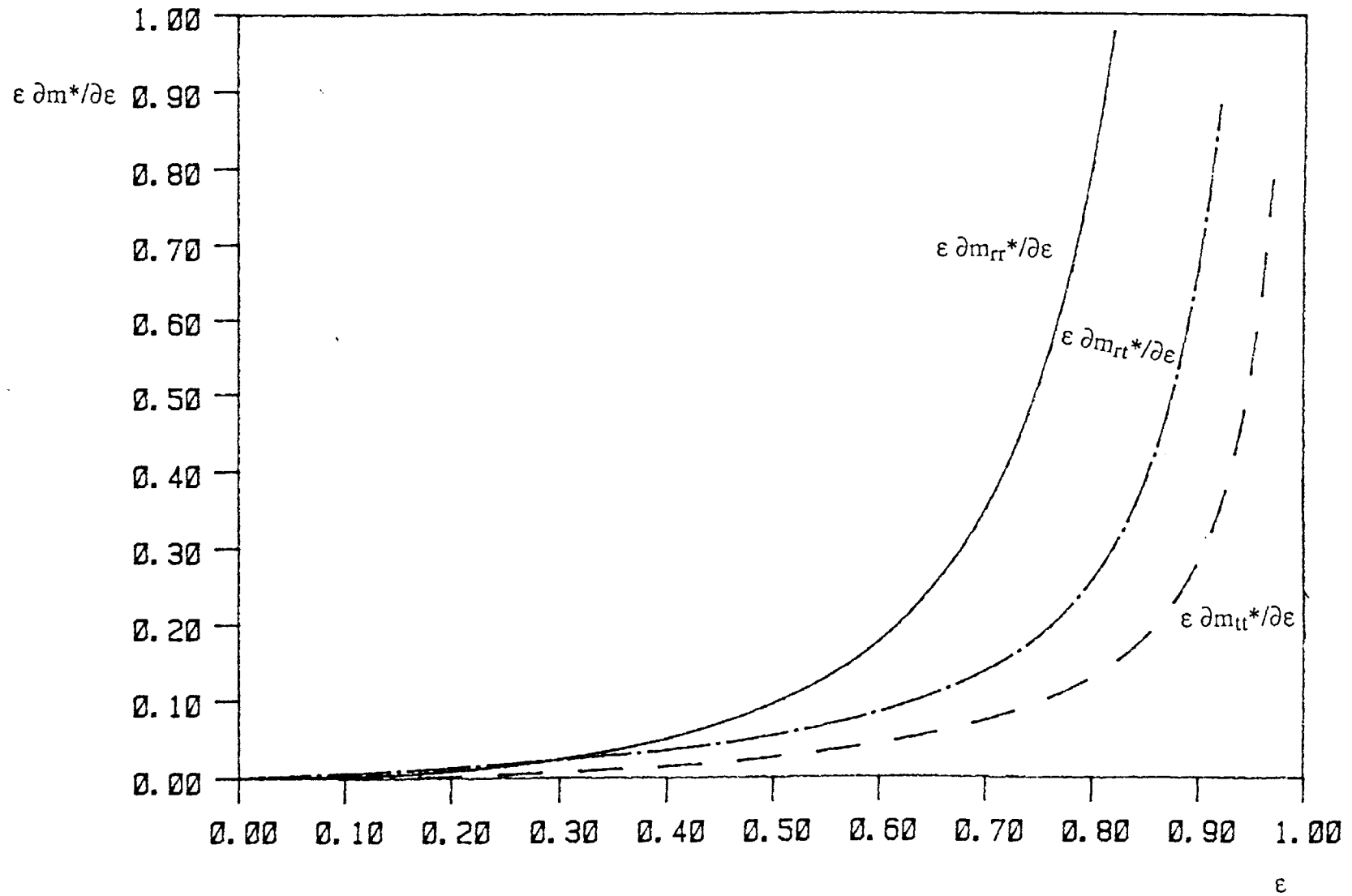


Figure 4.3 Nondimensional terms appearing in equations (4.16) and (4.17); short dampers

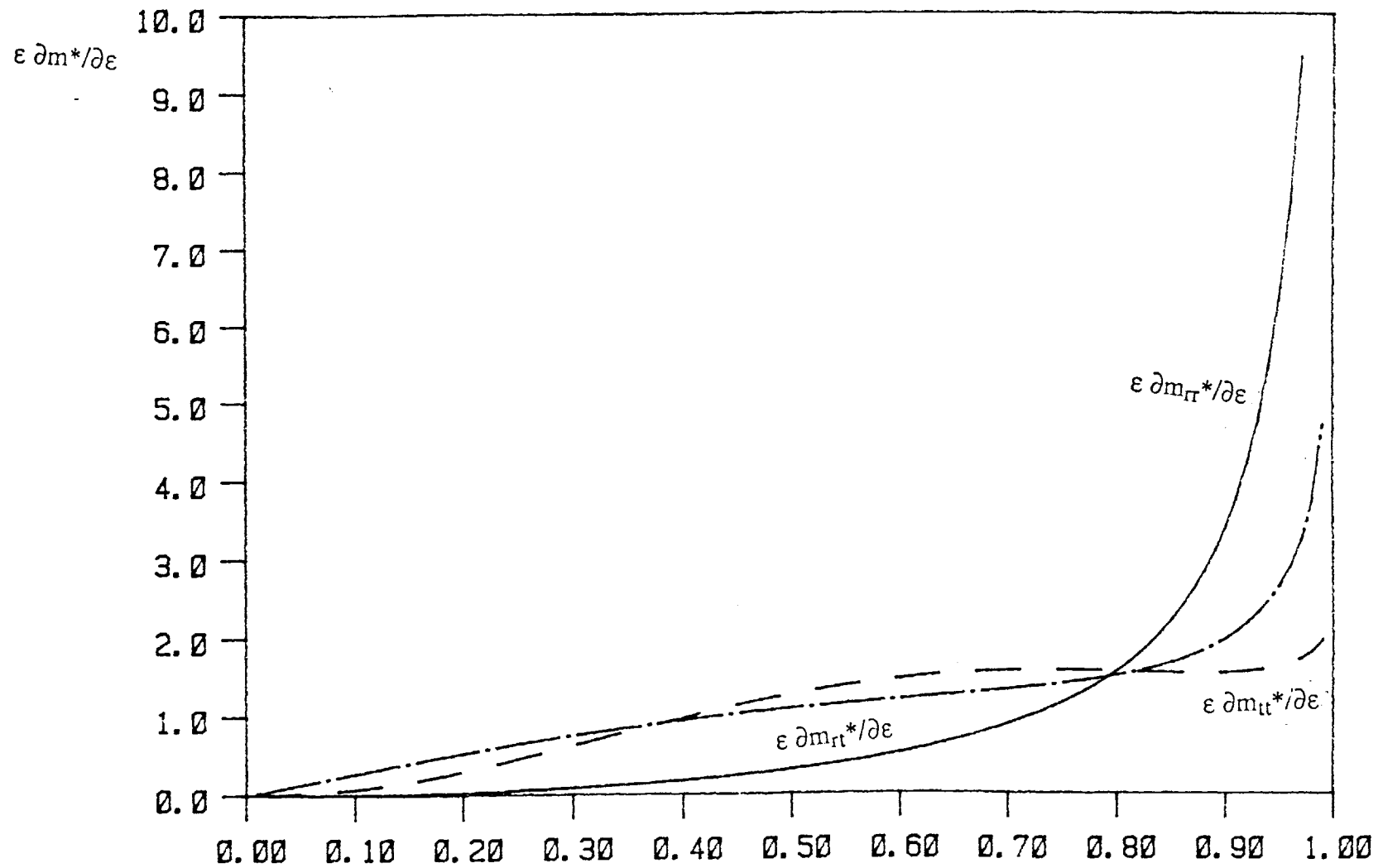


Figure 4.4 Nondimensional terms appearing in equations (4.16) and (4.17); long dampers

ϵ

$$(\mathbf{V} \cdot \hat{\mathbf{n}})_L = \begin{cases} w_L, & \theta_1 = \tan^{-1} \left(\frac{-\dot{e}}{e \dot{\psi}} \right) < \theta < \theta_1 + \pi \\ -w_L, & \theta_1 + \pi < \theta < \theta_1 + 2\pi \end{cases} \quad (4.21)$$

at $z=L/2$

$$(\mathbf{V} \cdot \hat{\mathbf{n}})_{-L} = \begin{cases} -w_{-L}, & \theta_1 = \tan^{-1} \left(\frac{-\dot{e}}{e \dot{\psi}} \right) < \theta < \theta_1 + \pi \\ w_{-L}, & \theta_1 + \pi < \theta < \theta_1 + 2\pi \end{cases} \quad (4.22)$$

and at $z=-L/2$

If we define R_{ri} and R_{ii} as the inertia forces due to the flux of the fluid particles across the control surface in the r - and t - directions respectively, and substituting equations (4.18-4.22) into equations (4.12) and (4.13) respectively, we get

$$R_{ri} = -m_{11} \frac{\dot{e}^2}{e} - 2 m_{21} \dot{e} \dot{\psi} - m_{12} e \dot{\psi}^2 \quad (4.23)$$

and

$$R_{ii} = -m_{21} \frac{\dot{e}^2}{e} - 2 m_{12} \dot{e} \dot{\psi} - m_{22} e \dot{\psi}^2 \quad (4.24)$$

where

$$m_{11} = \frac{54}{140} \frac{\rho R L^3}{c} \epsilon \int_{\theta_1}^{\theta_1 + \pi} \frac{\cos^3 \theta}{(1 - \epsilon \cos \theta)^2} d\theta - \frac{27}{140} \frac{\rho R L^3}{c} \epsilon \int_{\theta_1 + \pi}^{\theta_1 + 2\pi} \frac{\cos^3 \theta}{(1 - \epsilon \cos \theta)^2} d\theta$$

$$m_{21} = \frac{54}{140} \frac{\rho R L^3}{c} \epsilon \int_{\theta_1}^{\theta_1 + \pi} \frac{\sin \theta \cos^2 \theta}{(1 - \epsilon \cos \theta)^2} d\theta - \frac{27}{140} \frac{\rho R L^3}{c} \epsilon \int_{\theta_1 + \pi}^{\theta_1 + 2\pi} \frac{\sin \theta \cos^2 \theta}{(1 - \epsilon \cos \theta)^2} d\theta$$

$$m_{12} = \frac{54}{140} \frac{\rho R L^3}{c} \epsilon \int_{\theta_1}^{\theta_1 + \pi} \frac{\sin^2 \theta \cos \theta}{(1 - \epsilon \cos \theta)^2} d\theta - \frac{27}{140} \frac{\rho R L^3}{c} \epsilon \int_{\theta_1 + \pi}^{\theta_1 + 2\pi} \frac{\sin^2 \theta \cos \theta}{(1 - \epsilon \cos \theta)^2} d\theta$$

$$m_{22} = \frac{54}{140} \frac{\rho R L^3}{c} \epsilon \int_{\theta_1}^{\theta_1+\pi} \frac{\sin^3 \theta}{(1 - \epsilon \cos \theta)^2} d\theta - \frac{27}{140} \frac{\rho R L^3}{c} \epsilon \int_{\theta_1+\pi}^{\theta_1+2\pi} \frac{\sin^3 \theta}{(1 - \epsilon \cos \theta)^2} d\theta$$

For a π -bearing, with a journal executing a nearly circular counter-clockwise whirl, the limits of integration can be taken to be $\theta_1 = 0$ and $\theta_2 = \pi$, and the coefficients m_{11} , m_{22} , m_{12} and m_{21} take the form

$$m_{11} = \frac{\rho R L^3}{c} m_{11}^*, \quad m_{22} = \frac{\rho R L^3}{c} m_{22}^*, \quad m_{12} = \frac{\rho R L^3}{c} m_{12}^*, \quad m_{21} = \frac{\rho R L^3}{c} m_{21}^*$$

where

$$m_{11}^* = \frac{27}{140} \frac{\pi}{\epsilon^2} \left[2 - \frac{(2 - 3\epsilon^2)}{(1 - \epsilon^2)^{1.5}} \right] \quad (4.25)$$

$$m_{22}^* = -\frac{27}{140} \frac{1}{\epsilon} \left[4 + \frac{2}{\epsilon} \log \left(\left| \frac{1 - \epsilon}{1 + \epsilon} \right| \right) \right] \quad (4.26)$$

$$m_{12}^* = -\frac{27}{140} \frac{\pi}{\epsilon^2} \left[2 - \frac{(2 - \epsilon^2)}{(1 - \epsilon^2)^{1/2}} \right] \quad (4.27)$$

$$m_{21}^* = \frac{27}{140} \frac{1}{\epsilon} \left[\frac{2}{(1 - \epsilon^2)} + \frac{2}{\epsilon} \log \left(\left| \frac{1 - \epsilon}{1 + \epsilon} \right| \right) + 2 \right] \quad (4.28)$$

These coefficients are plotted in Figure 4.5 versus the eccentricity ϵ . For a 2π -bearing the coefficients m_{21} and m_{22} are twice those for a π -bearing, while m_{11} and m_{12} are zero.

To calculate the flux terms in equations (4.12) and (4.13) for the long squeeze film damper, we note that the long uncavitated damper has no fluid flux through its control surface, thus there is no flux terms in the inertia forces for the long uncavitated damper. For the long cavitated damper, the control surface is determined by the boundaries of the cavitated film and there is fluid flux through those boundaries. Thus the flux terms for the cavitated damper depend heavily on the cavitation theory being used and the orbit the journal is executing in the damper bearing. Here, as discussed earlier, we are interested in the π -film theory and circular centered whirl of the journal in the bearing, and in this case

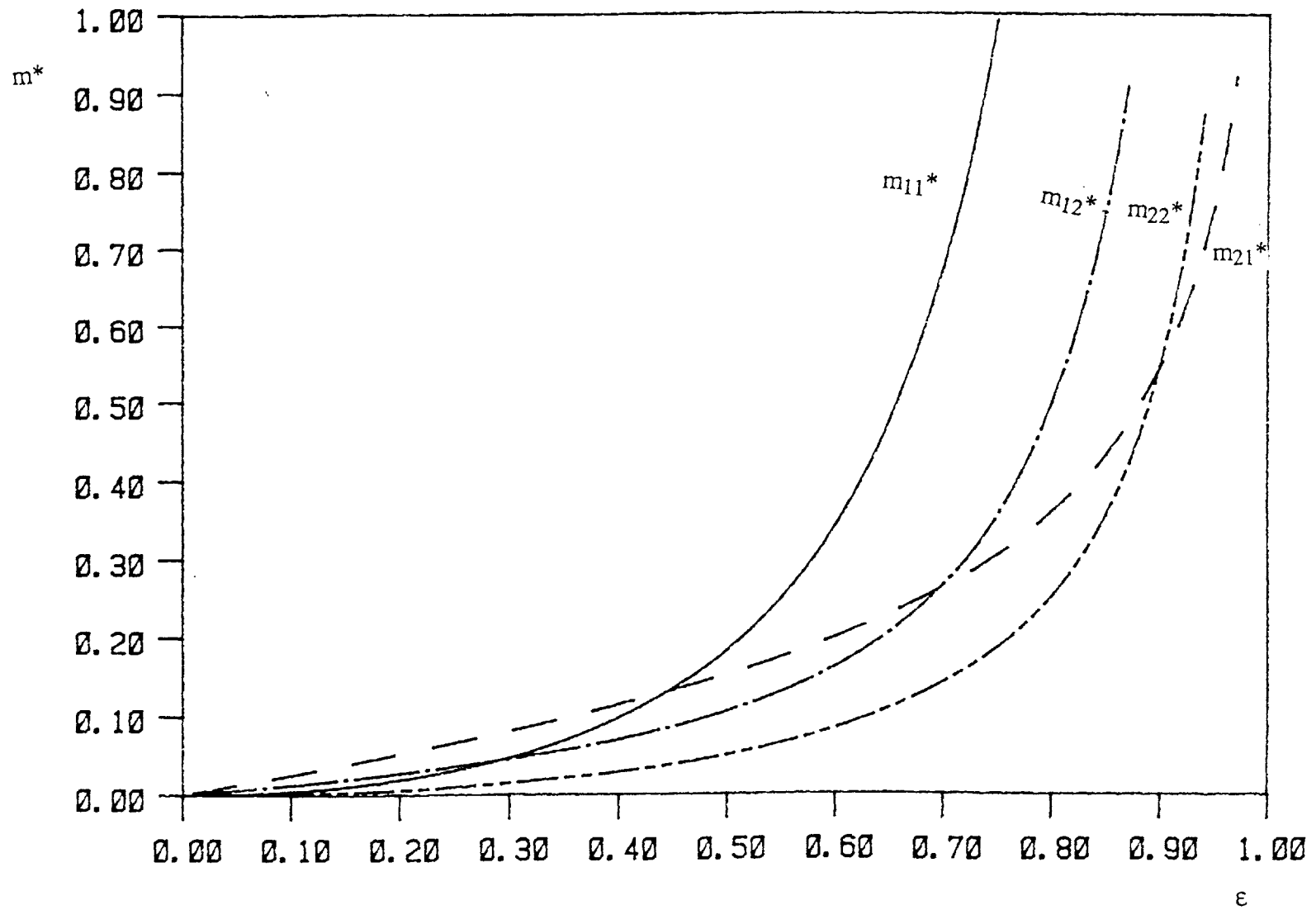


Figure 4.5 Supplemental inertia coefficients for short dampers.

the velocity vector \mathbf{V} depends on the circumferential velocity profile at $\theta = 0$ and $\theta = \pi$, termed u_0 and u_π , respectively, and on the velocity of the control surface $R \dot{\psi}$.

For a circular centered whirl \dot{e} is zero and the circumferential velocity profile u , equation (2.25), at $\theta = 0$ becomes

$$u_0 = \frac{6R}{h_0} \left(\frac{Y}{h_0} - \frac{Y^2}{h_0^2} \right) \left(\frac{3\epsilon}{2 + \epsilon^2} - 1 \right) e \dot{\psi} \quad (4.29)$$

and at $\theta = \pi$, u becomes

$$u_\pi = \frac{6R}{h_\pi} \left(\frac{Y}{h_\pi} - \frac{Y^2}{h_\pi^2} \right) \left(\frac{3\epsilon}{2 + \epsilon^2} + 1 \right) e \dot{\psi} \quad (4.30)$$

where h_0 is the the film thickness at $\theta = 0$, and h_π is the film thickness at $\theta = \pi$. Thus the kinetic coenergy per unit volume at $\theta = 0$, t_0^* , becomes

$$t_0^* = \frac{1}{2} \rho \frac{36R^2}{h_0^2} \left(\frac{Y}{h_0} - \frac{Y^2}{h_0^2} \right)^2 \left(\frac{3\epsilon}{2 + \epsilon^2} - 1 \right)^2 e^2 \dot{\psi}^2 \quad (4.31)$$

and at $\theta = \pi$, t_π^* , becomes

$$t_\pi^* = \frac{1}{2} \rho \frac{36R^2}{h_\pi^2} \left(\frac{Y}{h_\pi} - \frac{Y^2}{h_\pi^2} \right)^2 \left(\frac{3\epsilon}{2 + \epsilon^2} + 1 \right)^2 e^2 \dot{\psi}^2 \quad (4.32)$$

The velocity $\mathbf{V} \cdot \hat{\mathbf{n}}$ is given by

$$\mathbf{V} \cdot \hat{\mathbf{n}} = \begin{cases} u_0 + R \dot{\psi}, & \theta = 0 \\ u_\pi - R \dot{\psi}, & \theta = \pi \end{cases} \quad (4.33)$$

Substituting in (4.13), the component of the tangential inertia force due to the flux of the fluid through the control surface is

$$R_{ii} = -m_{22} e \dot{\psi}^2 \quad (4.34)$$

where

$$m_{22} = \frac{\rho R^3 L}{c} m_{22}^*$$

and

$$m_{22}^* = \frac{54}{35} \epsilon \left[\frac{\left(\frac{3\epsilon}{2+\epsilon^2} - 1 \right)^3}{(1-\epsilon)^2} + \frac{\left(\frac{3\epsilon}{2+\epsilon^2} + 1 \right)^3}{(1+\epsilon)^2} \right] + \frac{3}{5} \left[\frac{\left(\frac{3\epsilon}{2+\epsilon^2} - 1 \right)^2}{(1-\epsilon)} - \frac{\left(\frac{3\epsilon}{2+\epsilon^2} + 1 \right)^2}{(1+\epsilon)} \right] \quad (4.35)$$

Figure 4.6 shows a plot of m_{22}^* versus ϵ .

For future reference, the general form of the forces acting on the journal of a squeeze film damper is given below. The radial force, from equations (2.18), (4.16) and (4.23), is

$$F_r = -m_{rr} \ddot{e} - \left(\frac{1}{2} e \frac{\partial m_{rr}}{\partial e} + m_{11} \right) \frac{\dot{e}^2}{e} - m_{21} 2 \dot{e} \dot{\psi} + \left(m_{tt} + \frac{1}{2} e \frac{\partial m_{tt}}{\partial e} - m_{12} \right) e \dot{\psi}^2 - m_{rt} e \ddot{\psi} - C_{rr} \dot{e} - C_{rt} e \dot{\psi} \quad (4.36)$$

while the tangential force, from equations (2.19), (4.17) and (4.24), is

$$F_t = -m_{rt} \ddot{e} - \left(m_{rt} + e \frac{\partial m_{rt}}{\partial e} + m_{21} \right) \frac{\dot{e}^2}{e} - \left(m_{tt} + \frac{1}{2} e \frac{\partial m_{tt}}{\partial e} + m_{12} \right) 2 \dot{e} \dot{\psi} - m_{22} e \dot{\psi}^2 - m_{tt} e \ddot{\psi} - C_{tr} \dot{e} - C_{tt} e \dot{\psi} \quad (4.37)$$

Equations (4.36) and (4.37) are valid for both the long and short dampers, provided that coefficients of each model are used, and with the understanding that $m_{11} = m_{22} = m_{12} = m_{21} = 0$ for the long uncavitated dampers. These equations are the most general form of the forces acting on the journal of a SFD, except for the assumption that the inertia coefficients are velocity independent.

The centrifugal inertia force is determined by the quantity $m_t = m_{tt} + \frac{1}{2} e \frac{\partial m_{tt}}{\partial e} - m_{12}$, as can be seen from equation (4.36). Figure 4.7 shows a plot of m_t versus ϵ for a short SFD with π -film, from which it can be seen that m_t is nearly

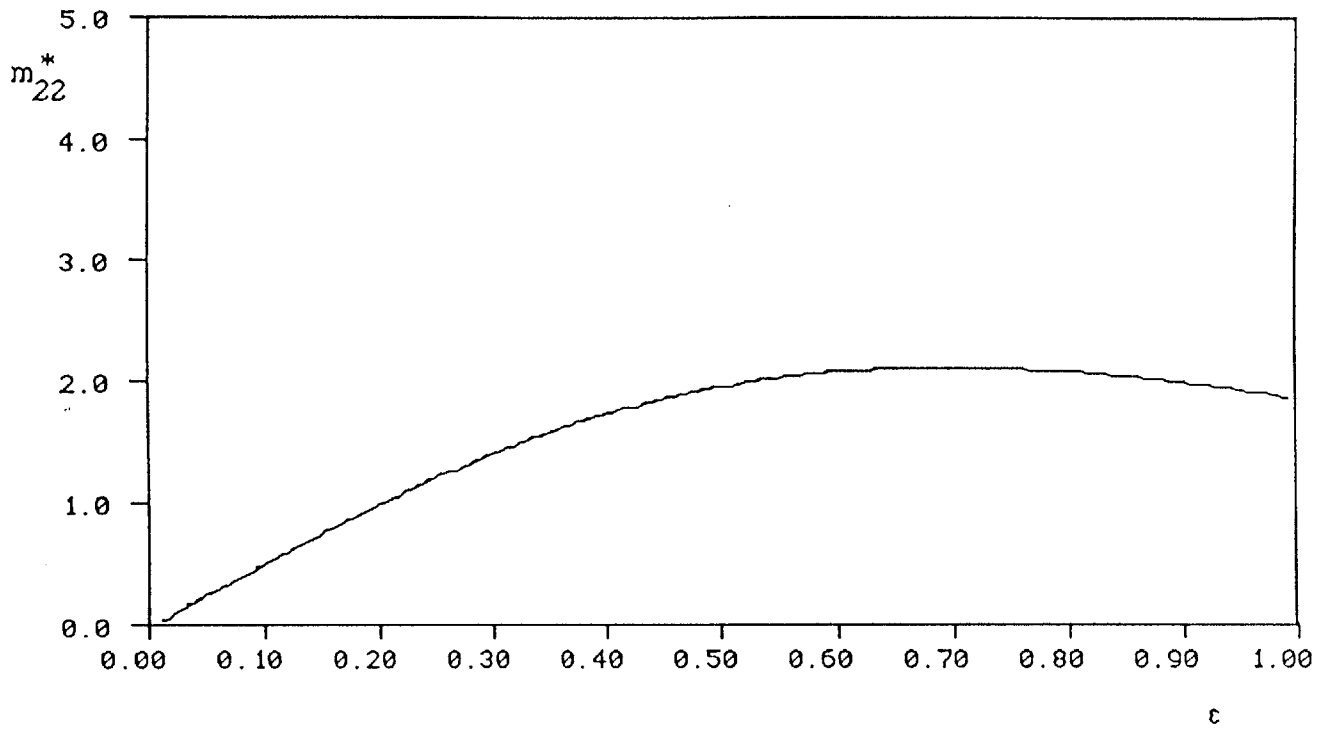
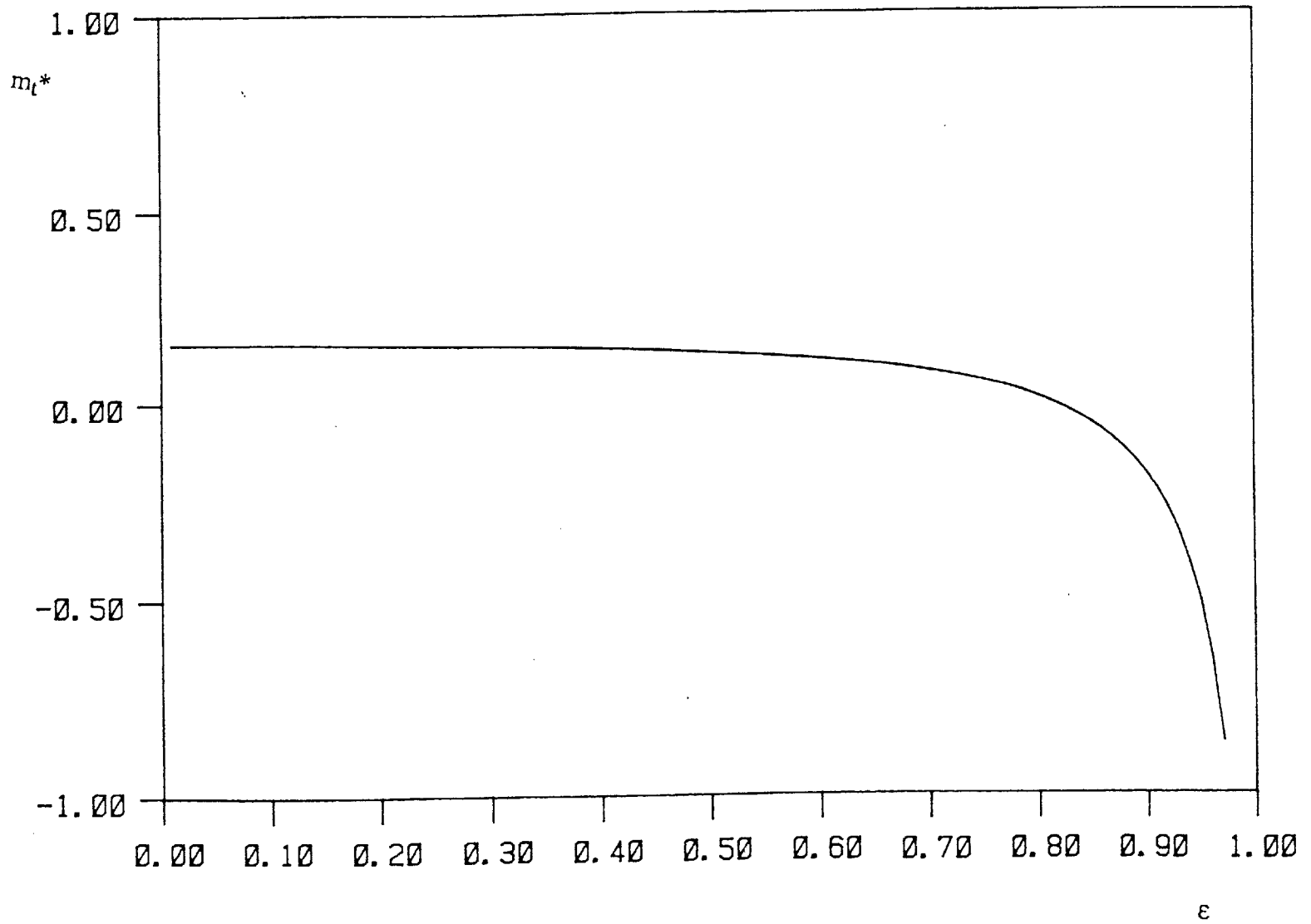


Figure 4.6 Supplemental inertia coefficient for long dampers

Figure 4.7 m_t^* versus ϵ

constant for small to moderate values of ϵ , but for excessively high eccentricities ($\epsilon > 0.8$), m_t becomes negative. Thus for high eccentricities, the centrifugal inertia force reverses its direction, and acts inwards. This is due to the m_{12} coefficient, thus it occurs only in cavitated short squeeze film dampers.

4.4 Solution of the governing equations for a small circular centered whirl

In this section we are going to present the solution of the partial differential equations describing the fluid in the damper for one of the few special cases in which these equations are solvable, namely a small circular centered whirl of the journal. Then we will show that the inertia forces predicted by the kinetic coenergy method described above, are the same as that of the solution of the partial differential equations in this special case.

For a small circular centered whirl, that is with $e \ll c$, the convective acceleration terms in the Navier-Stokes equations can be neglected, and equations (2.32 - 2.34) become

$$\frac{\partial u}{\partial t} = -\frac{1}{\rho} \frac{\partial p}{\partial X} + \mu \frac{\partial^2 u}{\partial Y^2} \quad (4.38)$$

$$\frac{\partial p}{\partial Y} = 0 \quad (4.39)$$

$$\frac{\partial w}{\partial t} = -\frac{1}{\rho} \frac{\partial p}{\partial Z} + \mu \frac{\partial^2 w}{\partial Y^2} \quad (4.40)$$

Furthermore, the boundary conditions on the upper surface of Figure 2.2, can be satisfied on the average. Thus the boundary conditions that equations (4.38 - 4.40) have to satisfy are

$$\text{At } y = 0 \quad u = 0 \quad v = 0 \quad w = 0 \quad (4.41)$$

$$\text{At } y = c \quad u = U \quad v = V \quad w = 0$$

where, for a circular whirl U and V are given by (see equation (2.8))

$$U = e \dot{\psi} \cos \theta$$

$$V = -e \dot{\psi} \sin \theta$$

or

$$U = \text{Real} \{ e \omega e^{i\theta} \}$$

$$V = \text{Real} \{ i e \omega e^{i\theta} \}$$

where $i = (-1)^{1/2}$ and $\omega = \dot{\psi}$ is the frequency of the whirl. In this case $\theta = \phi - \omega t$ which suggests that the upper surface of Figure 2.2, travels like a wave, and thus we should seek a solution in the form

$$u = U_0 e^{i\theta} \quad v = V_0 e^{i\theta} \quad w = W_0 e^{i\theta} \quad p = P_0 e^{i\theta} \quad (4.42)$$

where U_0 , V_0 and W_0 are functions of Y and Z , while P_0 is a function of Z only.

Substituting (4.42) into (4.38), we get

$$\frac{d^2 U_0}{dY^2} + \frac{i \rho \omega}{\mu} U_0 = \frac{i}{\mu R} P_0$$

which can be solved for U_0 using the boundary conditions (4.41), thus, neglecting terms of $O(c/R)$, we get

$$U_0 = \frac{P_0}{\rho \omega R} \left[\frac{\sinh(s(Y-c)) - \sinh(sY) + \sinh(sc)}{\sinh(sc)} \right] \quad (4.43)$$

where

$$s = \frac{1}{c} \sqrt{\frac{\text{Re}}{2}} (1-i)$$

and $\text{Re} = \rho \omega c^2 / \mu$ is the Reynolds number. Substituting (4.42) into (4.40), we get

$$\frac{d^2 W_0}{dY^2} + \frac{i \rho \omega}{\mu} W_0 = \frac{1}{\mu} \frac{dP_0}{dZ}$$

which can be solved for W_0 using the boundary conditions (4.41), thus

$$W_0 = -\frac{i}{\rho \omega} \frac{dP_0}{dZ} \left[\frac{\sinh(s(Y-c)) - \sinh(sY) + \sinh(sc)}{\sinh(sc)} \right] \quad (4.44)$$

Substituting (4.42), (4.43) and (4.44) into the continuity equation, equation (2.6), we get

$$\frac{\partial V_0}{\partial Y} = \frac{i}{\rho \omega} \left(\frac{d^2 P_0}{dZ^2} - \frac{1}{R^2} P_0 \right) \left[\frac{\sinh(s(Y-c)) - \sinh(sY) + \sinh(sc)}{\sinh(sc)} \right]$$

The above equation can be integrated over Y to obtain

$$V_0 = \frac{i}{\rho \omega} \left(\frac{d^2 P_0}{dZ^2} - \frac{1}{R^2} P_0 \right) \left[\frac{\cosh(s(Y-c)) - \cosh(sY) + sY \sinh(sc)}{s \sinh(sc)} \right] + C_1$$

But at $Y = 0$, $V_0 = 0$, thus

$$C_1 = -\frac{i}{\rho \omega} \left(\frac{d^2 P_0}{dZ^2} - \frac{1}{R^2} P_0 \right) \left[\frac{\cosh(sc) - 1}{s \sinh(sc)} \right]$$

and V_0 becomes

$$V_0 = \frac{i}{\rho \omega} \left(\frac{d^2 P_0}{dZ^2} - \frac{1}{R^2} P_0 \right) \left[\frac{\cosh(s(Y-c)) - \cosh(sY) + sY \sinh(sc) + 1 - \cosh(sc)}{s \sinh(sc)} \right]$$

The other boundary condition that V_0 has to satisfy, namely, at $Y=c$ the velocity $V_0 = i e \omega$, gives us

$$\frac{d^2 P_0}{dZ^2} - \frac{1}{R^2} P_0 = \frac{\rho e \omega^2}{c} \left[\frac{sc \sinh(sc)}{2 - 2 \cosh(sc) + sc \sinh(sc)} \right] \quad (4.45)$$

which is a differential equation that the pressure P_0 has to satisfy together with the boundary conditions

$$P_0 = 0 \quad \text{at} \quad Z = \pm L/2$$

and on solving (4.45) we get

$$P_0 = \frac{\rho e \omega^2 R^2}{c} \left[\frac{sc \sinh(sc)}{2 - 2 \cosh(sc) + sc \sinh(sc)} \right] \left\{ \frac{\cosh\left(\frac{2Z}{D}\right)}{\cosh\left(\frac{L}{D}\right)} - 1 \right\} \quad (4.46)$$

where $D = 2R$ is the diameter of the damper. Equation (4.46) is a finite length solution for the pressure P_0 in a squeeze film damper whose journal executes a small circular-centered whirl, which is valid for all Re (in the laminar region).

The pressure in the damper is given by

$$p = \text{Real} \left\{ \left[\frac{\rho e \omega^2 R^2}{c} \frac{sc \sinh(sc)}{2 - 2 \cosh(sc) + sc \sinh(sc)} \right] \left[\frac{\cosh\left(\frac{2Z}{D}\right)}{\cosh\left(\frac{L}{D}\right)} - 1 \right] e^{i\theta} \right\} \quad (4.47)$$

The pressure in equation (4.47) depends on Re only through the terms inside the first square bracket, namely

$$f(Re) = \left[\frac{\rho e \omega^2 R^2}{c} \frac{s c \sinh (s c)}{2 - 2 \cosh (s c) + s c \sinh (s c)} \right] \quad (4.48)$$

If we take the limit as $Re \rightarrow 0$ of equation (4.48) we get

$$\lim_{Re \rightarrow 0} f(Re) = \frac{12 R^2 \mu e \omega}{c^3} \left(i + \frac{Re}{10} \right) \quad (4.49)$$

Figure 4.8 shows a plot of the real and imaginary parts of $f(Re)$ versus Re as predicted from equation (4.48). Also plotted on Figure 4.8 are the real and imaginary parts of the limit of $f(Re)$ as $Re \rightarrow 0$, equation (4.49), from which it is clear that equation (4.49) is a good approximation of equation (4.48) for Re up to about 50.

The forces acting on the journal can be obtained by integrating equation (4.47), thus (see Figure 2.4)

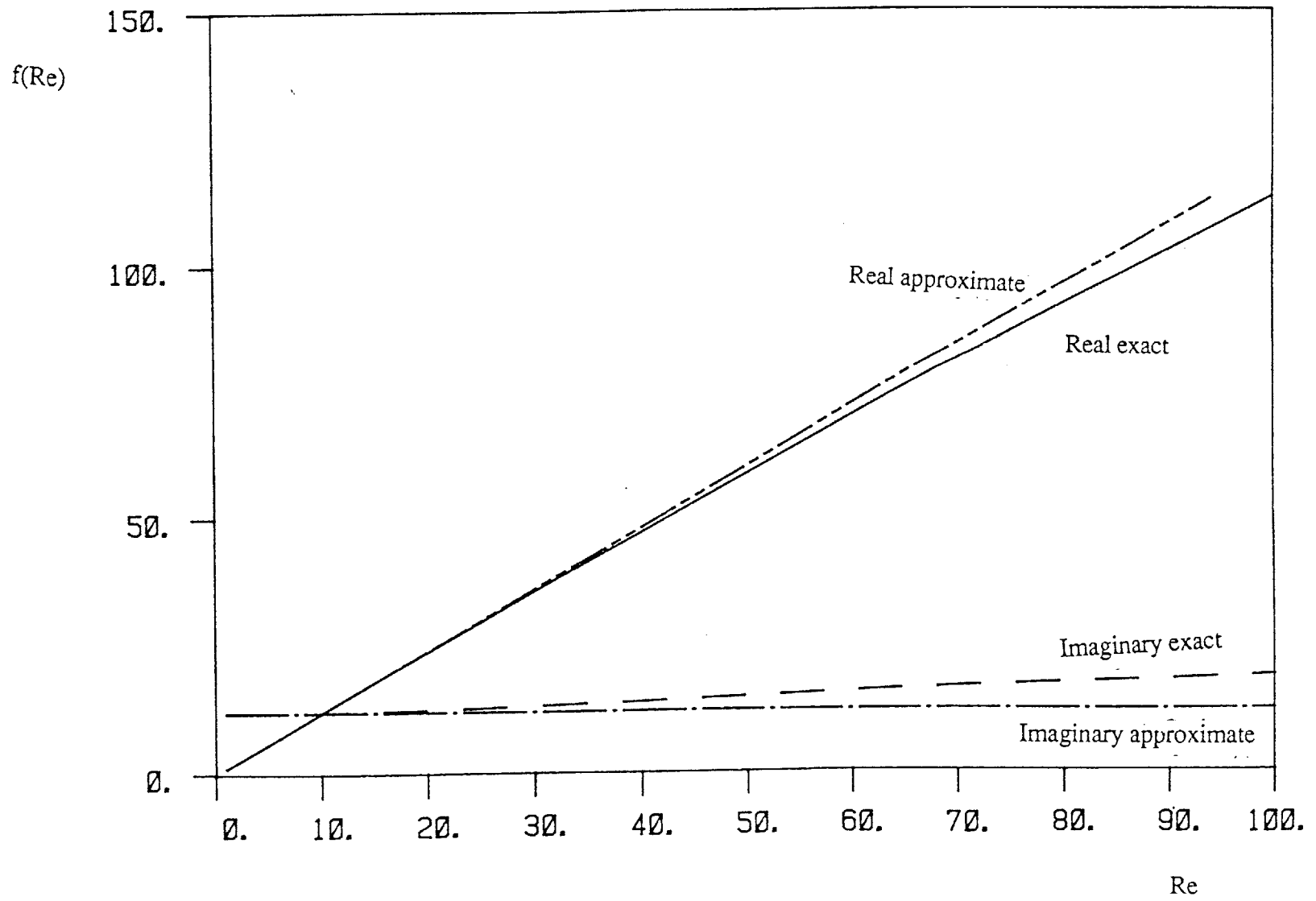
$$F_r = - \int_{-\frac{L}{2}}^{\frac{L}{2}} \int_{\theta_1}^{\theta_2} p \cos \theta R d\theta dZ$$

$$F_t = - \int_{-\frac{L}{2}}^{\frac{L}{2}} \int_{\theta_1}^{\theta_2} p \sin \theta R d\theta dZ$$

Now using the limit of $f(Re)$, equation (4.49), in equation (4.47), the forces acting on the journal become

$$F_r = 12 \frac{\mu R^3 L}{c^3} e \omega \left\{ 1 - \frac{\tanh\left(\frac{L}{D}\right)}{\frac{L}{D}} \right\} \left[- \int_{\theta_1}^{\theta_2} \sin \theta \cos \theta d\theta + \frac{Re}{10} \int_{\theta_1}^{\theta_2} \cos^2 \theta d\theta \right] \quad (4.50)$$

$$F_t = 12 \frac{\mu R^3 L}{c^3} e \omega \left\{ 1 - \frac{\tanh\left(\frac{L}{D}\right)}{\frac{L}{D}} \right\} \left[- \int_{\theta_1}^{\theta_2} \sin^2 \theta d\theta + \frac{Re}{10} \int_{\theta_1}^{\theta_2} \sin \theta \cos \theta d\theta \right] \quad (4.51)$$

Figure 4.8 $f(\text{Re})$ versus Re

where the quantity

$$K_L = \left\{ 1 - \frac{\tanh\left(\frac{L}{D}\right)}{\frac{L}{D}} \right\}$$

has been termed a leakage factor by Warner [100] which accounts for the finiteness of the damper. Equations (4.50) and (4.51) represent a finite length solution to the governing equations. To be able to compare the results of the kinetic coenergy method with the above equations, we have to consider the limiting cases of long and short dampers. For a long damper $L/D \rightarrow \infty$ thus $K_L \rightarrow 1$, and for a short damper $L/D \rightarrow 0$ thus $K_L \rightarrow \frac{1}{3} \left(\frac{L}{D}\right)^2$

For a long 2π -bearing equations (4.50) and (4.51) become

$$F_r = 12 \frac{\rho R^3 L}{10 c} \pi e \omega^2$$

$$F_t = -12 \frac{\mu R^3 L}{c^3} \pi e \omega$$

The radial force is the centrifugal force and the tangential force is the damping force. These forces are the forces acting on the journal when it executes a small circular-centered orbit in a 2π -bearing. These are the same forces as those predicted by equation (4.36) for F_r and (4.37) for F_t , if we take the limit as ϵ tends to zero of the inertia and damping coefficients, which is the condition of a small orbit. It can be shown that for the π -bearing we get half the forces for a 2π -bearing, when we apply each of the above techniques.

Similarly, for a short 2π -bearing equations (4.50) and (4.51) become

$$F_r = \frac{\rho R L^3}{10 c} \pi e \omega^2$$

$$F_t = -\frac{\mu R L^3}{c^3} \pi e \omega$$

The radial force is the centrifugal force and the tangential force is the damping force. These forces are the forces acting on the journal when it executes a small circular-centered orbit in

a 2π -bearing. These are the same forces as those predicted by equation (4.36) for F_r and (4.37) for F_t , if we take the limit as ϵ tends to zero of the inertia and damping coefficients, which is the condition of a small orbit. It can be shown that for the π -bearing we get half the forces for a 2π -bearing, when we apply each of the above techniques.

Thus in this section we have shown that the forces acting on the journal when it executes a small circular-centered orbit in a squeeze film damper, obtained by taking the limit as $Re \rightarrow 0$ of the solution of the governing partial differential equations, are the same as those predicted by the kinetic coenergy method. Also it was shown that the limit as $Re \rightarrow 0$ of the pressure, and thus the forces, is nearly constant up to $Re = 50$, which is the region of application of squeeze film dampers in practice. Thus we may conclude that the kinetic coenergy method reliably predicts the inertia forces in squeeze film dampers.

Concluding this chapter, we have now completed the development of the squeeze film damper model, including both the damping forces (chapter 2) and the inertia forces (this chapter), and for both the long and short dampers. This model is going to be employed in the next chapter to study the dynamics of a rotor incorporating squeeze film dampers.

Chapter 5

Dynamics of Rotors Incorporating Squeeze Film Dampers

In this chapter we employ the model we derived in chapters 2 and 4, for a squeeze film damper (SFD), in the analysis of the steady state whirl of a rotor incorporating SFDs. We consider a simplified rotor system which consists of a massive disk and a massless flexible shaft. This model is referred to as the Jeffcott rotor. The Jeffcott rotor can be considered as a one degree of freedom rotor system, thus it is valid below the second bending critical speed of the rotor.

The main emphasis is going to be on the effect of fluid inertia on the dynamics of the rotor. In particular, the effect of fluid inertia on the critical speeds, jump resonance characteristics, and on the stability of the steady state.

5.1 Jeffcott rotor incorporating a SFD

Figure 5.1 shows a Jeffcott rotor mounted on two identical ball bearings, each of which is surrounded by a squeeze film. The outer race of each ball bearing, which is assumed rigid and massless, is constrained from rotating by a retainer spring of stiffness K_r , which also acts to center the journal in the clearance of the oil film. The rotor has mass $2m$, stiffness $2K$, and damping acting at its center with a damping coefficient of $2C$.

The rotor is spinning in the bearings but this spinning does not reach the oil film, because of the constraint on the outer races of the ball bearings. Also the rotor can experience bending vibration.

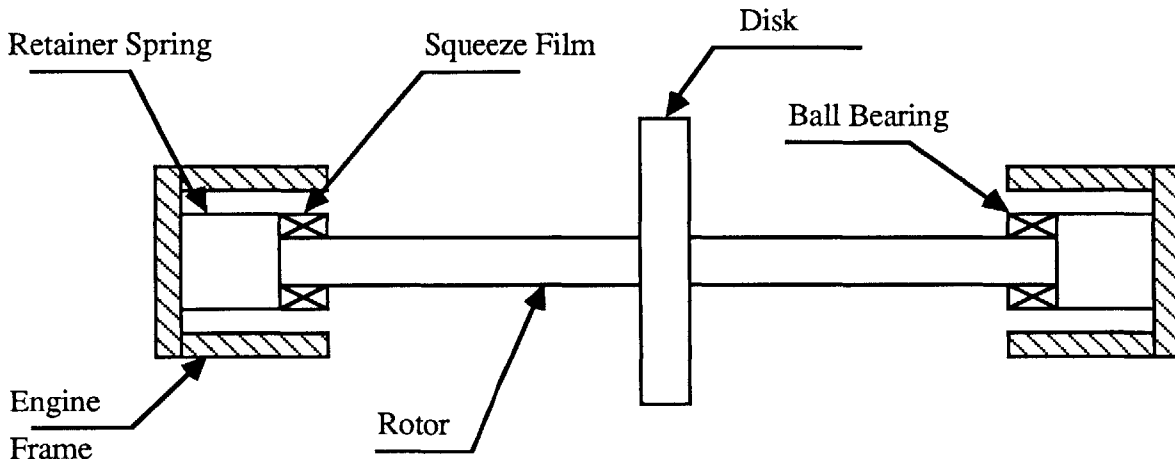


Figure 5.1 Jeffcott Rotor on squeeze film dampers

The oil film acts to damp this bending vibration. The rotor can experience bending vibration both in the horizontal and vertical planes. If the frequencies of vibration in both planes are the same, then the resulting motion is a whirling orbit.

The whirling vibration can either be a free vibration due to disturbances, or a forced vibration due to a force applied to the rotor. The most common force applied to rotating machinery is the centrifugal force arising from an unbalance. This occurs when the mass center of the rotor does not coincide with the geometric center.

Usually high speed rotating machinery are well balanced, but there is always some residual unbalance in the machine (which usually degrades with operation), that causes the rotor to resonate as it passes the critical speed. This is the main reason that dampers are used in rotating machinery, to aid in passing the critical speeds and to reduce the forces

acting on the bearings and the engine frame due to unbalance. Also dampers dissipate energy from the free vibration of the rotor. In the rest of the chapter, we study the unbalance response of the Jeffcott rotor of Figure 5.1, with particular emphasis on the performance of the squeeze film dampers.

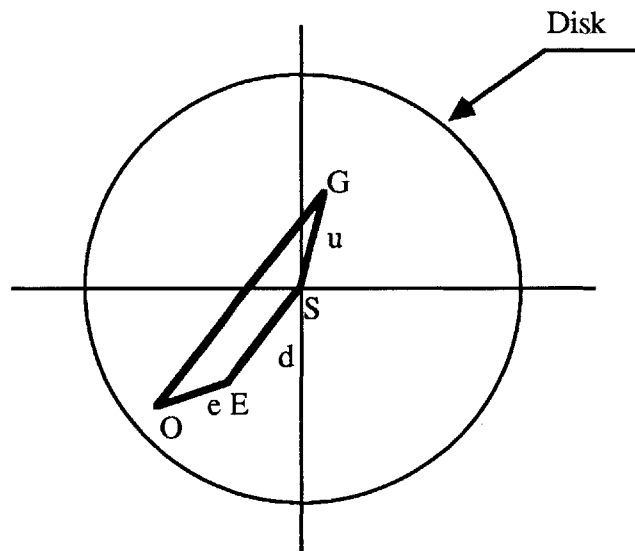


Figure 5.2 Side view of rotor

Figure 5.2 shows a side view of the Jeffcott rotor of Figure 5.1. Point O represents the center of bearings, while point E represents the center of the journal. Thus the distance OE is equal to the eccentricity (e) of the journal in the damper. Point S represents the geometric center of the disk, thus the distance SE is the deflection (d) of the rotor at its midspan; and point G represents the center of mass of the disk, thus the distance GS is the unbalance (u). Since the rotor is symmetrical, the eccentricities of the journals in each bearing are the same.

Figure 5.3 shows the notation and the coordinate frames used in the analysis of the rotor. The (x,y) frame is a stationary frame whose center is at the bearings center O. The rotating (r,t) frame is rotating at the whirl frequency of the journal in the damper. The

positive r-axis joins the center of the bearing O and the center of the journal E, and makes an angle ψ with the positive x-axis. The rotor deflection d can in general be in a direction making an angle α with the positive r-axis, and the unbalance u makes an angle β with positive r-axis as shown in Figure 5.3.

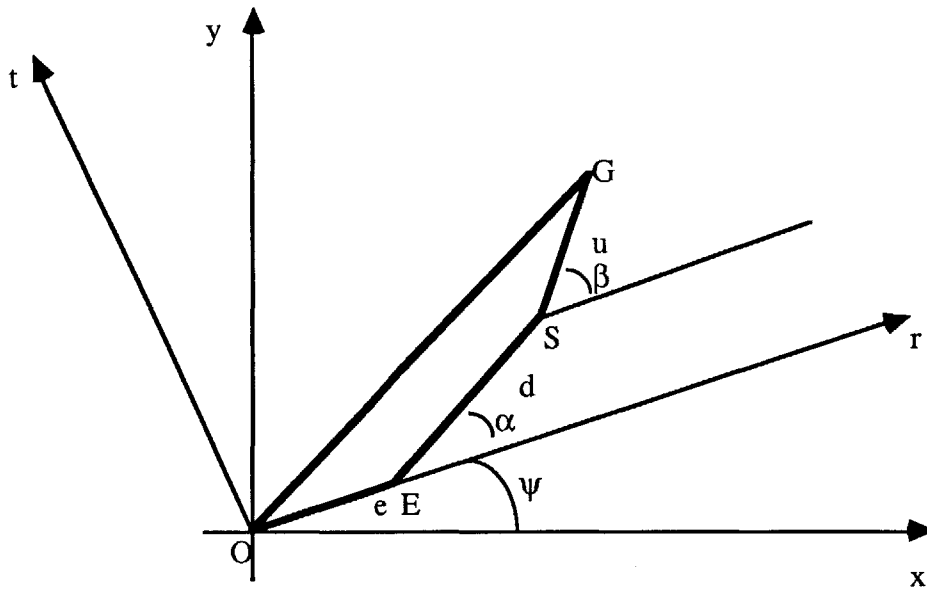


Figure 5.3 Coordinate Frame for Jeffcott rotor

5.2 Equations of motion

We can consider the (x,y) plane of Figure 5.3 to be a complex plane, in which the position vector of a point in the plane is determined by a complex number $z = x + i y$. Using this complex notation the equations of motion for the Jeffcott rotor of Figure 5.1, become

$$2 m \ddot{z}_G = -2 K (z_S - z_E) - 2 C \dot{z}_S \quad (5.1)$$

$$2 K (z_S - z_E) - 2 K_r z_E + 2 (F_r + i F_t) e^{i\psi} = 0 \quad (5.2)$$

where z_G , z_S , and z_E are the position vectors in the complex plane of the points G, S and E respectively. The dot implies differentiation with respect to time, and F_r and F_t are the forces acting on the journal due to the squeeze film damper. Equation (5.1) is the equation of motion of the disk, while equation (5.2) represents the force balance at the center of the journal. The position vectors z_G , z_S , and z_E are given by

$$\begin{aligned} z_E &= e e^{i\psi} \\ z_S &= (e + d e^{i\alpha}) e^{i\psi} \\ z_G &= (e + d e^{i\alpha} + u e^{i\beta}) e^{i\psi} \end{aligned}$$

Thus equation (5.1) becomes

$$\begin{aligned} m \{ \ddot{e} - e \dot{\psi}^2 + i (e \ddot{\psi} + 2 \dot{e} \dot{\psi}) + [(d - d (\dot{\alpha} + \dot{\psi})^2) + i (d (\ddot{\alpha} + \ddot{\psi}) + 2 d (\dot{\alpha} + \dot{\psi}))] e^{i\alpha} \\ + [-u (\dot{\beta} + \dot{\psi})^2 + i u (\ddot{\beta} + \ddot{\psi})] e^{i\beta} \} + C \{ \dot{e} + i e \dot{\psi} + [\dot{d} + i d (\dot{\alpha} + \dot{\psi})] e^{i\alpha} \} \\ + K d e^{i\alpha} = 0 \end{aligned} \quad (5.3)$$

and equation (5.2) becomes

$$K d e^{i\alpha} - K_r e + F_r + i F_t = 0 \quad (5.4)$$

where the forces F_r and F_t are given by equations (4.36) and (4.37). Also the condition that the unbalance u is rotating at the speed of rotation of the rotor Ω , is given by

$$\dot{\beta} + \dot{\psi} = \Omega \quad (5.5)$$

which gives an additional condition on the motion of the system.

It is desirable to nondimensionalize equations (5.3), (5.4) and (5.5) to generalize the analysis and to reduce the number of independent parameters. To do so, we divide each of equations (5.3) and (5.4) by $m \omega_n^2 c$, where c is the clearance of the damper, $\omega_n^2 = (K_{eq}/m)$ is the natural frequency of the rotor-bearing system and $K_{eq} = K_r K / (K_r + K)$ is the equivalent stiffness of the rotor and the retainer spring. We also define the following nondimensional parameters:

$$\varepsilon = e/c = \text{eccentricity ratio}$$

$D = d/c =$ nondimensional deflection

$U = u/c =$ nondimensional unbalance

$K^* = K/m \omega_n^2 =$ nondimensional rotor stiffness

$K_r^* = K_r/m \omega_n^2 =$ nondimensional retainer spring stiffness

$\Omega^* = \Omega/\omega_n =$ nondimensional rotor speed

$\eta = C/m \omega_n =$ damping loss factor

$R_k = K_r^*/K^* =$ stiffness ratio

$F_r^* = F_r/m c \omega_n^2 =$ nondimensional radial damper force

$F_t^* = F_t/m c \omega_n^2 =$ nondimensional tangential damper force

$\tau = \omega_n t =$ nondimensional time

It should be noted that since we chose to nondimensionalize the parameters by using the natural frequency ω_n , then K^* and K_r^* are determined completely by the knowledge of R_k , since $K_{eq}^*=1$, then

$$K^* = 1 + 1/R_k$$

and $K_r^* = 1 + R_k$

This is a restriction that conveniently results in a reduction of the number of parameters under investigation. It is not necessary to use such a nondimensionalizing scheme, we could have chosen any other datum frequency (although in this case the undamped critical speed will not be at $\Omega^*=1$), if it is required to study the effects of the rotor stiffness and the retainer spring stiffness separately.

Thus equations (5.3) and (5.4) become

$$\begin{aligned} & \varepsilon'' - \varepsilon \psi'^2 + i (\varepsilon \psi'' + 2 \varepsilon' \psi') \\ & + [D'' - D (\alpha' + \psi')^2 + i (D (\alpha'' + \psi'') + 2 D' (\alpha' + \psi'))] e^{i\alpha} \\ & + [-U (\beta' + \psi')^2 + i U (\beta'' + \psi'')] e^{i\beta} \\ & + \eta \{ \varepsilon' + i \varepsilon \psi' + [D' + i D (\alpha' + \psi')] e^{i\alpha} \} + K^* D e^{i\alpha} = 0 \end{aligned} \quad (5.6)$$

and

$$K^* D e^{i\alpha} - K_r^* \varepsilon + F_r^* + i F_t^* = 0 \quad (5.7)$$

Dividing equation (5.5) by ω_n , we get

$$\beta' + \psi' = \Omega^* \quad (5.8)$$

where $()'$ denotes differentiation with respect to τ .

Substituting for ψ' from equation (5.8) into equations (5.6) and (5.7), they become two complex differential equations, i.e. four real differential equations, in four unknowns: ε , D , α and β . They are nonlinear equations since F_r^* and F_t^* are nonlinearly dependent on the position of the journal in the damper. These equations are difficult to solve analytically, and it has been reported [85] that they exhibit the following problems, when solved numerically:

- a) false convergence to steady state.
- b) regions of multiple solution tend to involve a tedious and time consuming trial and error.
- c) only stable solutions can be found, and
- d) the particular algorithm and convergence criteria used in the iterative approach determine the accuracy and credibility of the results.

Also if these algorithms are used for multi-mass rotor systems, they will become very time consuming.

5.3 Steady state unbalance response

Fortunately since the rotor of Figure 5.1 is symmetric, we can assume that at steady state, the points E, S and G execute circular centered whirling orbits, at the frequency of the rotation of the rotor Ω^* (since this is a forced response due to unbalance). Thus the polygon OESG of Figures 5.2 and 5.3 is locked at steady state and is not changing, and rotating at a constant frequency Ω^* . Also at steady state $\varepsilon' = \varepsilon'' = D' = D'' = \alpha' = \alpha'' = \beta' =$

$\beta'' = 0$. Applying these conditions and substituting (5.8) into equations (5.6) and (5.7), their real and imaginary parts become

$$\Omega^{*2} U \cos \beta = -\varepsilon \Omega^{*2} + (K^* - \Omega^{*2}) D \cos \alpha - \eta \Omega^* D \sin \alpha \quad (5.9)$$

$$\Omega^{*2} U \sin \beta = \eta \Omega^* \varepsilon + (K^* - \Omega^{*2}) D \sin \alpha + \eta \Omega^* D \cos \alpha \quad (5.10)$$

$$K^* D \cos \alpha = K_r^* \varepsilon + B C_{tt}^* \varepsilon \Omega^* - M m_t^* \varepsilon \Omega^{*2} \quad (5.11)$$

$$K^* D \sin \alpha = B C_{tt}^* \varepsilon \Omega^* + M m_{22}^* \varepsilon \Omega^{*2} \quad (5.12)$$

where

$$m_t^* = m_{tt}^* + \frac{1}{2} \varepsilon \frac{\partial m_{tt}^*}{\partial \varepsilon} - m_{12}^*$$

B = bearing parameter

$$= \mu R L^3 / m \omega_n c^3 \quad \text{for short dampers}$$

$$= \mu R^3 L / m \omega_n c^3 \quad \text{for long dampers}$$

M = Inertia parameter

$$= \rho R L^3 / m c \quad \text{for short dampers}$$

$$= \rho R^3 L / m c \quad \text{for long dampers}$$

The nondimensional damping and inertia parameters C_{ij}^* and m_{ij}^* are given by equations (2.28-2.31), (4.9-4.11) and (4.35) for long dampers, and by equations (2.20-2.22), (4.4-4.6) and (4.22-4.25) for short dampers.

Equations (5.9) - (5.12) are four nonlinear algebraic equations in the four unknowns ε , D , α and β . Instead of solving these equations numerically using a nonlinear equation solver like the Newton-Raphson technique, which will involve a tedious trial and error in regions of multiple solution, we are going to manipulate equations (5.9-5.12) further. The goal is to obtain a polynomial in Ω^* whose coefficients are functions of ε . Taylor and Kumar [86] were successful in doing so, for a rigid rotor mounted on squeeze film dampers. They solved the resulting fourth order polynomial in closed form to obtain the unbalance response.

Squaring (5.9) and (5.10) and adding, we get

$$U^2 \Omega^{*4} = (\eta^2 + \Omega^{*2}) \epsilon^2 \Omega^{*2} + [(K^* - \Omega^{*2})^2 + \eta^2 \Omega^{*2}] D^2 (\cos^2 \alpha + \sin^2 \alpha) \\ + 2 \epsilon \Omega^* [\eta K^* D \sin \alpha + \Omega^* (\eta^2 - K^* + \Omega^{*2}) D \cos \alpha]$$

Substituting for $D \cos \alpha$ and $D \sin \alpha$ from (5.11) and (5.12), respectively, into the above equation, and after some extensive algebraic manipulation we get

$$a_1 \Omega^{*8} + a_2 \Omega^{*7} + a_3 \Omega^{*6} + a_4 \Omega^{*5} + a_5 \Omega^{*4} + a_6 \Omega^{*3} + a_7 \Omega^{*2} + a_8 \Omega^* + a_9 = 0 \quad (5.13)$$

where

$$a_1 = \frac{M^2}{K^{*2}} (m_t^{*2} + m_{22}^{*2})$$

$$a_2 = \frac{2MB}{K^{*2}} (C_{tt}^* m_{22}^* - C_{rt}^* m_t^*)$$

$$a_3 = \frac{1}{K^{*2}} [B^2 (C_{tt}^{*2} + C_{rt}^{*2}) - 2MK_r^* m_t^* + M^2 (\eta^2 - 2K^*) (m_t^{*2} + m_{22}^{*2}) \\ - 2MK^* m_t^*]$$

$$a_4 = \frac{2B}{K^{*2}} [C_{rt}^* (K^* + K_r^*) + M (\eta^2 - 2K^*) (C_{tt}^* m_{22}^* - C_{rt}^* m_t^*)]$$

$$a_5 = 1 - \frac{U^2}{\epsilon^2} - \frac{2M\eta^2 m_t^*}{K^*} + 2M m_t^* + \frac{2K_r^*}{K^*} + \frac{K_r^{*2}}{K^{*2}} + M^2 (m_t^{*2} + m_{22}^{*2}) \\ + \frac{(\eta^2 - 2K^*)}{K^{*2}} [B^2 (C_{tt}^{*2} + C_{rt}^{*2}) - 2MK_r^* m_t^*]$$

$$a_6 = 2M m_{22}^* \eta + \frac{2BC_{rt}^* \eta^2}{K^*} - 2BC_{rt}^* + \frac{2(\eta^2 - 2K^*) K_r^* B C_{rt}^*}{K^{*2}}$$

$$+ 2MB (C_{tt}^* m_{22}^* - C_{rt}^* m_t^*)$$

$$a_7 = \eta^2 + 2BC_{tt}^* \eta + 2\eta^2 \frac{K_r^*}{K^*} - 2K_r^* + B^2 (C_{tt}^{*2} + C_{rt}^{*2}) - 2MK_r^* m_t^*$$

$$+ (\eta^2 - 2K^*) \frac{K_r^{*2}}{K^{*2}}$$

$$a_8 = 2K_r^* B C_{rt}^*$$

$$a_9 = K_r^{*2}$$

Equation (5.13) is an eighth order polynomial in Ω^* , whose coefficients are functions of ε . This polynomial was solved numerically by the IMSL subroutine ZPOLR, which uses the Laguerre algorithm to obtain the roots of the polynomial. A value of ε is assumed and the subroutine is called to obtain the roots of (5.13). Complex roots were neglected, since they would not indicate a steady state. Since the rotor can rotate both in the clockwise and the counter-clockwise directions, the routine obtained both positive and negative roots which were mirror image. Knowing that, only the positive roots were retained, for counter-clockwise rotation. If the rotor rotates in the clockwise direction, then the system will exhibit similar behavior as when the rotor rotates in the counter-clockwise direction.

Knowing ε and Ω^* , it is possible to obtain the deflection D from equations (5.11) and (5.12), by squaring and adding, thus

$$D^2 = \frac{\varepsilon^2}{K^{*2}} \{ M^2 (m_t^{*2} + m_{22}^{*2}) \Omega^{*4} + 2 M B (C_{tt}^* m_{22}^* - C_{rt}^* m_t^*) \Omega^{*3} \\ + [B^2 (C_{tt}^{*2} + C_{rt}^{*2}) - 2 M K_r^* m_t^*] \Omega^{*2} + 2 K_r^* B C_{rt}^* \Omega^* + K_r^{*2} \} \quad (5.14)$$

Also if we divide (5.12) by (5.11), then α is

$$\alpha = \tan^{-1} \left\{ \frac{B C_{tt}^* \Omega^* + M m_{22}^* \Omega^{*2}}{K_r^* + B C_{rt}^* \Omega^* - M m_t^* \Omega^{*2}} \right\} \quad (5.15)$$

Similarly, dividing (5.10) by (5.9), then β is

$$\beta = \tan^{-1} \left\{ \frac{\eta \Omega^* \varepsilon + (K^* - \Omega^{*2}) D \sin \alpha + \eta \Omega^* D \cos \alpha}{-\varepsilon \Omega^{*2} + (K^* - \Omega^{*2}) D \cos \alpha - \eta \Omega^* D \sin \alpha} \right\} \quad (5.16)$$

It is sometimes convenient to describe the motion of the rotor by the runout at the rotor center, r , which is the distance OS in Figure 5.3. If we define $R^* = r/c$, as a nondimensional runout, then

$$R^* = \sqrt{(\varepsilon + D \cos \alpha)^2 + D^2 \sin^2 \alpha} \quad (5.17)$$

Another quantity that is important in determining SFD performance is the transmissibility Tr . It is defined as the ratio of the magnitude of the force transmitted to the engine frame with SFD support, to the magnitude of the force transmitted to the engine frame if the support was rigid. Thus

$$Tr = \frac{\sqrt{F_r^{*2} + F_t^{*2}}}{\frac{K^* U \Omega^{*2}}{\sqrt{(K^* - \Omega^{*2})^2 + \eta^2 \Omega^{*2}}}} \quad (5.18)$$

If $Tr < 1$, then the squeeze film damper is successful in attenuating the force transmitted to the engine frame. On the other hand, if $Tr > 1$, then the SFD magnifies the force transmitted to the engine frame. The transmissibility serves to determine the regions of successful SFD operation.

It should be noted that in this analysis we are assuming that the eccentricities in both dampers have the same phase, thus we are neglecting the excitation of the odd modes for this system. One would expect that this system would have three modes because of the three lumped masses: one due to the disk, and one each due to fluid inertia in the two dampers. Thus we expect that we have two even modes and one odd mode, while the analysis here provides only the two even modes. For this system the odd mode, because of symmetry, would result in no whirl at the disk center and whirl primarily in the journals. It appears that this mode would be unimportant since the motion essentially occurs in the dampers, and thus would be highly damped, which would result in relatively small amplitudes, and thus its neglect would not affect the unbalance response.

5.4 Parametric studies of unbalance response

The unbalance response of the system was obtained by a program UNBRES that employed the techniques described in the previous section. The program was extremely efficient, such that typically it took approximately 20 seconds to obtain the full steady state unbalance response on a PDP-11/44 computer. It has been reported [85] that, using numerical integration, the unbalance response of a simpler system (rigid rotor, no fluid inertia) took about 15 minutes on a PDP-11/34 computer.

In performing the parametric studies, we took a datum system, whose parameters are close to those reported in [85], and varied each parameter of interest to determine its effect on the unbalance response. This datum system exhibits the generic behavior resulting from the nonlinear characteristics of SFDs. The unbalance response of this generic system is shown in Figure 5.4, for a π -film short damper. The parameters defining the generic system are: $B = 0.1$, $M = 0.2$, $U = 0.3$, $R_k = 0.1$ and $\eta = 0.01$.

Figure 5.4 (a) illustrates the basic features of the unbalance response of the generic system. The eccentricity ratio ϵ is plotted versus the nondimensional frequency Ω^* . The jump phenomenon can be clearly seen in the figure, and also two high eccentricity steady state branches can be seen at Ω^* between 2.5 and 3.5. Regions II and III [85] in the figure are unstable steady states, while regions I, IV and V represent stable steady states that the rotor can achieve. Figure 5.4 (b) shows the nondimensional deflection D versus Ω^* . Regions III and IV are at a much larger amplitude (of the order of 3. to 5.) than regions I, II and V, and are not shown in the figure. Comparing Figures 5.4 (a) and (b), it can be seen that the rotor deflection D is much smaller than ϵ for regions I, II and V, but for regions III and IV the deflection is much larger than ϵ and consequently the rotor will probably be deflected beyond its limit if it were to operate in region IV. Figures 5.4 (c) and

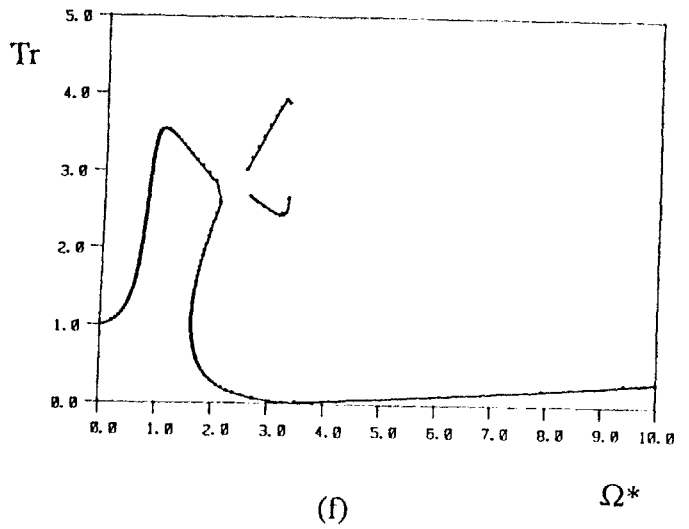
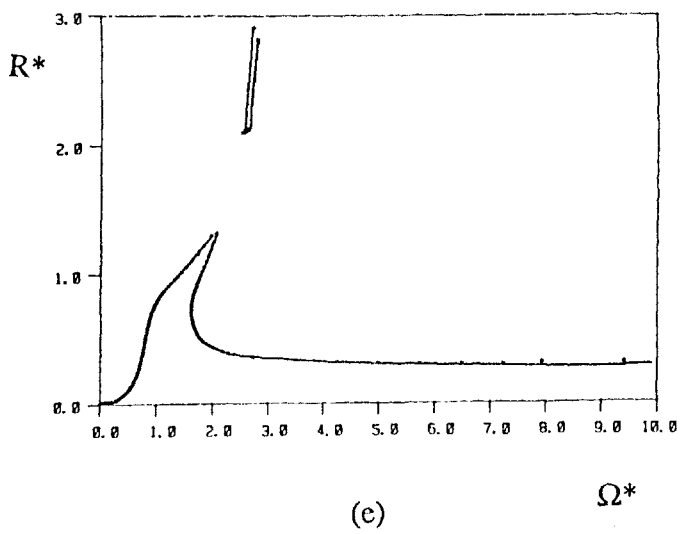
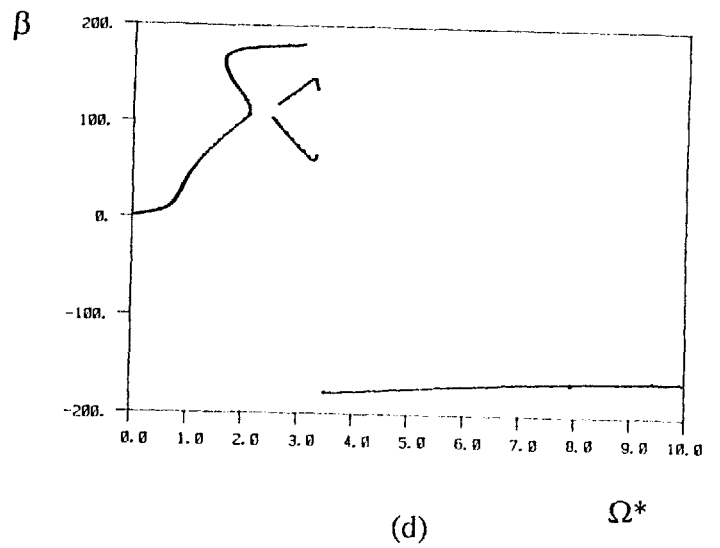
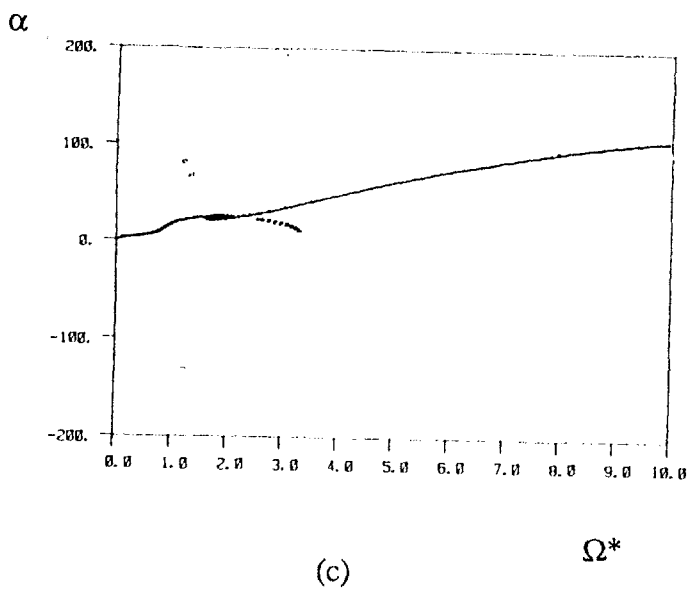
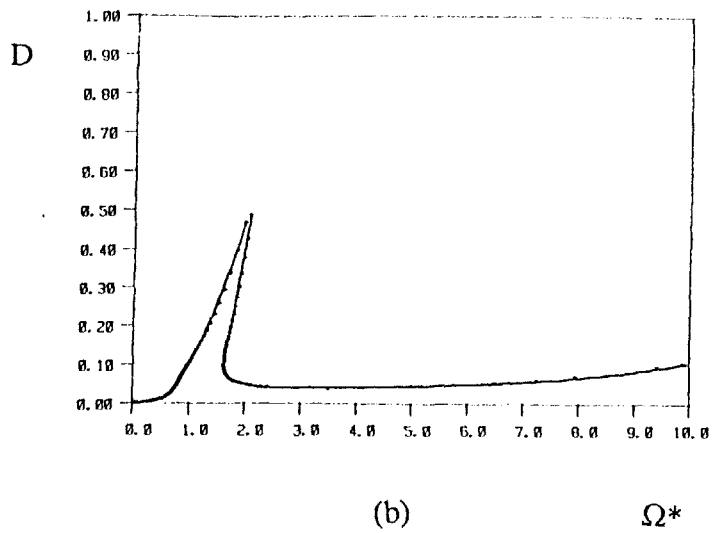
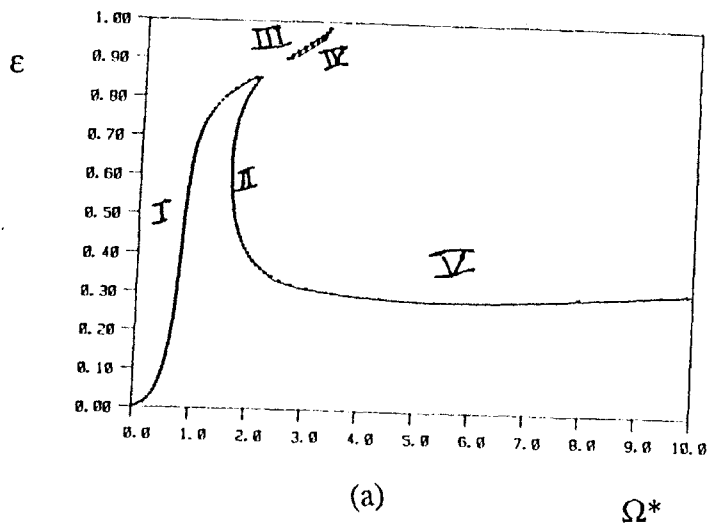


Figure 5.4 Unbalance response of generic system

(d) show the angles α and β versus Ω^* , respectively. These figures help in visualizing the mode shape and the phase differences for the rotor. Figure 5.4 (e) shows the nondimensional runout at the rotor center R^* versus Ω^* , from which the large deflections of the rotor in regions III and IV can be appreciated. Figure 5.4 (f) shows the transmissibility Tr versus Ω^* , from which it can be seen that the SFD will be a superior rotor support if it operates on branch V.

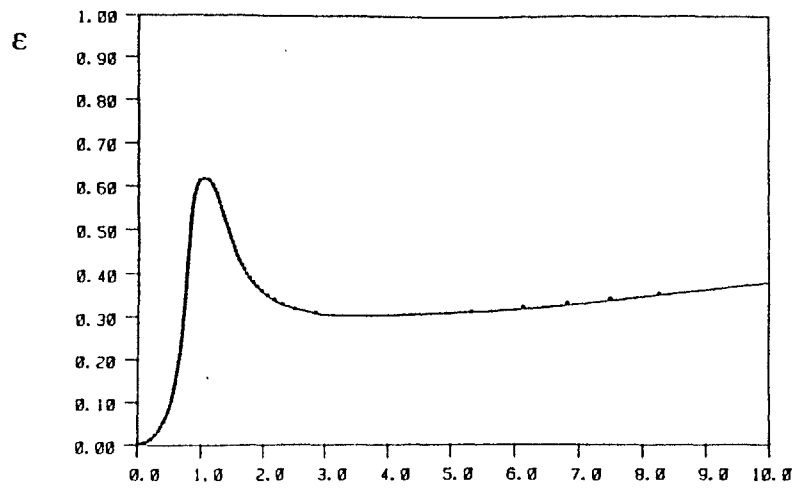
5.4.1 Short squeeze film dampers

In this sub-section we explore the effects of various parameters on the unbalance response of the rotor system with short squeeze film dampers. Long squeeze film dampers are discussed in the next sub-section. We are going to investigate the effect of each parameter essentially on three variables: ϵ , R^* and Tr . In each case we kept all the parameters at the values of those of the generic system, and changed only the parameter of interest.

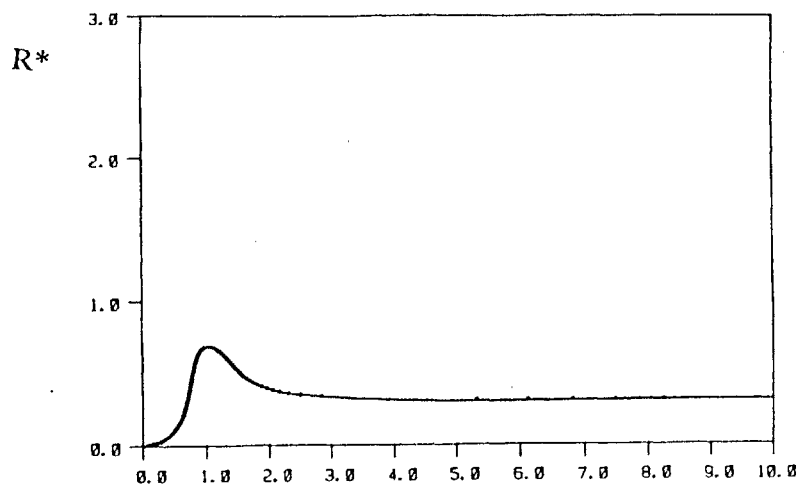
Figure 5.5 shows the effect of employing the 2π -film model on the unbalance response of the generic system. This would be a good model for a highly pressurized damper. It can be seen that the jump resonance disappeared and the peaks become smaller in magnitude. Overall, pressurization improves the performance of the damper. Yet at high frequencies it can be seen that the amplitudes start to build up for a second critical that is due to fluid inertia. This second critical will be investigated in detail later.

Figures 5.6, 5.7 and 5.8 illustrate the effects of changing the bearing parameter B on the unbalance response of the generic system. The bearing parameter, which was identified previously in the literature [101,57,85], is a measure of the amount of damping the SFD can provide. Figure 5.6 illustrates the effect of changing B on ϵ . For low values

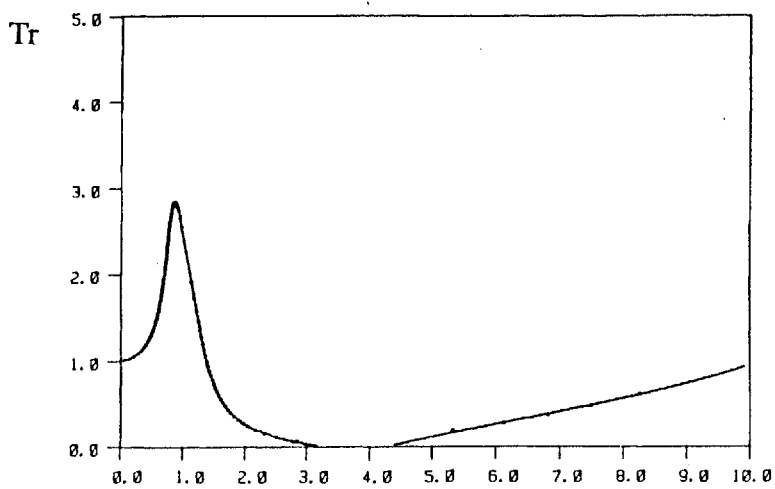
2 π -Film



(a)

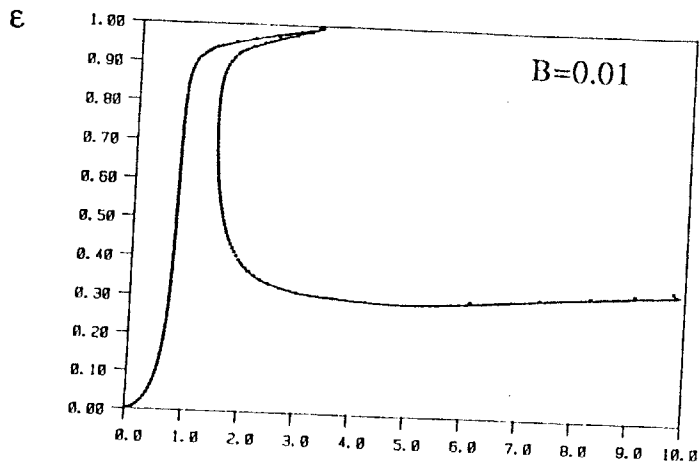


(b)

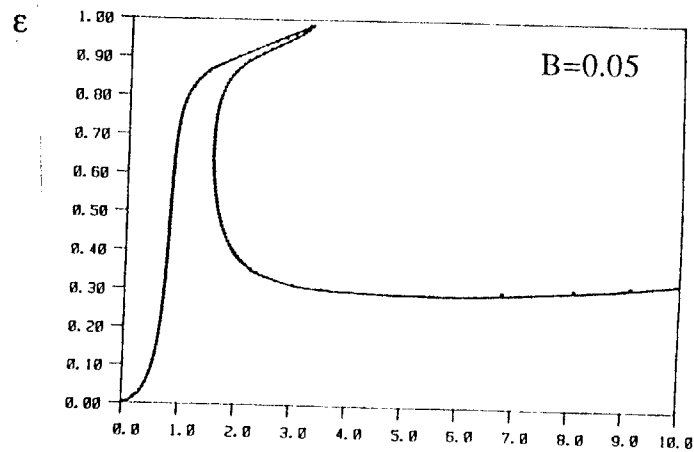


(c)

Figure 5.5 Unbalance response of generic system, 2 π -film

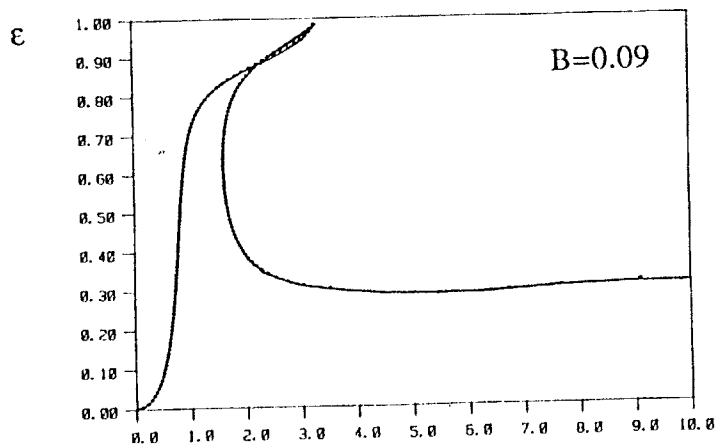


(a)



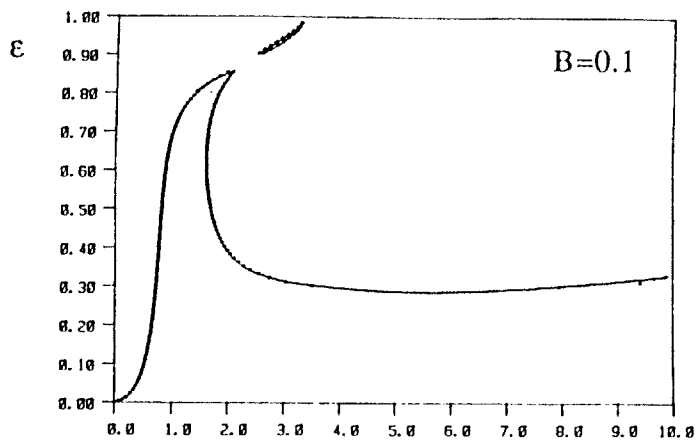
(b)

Ω^*



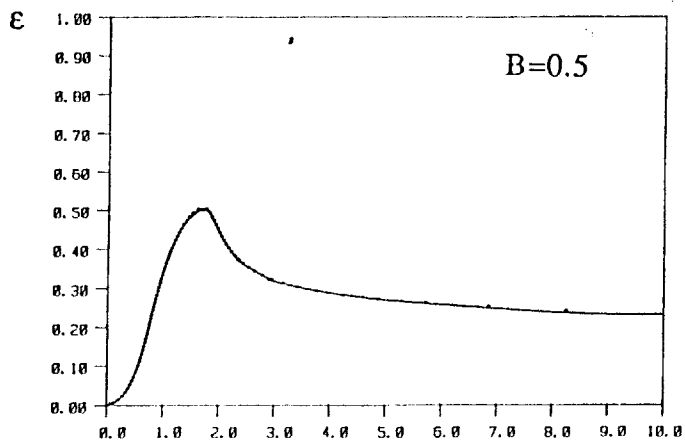
(c)

Ω^*

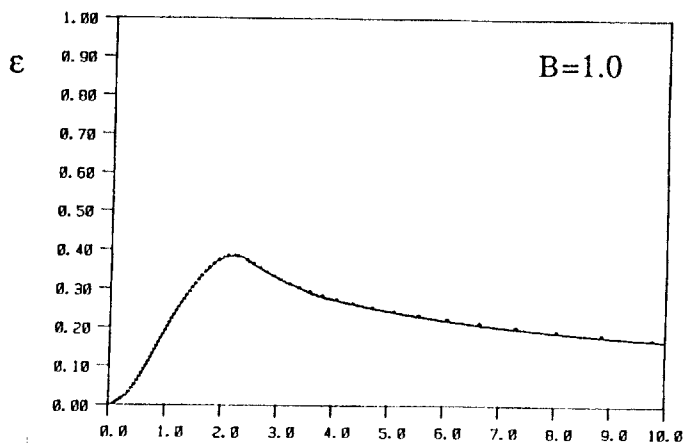


(d)

Ω^*



(e)



(f)

Ω^*

Figure 5.6 Effect of B on unbalance response of generic system, ϵ

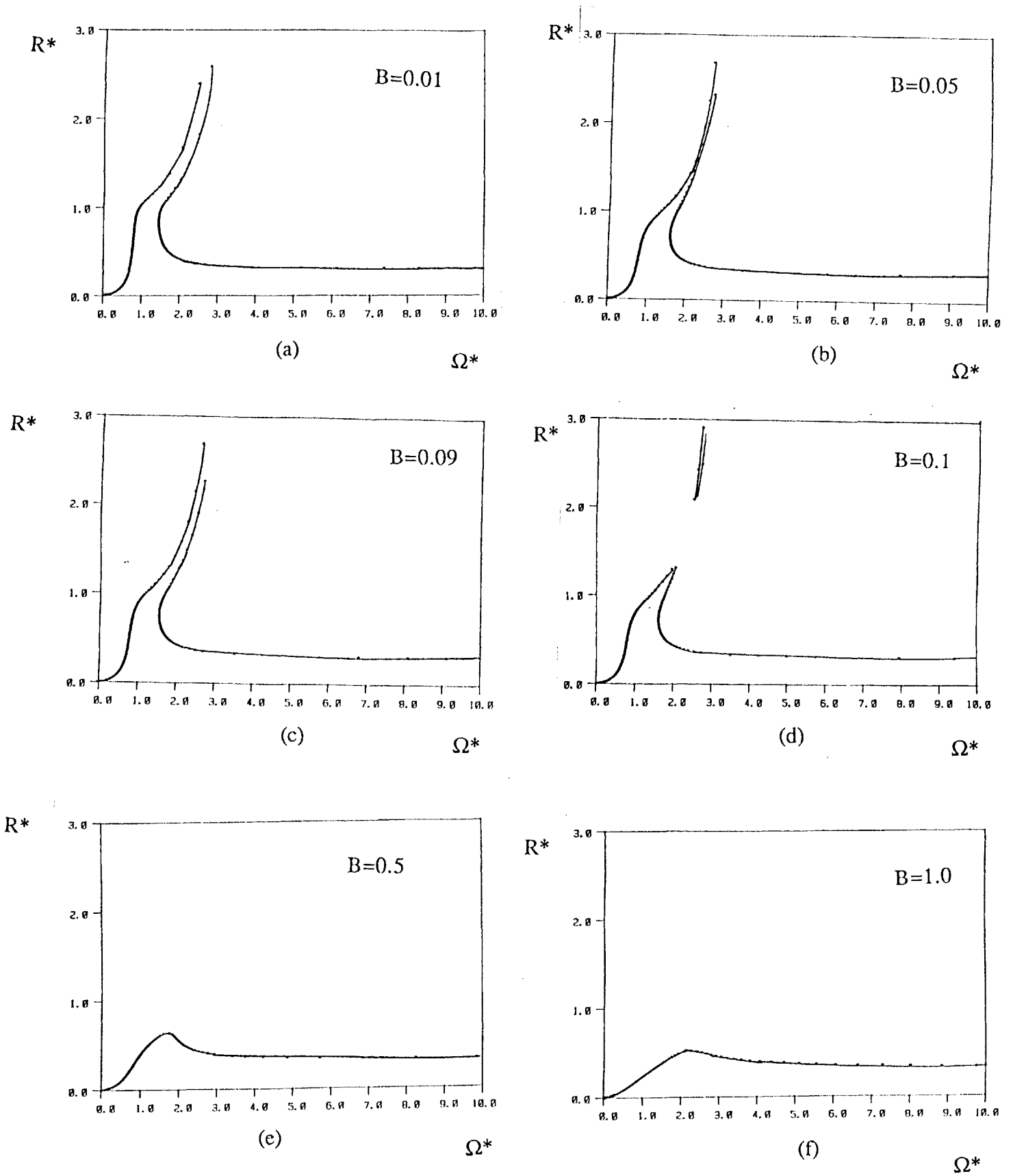


Figure 5.7 Effect of B on unbalance response of generic system, R^*

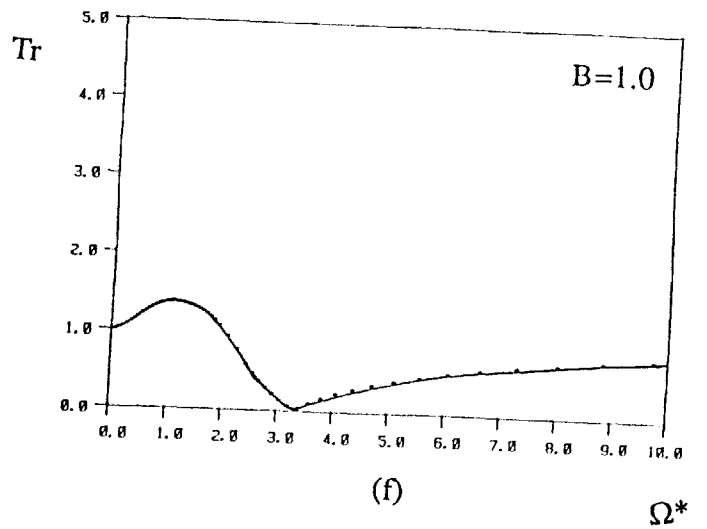
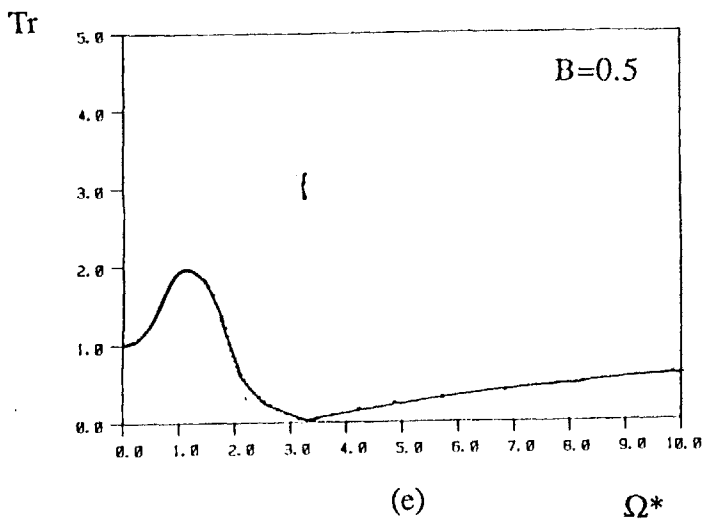
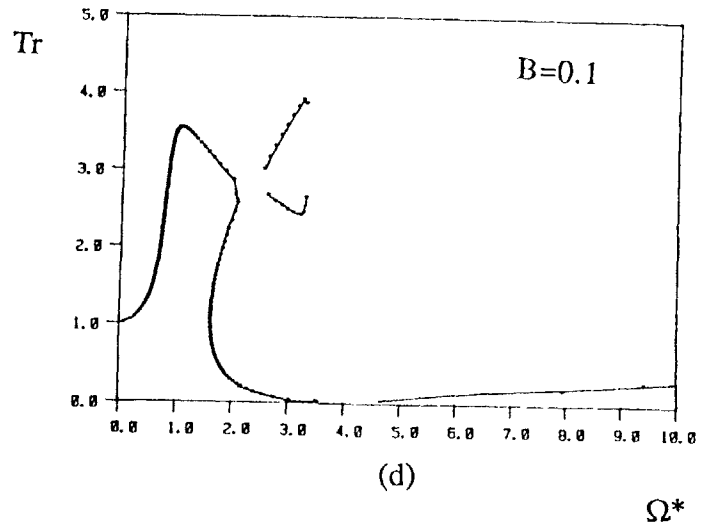
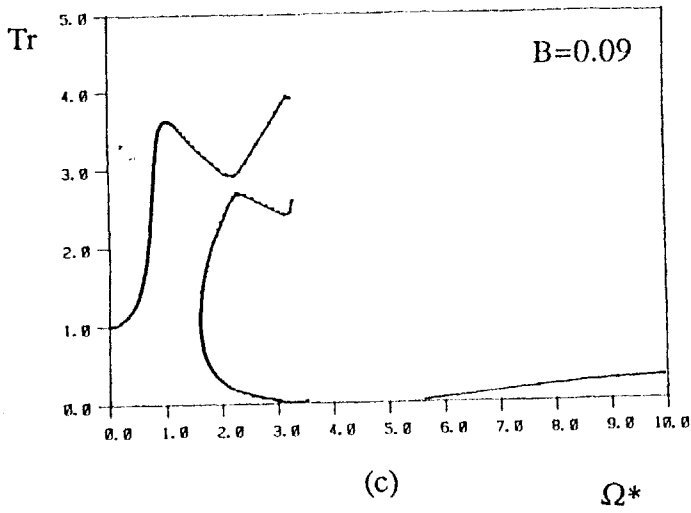
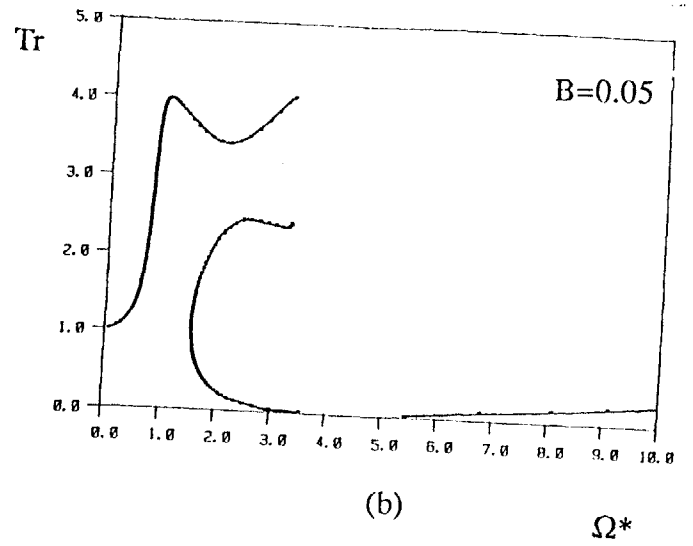
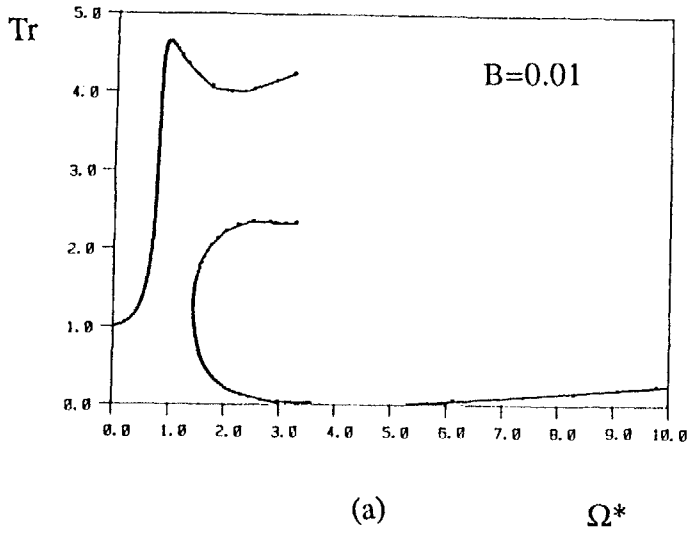


Figure 5.8 Effect of B on unbalance response of generic system, Tr

of B , regions III and IV disappear, and the jump resonance attains large amplitudes. The value of $B=0.09$ is interesting, regions III and IV are starting to appear, and are connected to regions I and II. It can be seen that region III is a continuation of region II and region IV is continuation of region I. Thus it is no surprise that region III is unstable, while region IV is stable. Increasing B further, the amplitude of the jump resonance decreases and regions III and IV separate from regions I and II. At large values of B , the jump resonance disappears and regions III and IV also decrease in size and eventually disappear. The same sequence is seen in Figure 5.7 which illustrates the effect of changing B on R^* . Figure 5.8 shows the effect of changing B on Tr . For low values of B the transmissibility is high in region I, and in region V the transmissibility is nearly zero. Thus low values of B result in a large speed range with low transmitted force. For large values of B the transmissibility is larger than 1.0 in region I, (but with values less than those for small B), and the jump resonance does not occur. Regions III and IV diminish, although they exhibit large transmissibilities. Region V has sizable Tr , but still less than 1. Thus in the useful speed range, large values of B result in larger Tr than low values of B .

Figures 5.9, 5.10 and 5.11 illustrate the effects of changing the inertia parameter M on the unbalance response of the generic system. Figure 5.9 illustrates the effect of changing M on ϵ . For low values of M , as for B , regions III and IV disappear and the jump resonance attains large amplitudes. the value of $M=0.00002$ should be considered to be similar to the case of no fluid inertia. We were not able to reduce M to zero, since the coefficient a_1 , of equation (5.13) would be zero and in this case the routine ZPOLR was not able to obtain the roots of the polynomial. For large values of M , regions III and IV appear and as M is increased they diminish, and the jump resonance magnitude also decreases until it disappears. Thus it may be concluded that large values of M are beneficial with regards to the jump resonance. Also for large values of M , a second mode appears in the frequency range under consideration. This mode is essentially due to fluid inertia in the

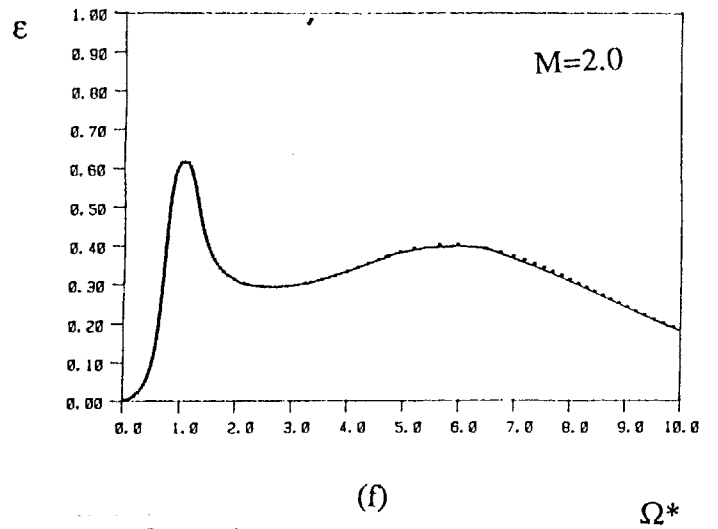
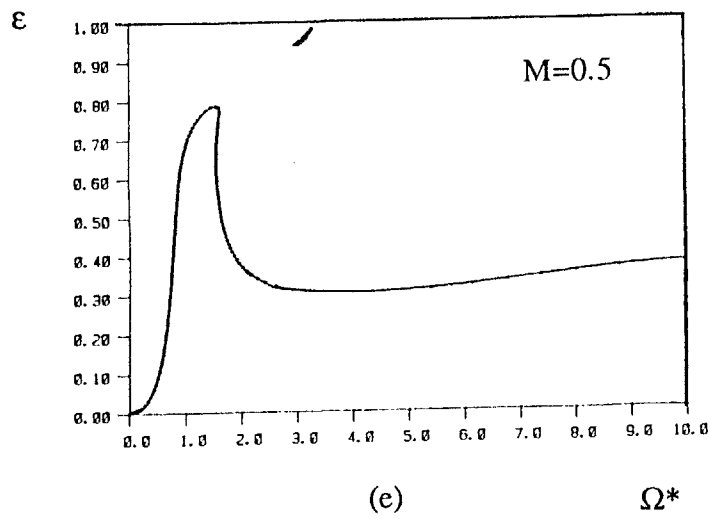
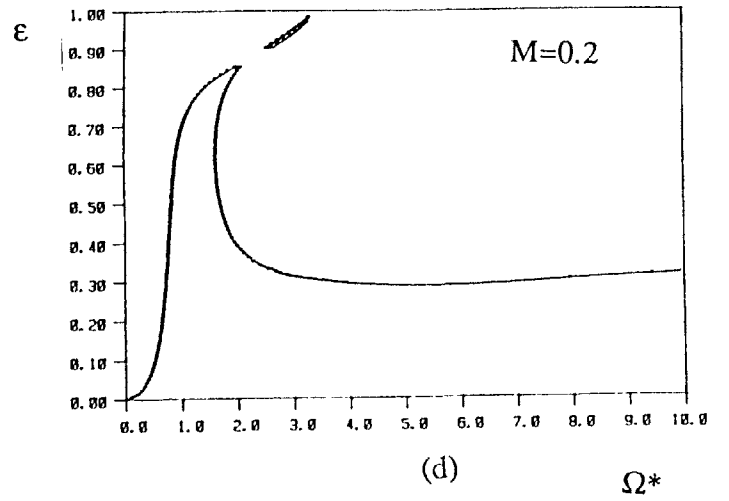
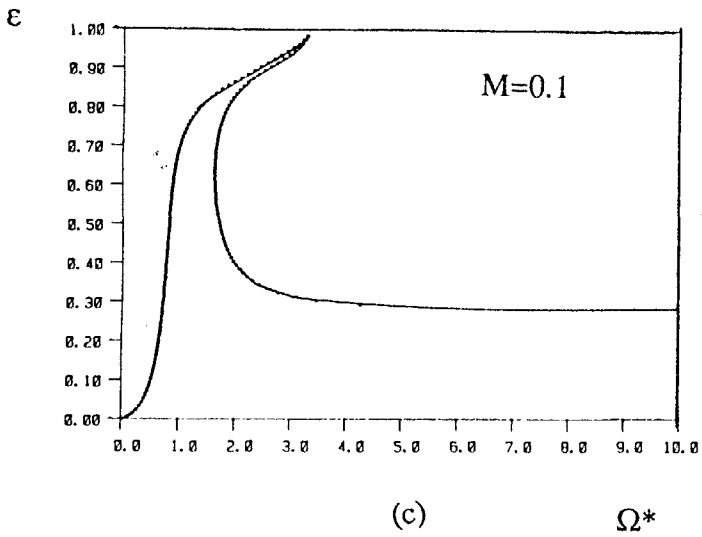
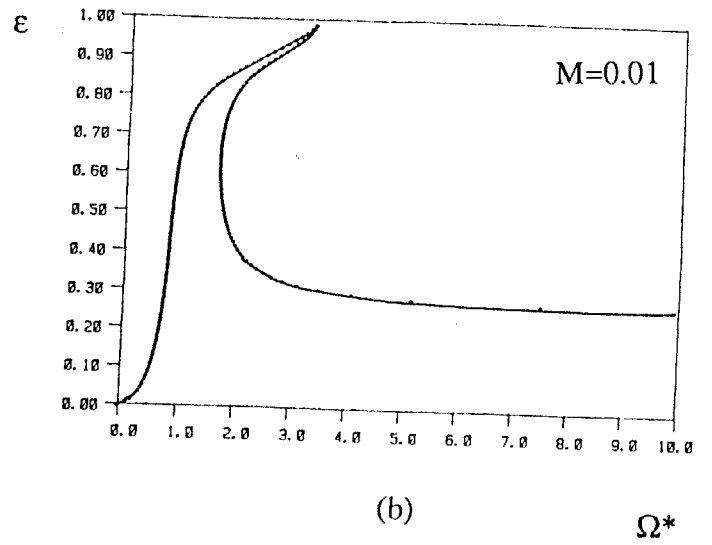
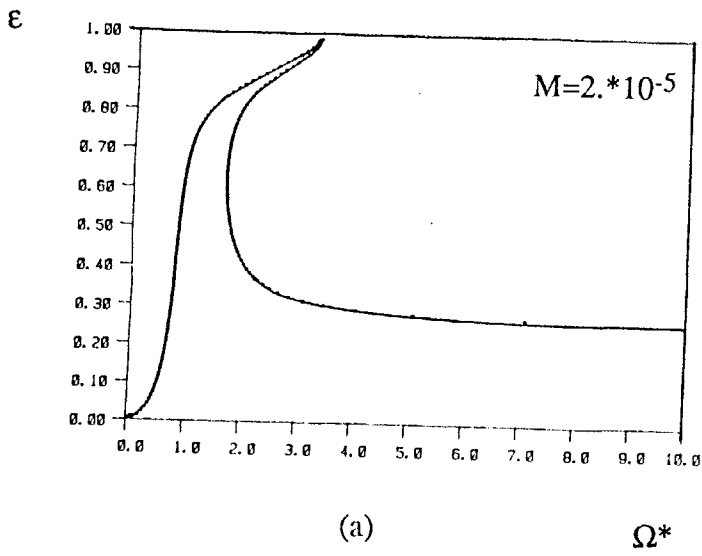


Figure 5.9 Effect of M on unbalance response of generic system, ϵ

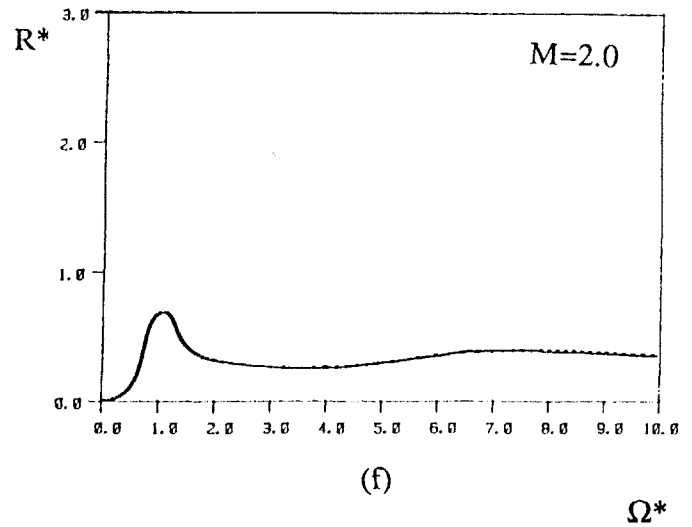
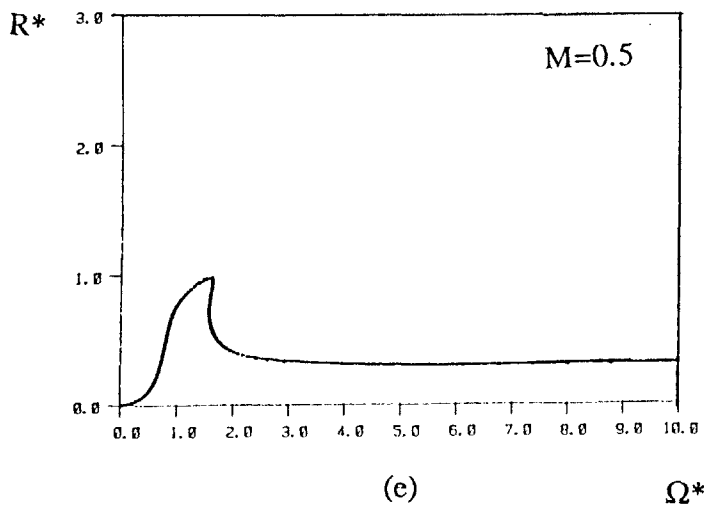
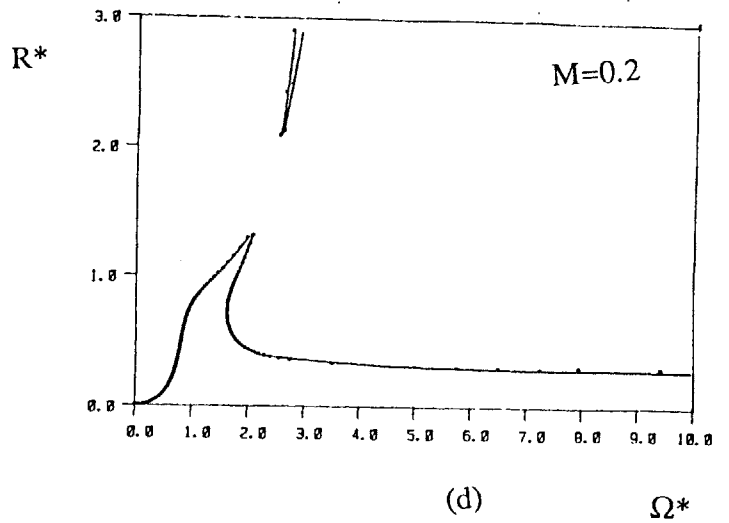
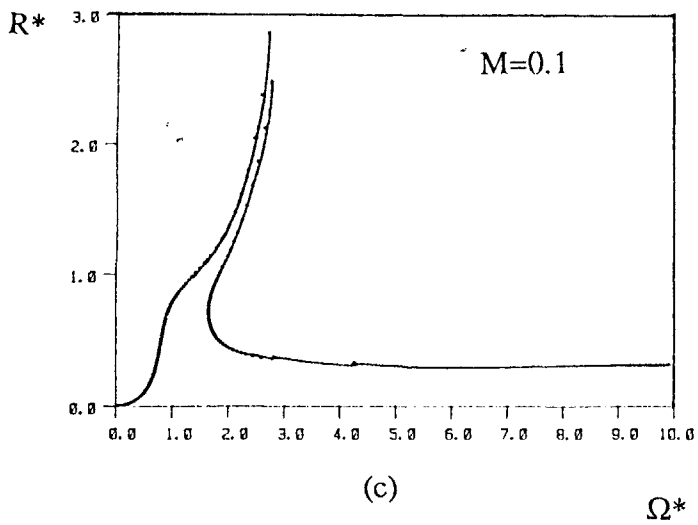
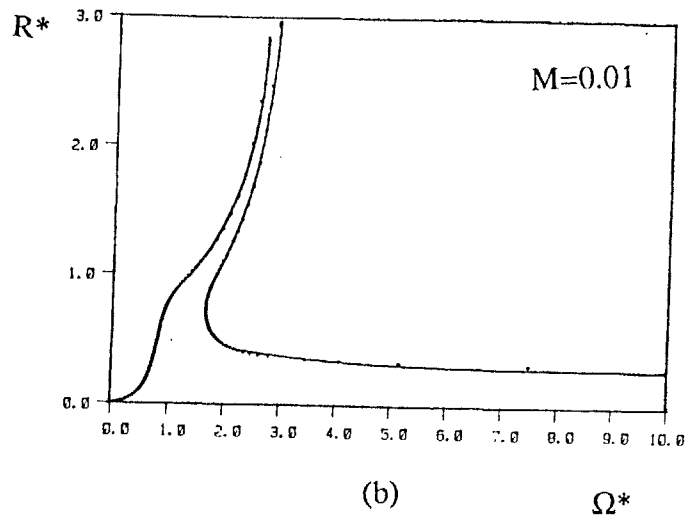
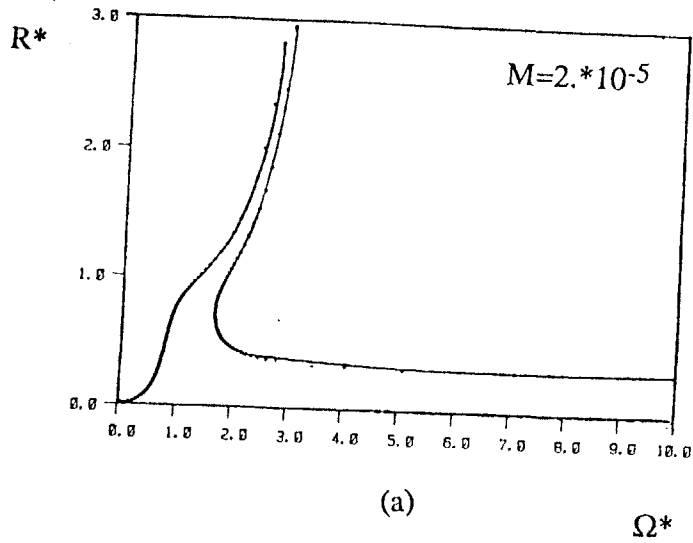
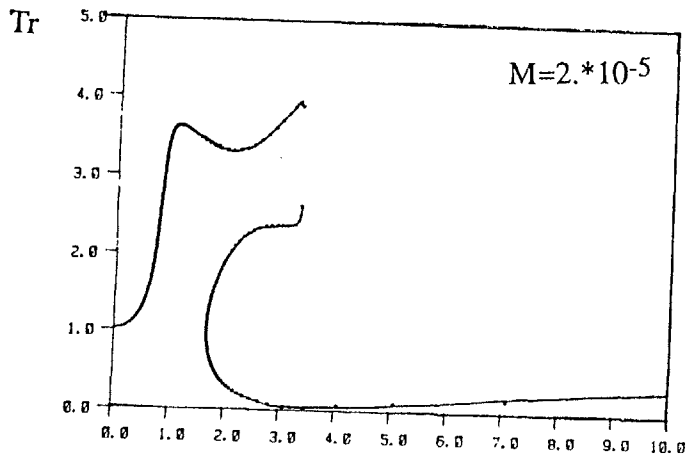
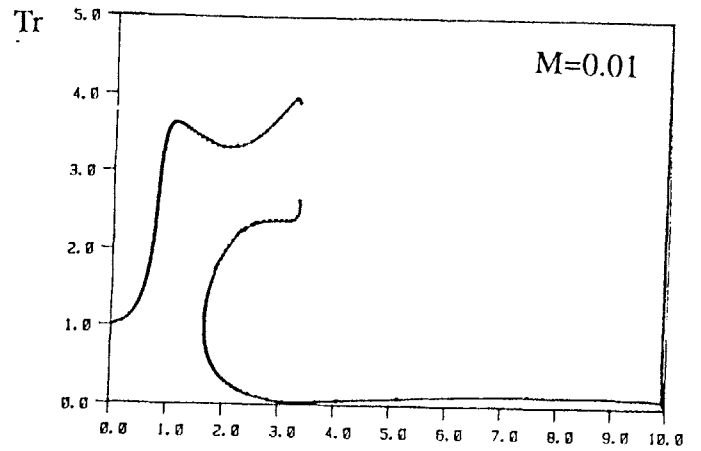


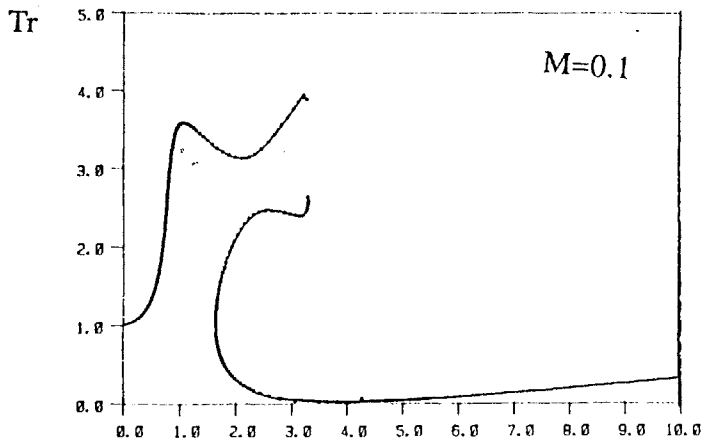
Figure 5.10 Effect of M on unbalance response of generic system, R^*



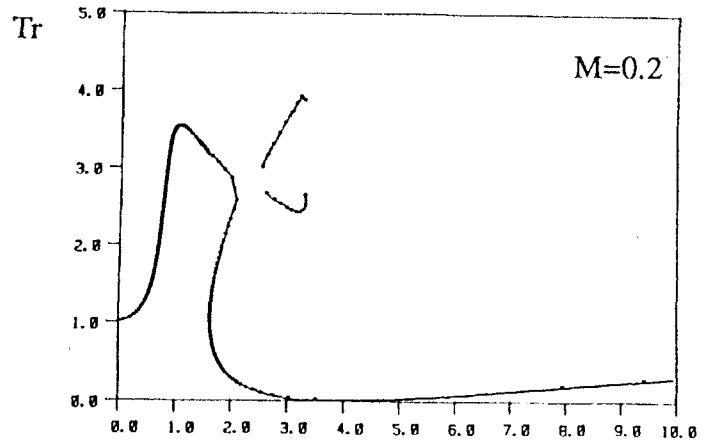
(a)

 Ω^* 

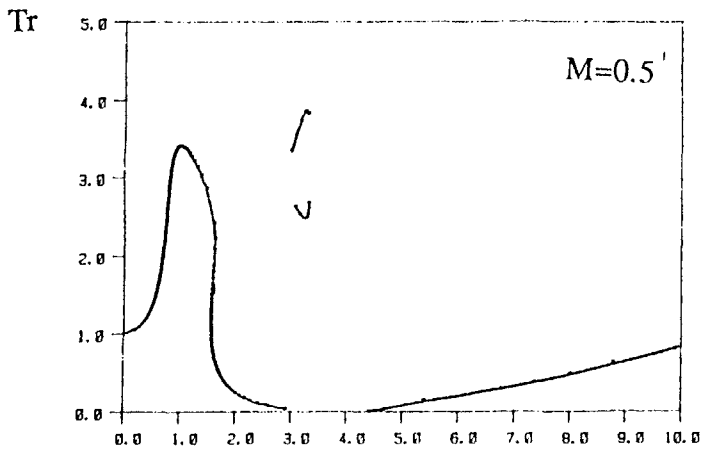
(b)

 Ω^* 

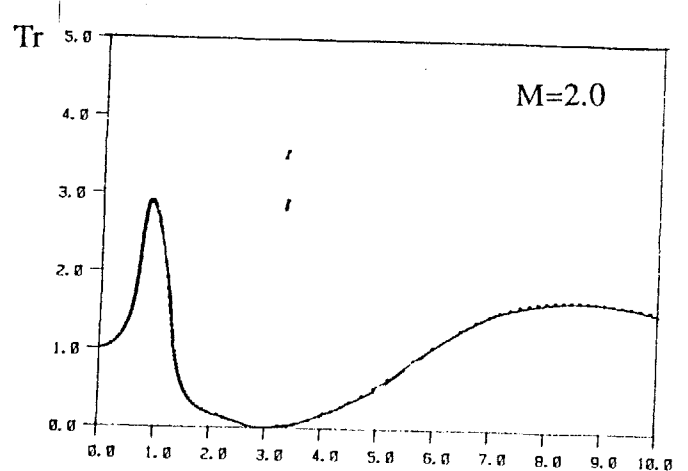
(c)

 Ω^* 

(d)

 Ω^* 

(e)

 Ω^* 

(f)

 Ω^* Figure 5. 11 Effect of M on unbalance response of generic system, Tr

dampers, and it exhibits a smaller peak relative to that due to the first mode. Figure 5.10 illustrates the effect of changing M on R^* , and it shows the same effects as for ϵ . Perhaps it should be pointed out that looking at the second critical speed (mode) from the point of view of ϵ and R^* would be quite misleading as illustrated in Figure 5.12 which shows the deflection D versus Ω^* at $M=2.0$. From which it is clear that the rotor is undergoing relatively large deflections at this mode which have to be taken into consideration when designing the rotor. Nevertheless these deflections are much smaller than those corresponding to regions III and IV, and a rotor should not be allowed to operate in region IV (region III is unstable so the rotor will never operate there). Figure 5.11 illustrates the effect of changing M on Tr . It is clear that for large M , the useful transmissibility range ($Tr < 1$) is reduced because of the second mode. For low values of M its effect is similar to that of B .

Another important parameter in determining the unbalance response of the rotor system, is the unbalance. An important question in the design of a rotor is how much unbalance would that rotor tolerate. Figures 5.13, 5.14 and 5.15 show the effect of changing the unbalance U on the unbalance response of the system. Figure 5.13 illustrates the effect of changing U on ϵ . It can be seen that for low values of U the jump resonance is reduced in magnitude, but not totally eliminated for this system. Probably as we go to lower values of U than those shown in Figure 5.13, the jump resonance would be eliminated. It has been reported in the literature [101,57,85] that decreasing the unbalance decreases the jump resonance, and would at a certain point disappear. Rotors incorporating SFDs are designed to operate at an unbalance that does not cause the rotor to exhibit the jump phenomenon. But apparently our generic system would exhibit the jump phenomenon at relatively low values of U . (Further investigation revealed that the jump could be eliminated by increasing B). For large values of U , the jump becomes pronounced and regions III and IV appear, and as U is increased regions III and IV unite

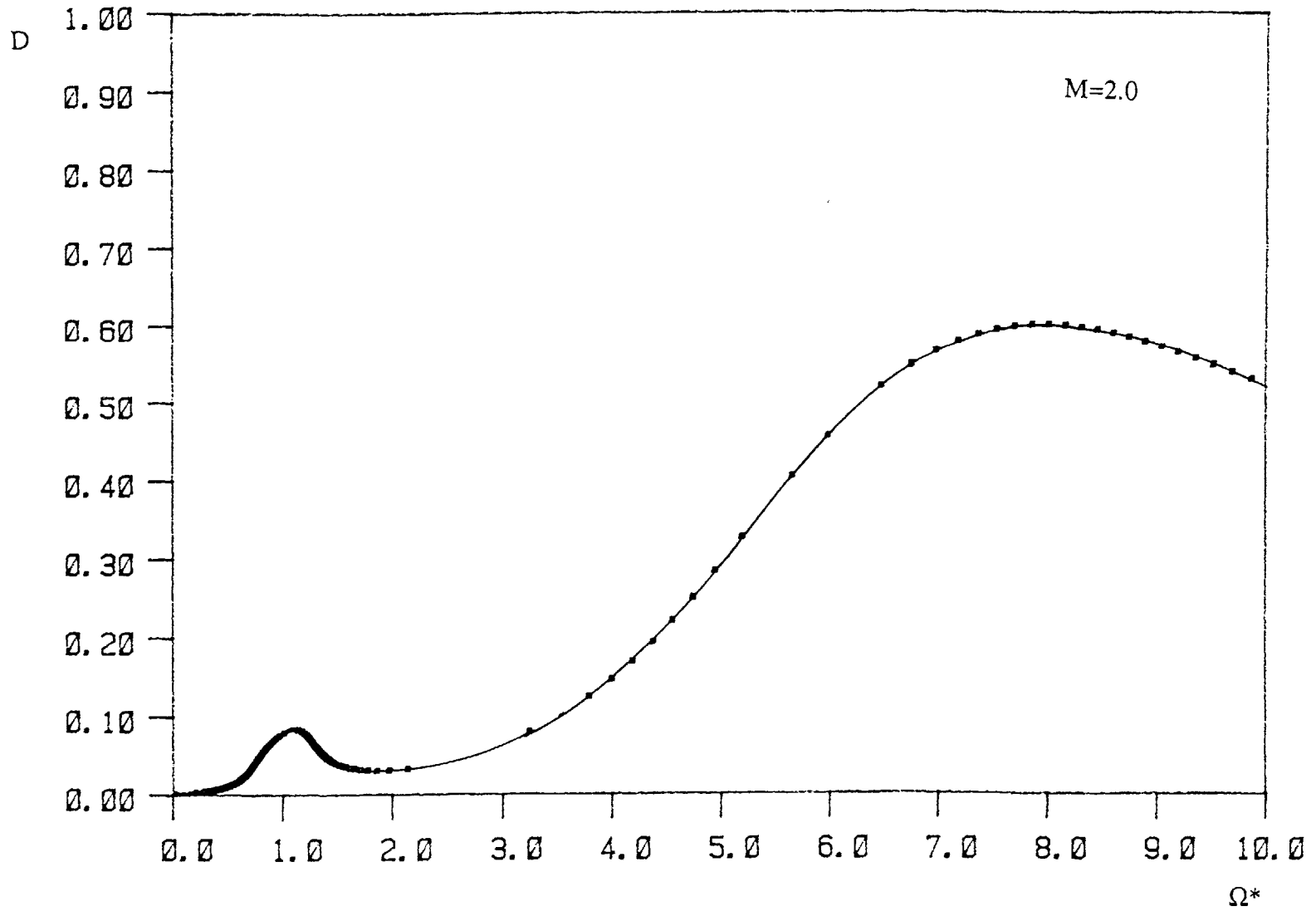


Figure 5.12 Steady state deflection of rotor at midspan for $M = 2.0$

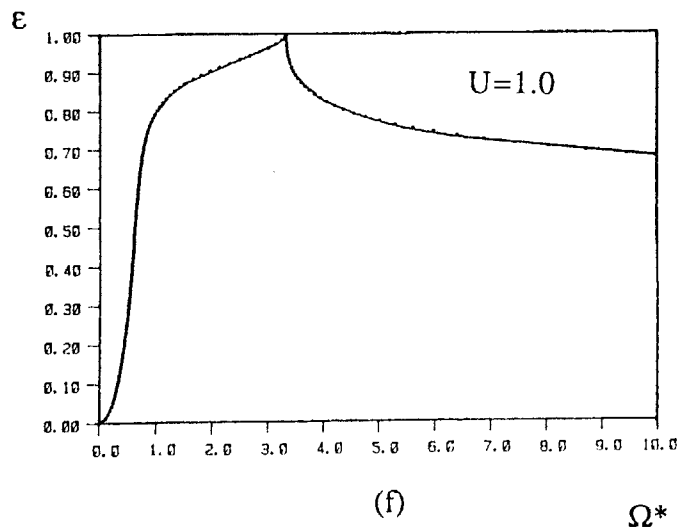
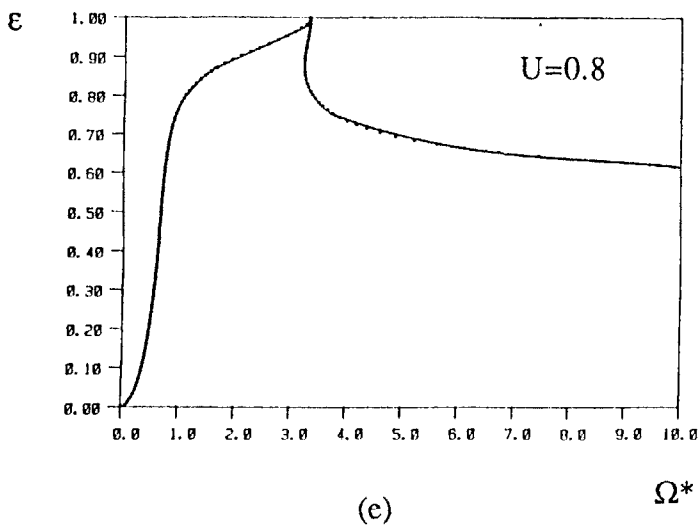
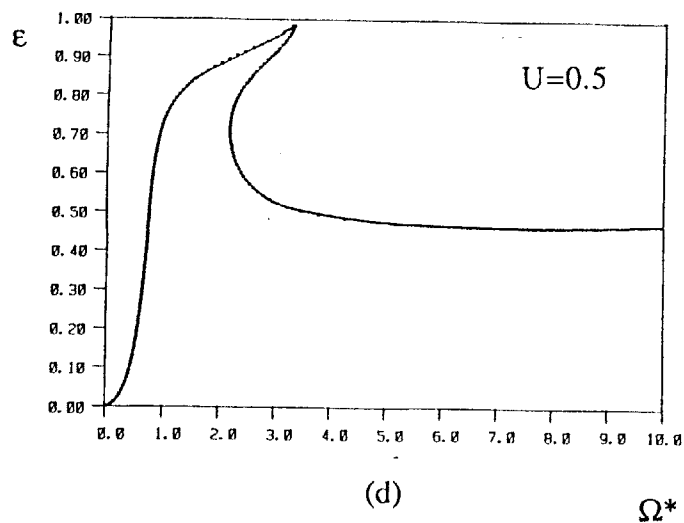
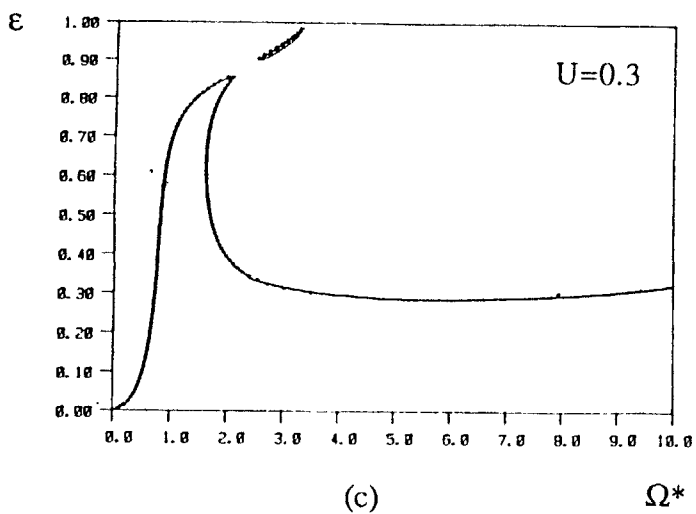
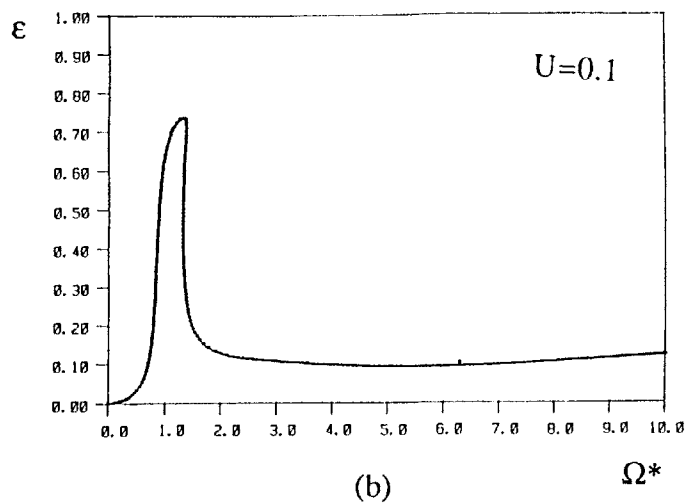
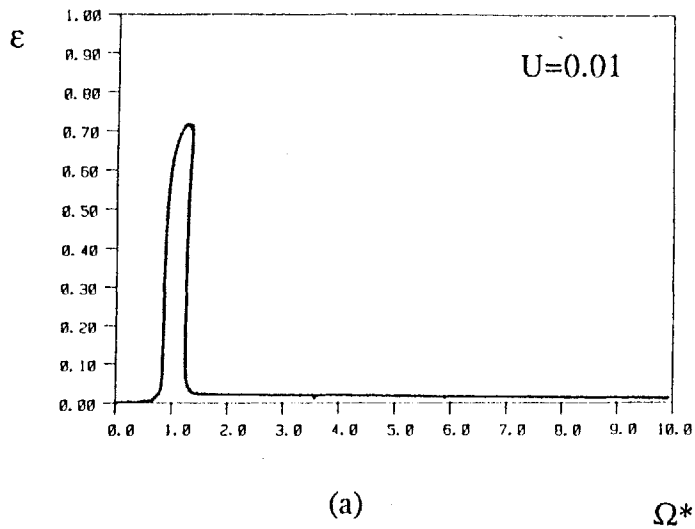


Figure 5.13 Effect of U on unbalance response of generic system, ϵ

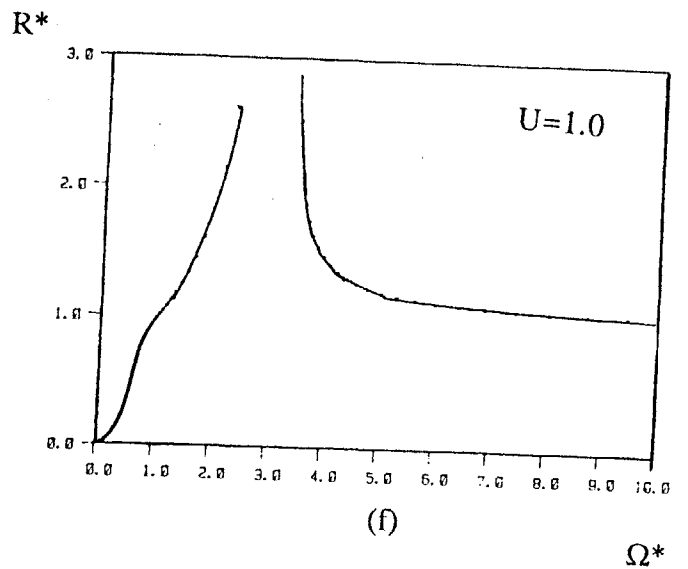
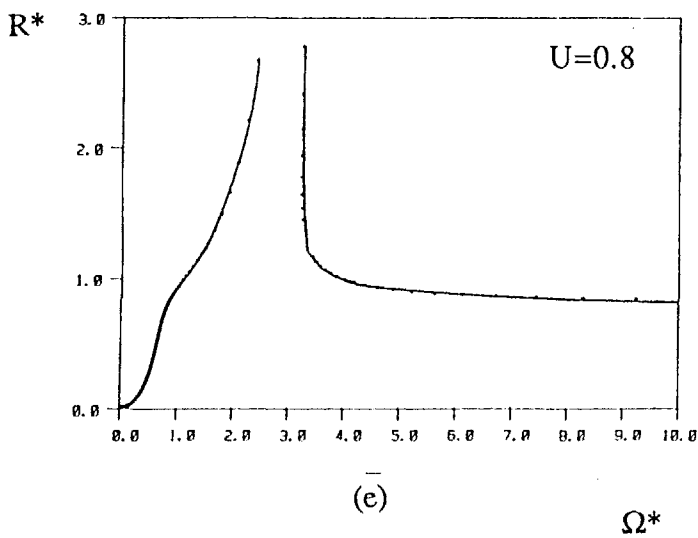
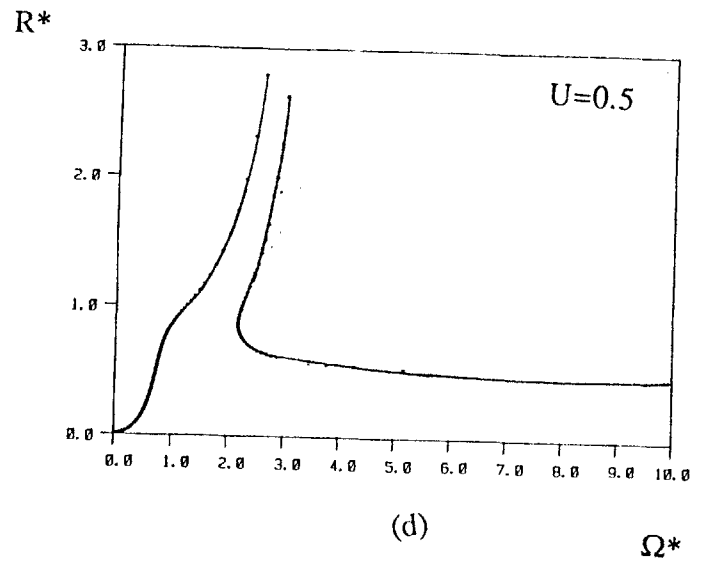
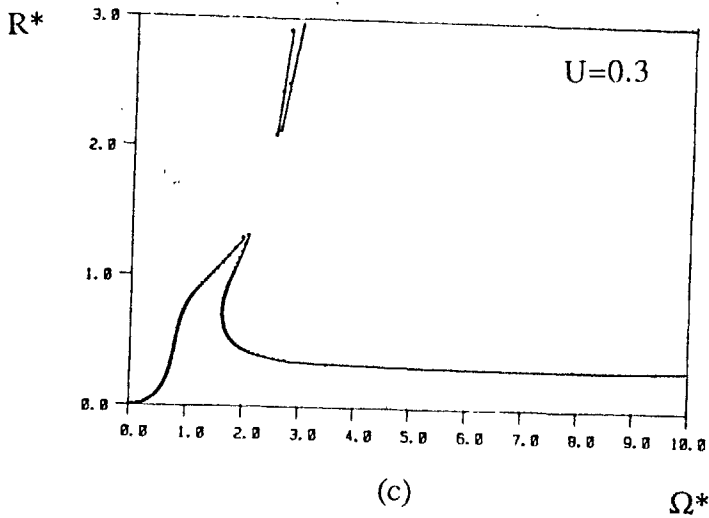
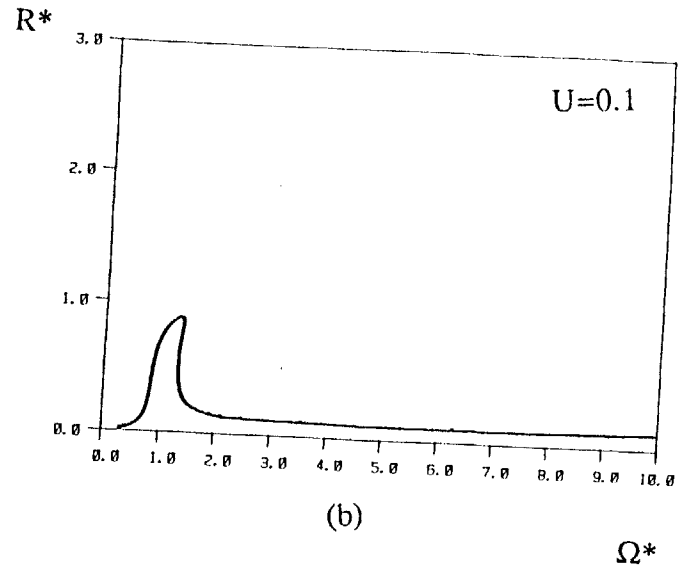
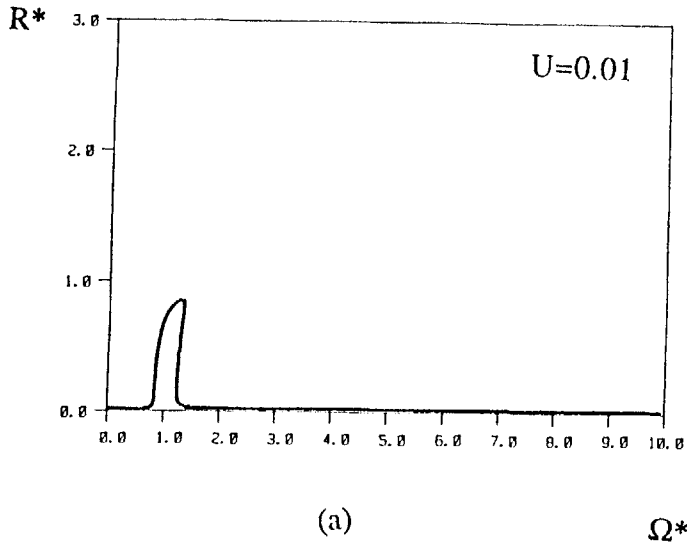
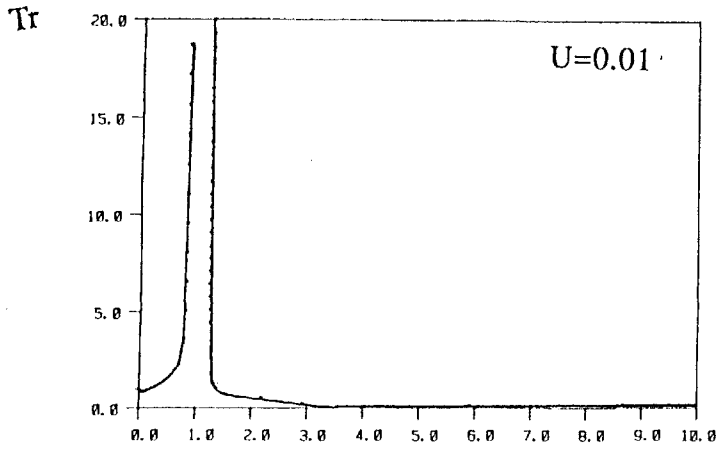
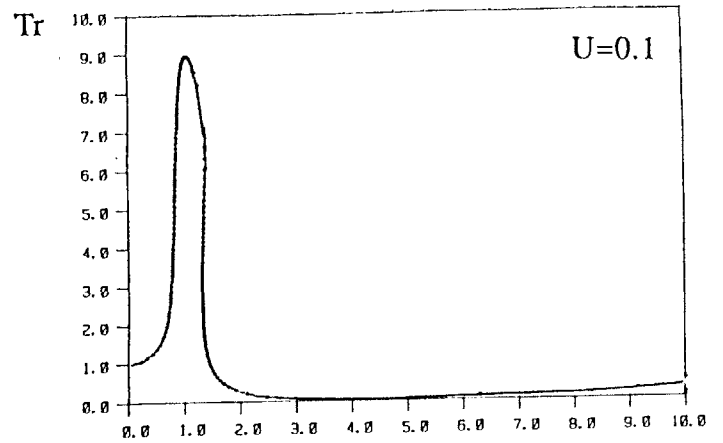


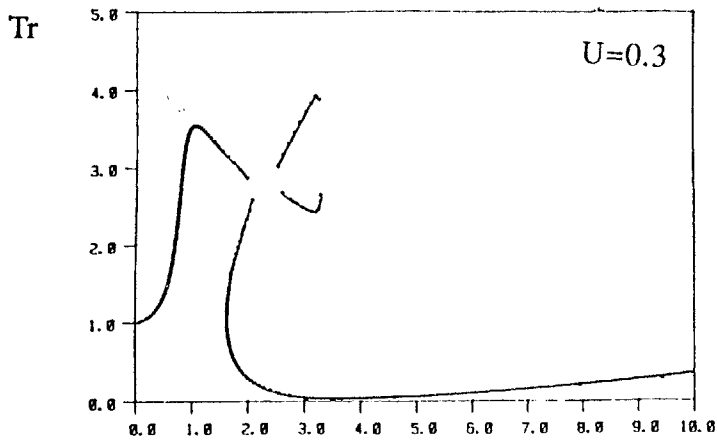
Figure 5.14 Effect of U on unbalance response of generic system, R^*



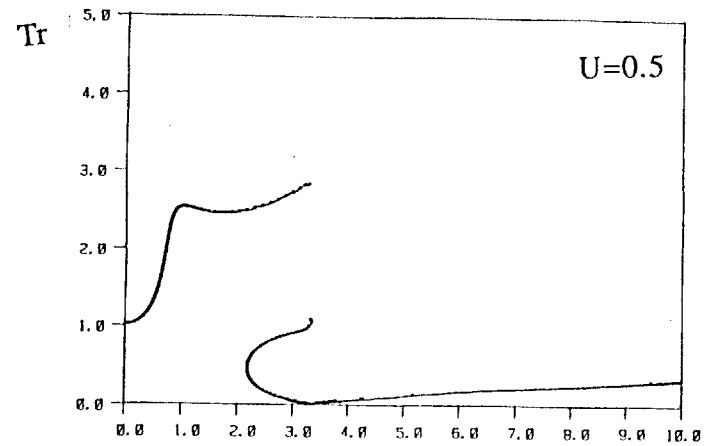
(a)

 Ω^* 

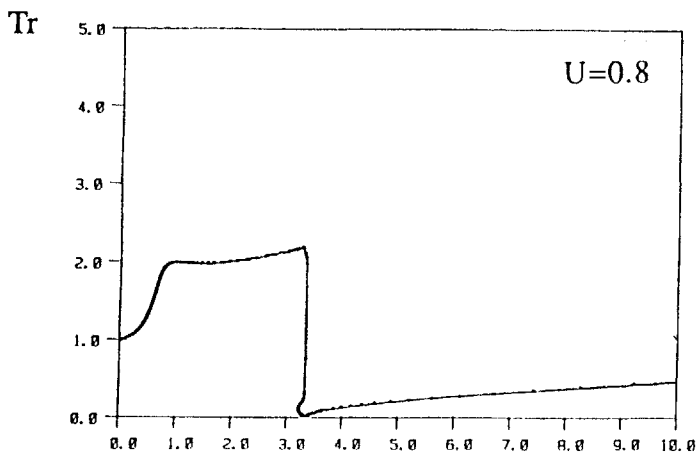
(b)

 Ω^* 

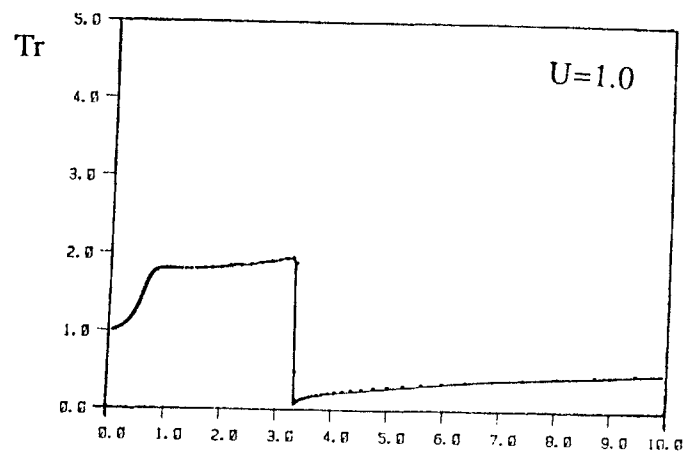
(c)

 Ω^* 

(d)

 Ω^* 

(e)

 Ω^* 

(f)

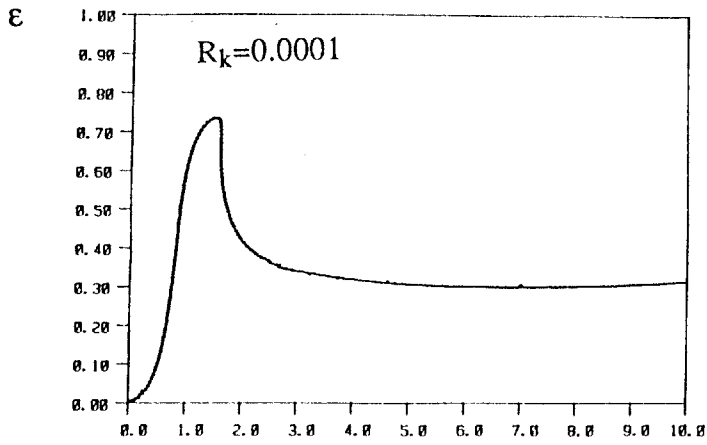
 Ω^* Figure 5.15 Effect of U on unbalance response of generic system, Tr

with regions II and I, respectively, to form an even sharper resonance. At even larger values of U , the rotor exhibits a totally unacceptable response. Figure 5.14 shows the effect of changing U on R^* , which exhibits the same characteristics as for ϵ . The same effects are illustrated in figure 5.15, which shows the effect of changing U on Tr and it reveals that, at low U , the SFD has a low transmissibility for nearly all the speed range, except at resonance. Curiously this large Tr at resonance increases with the decrease of U . This is because the force in the damper depends on ϵ and Ω^* only, which do not change much with decreasing U , (see Figure 5.13), but the damperless system would have a much lower force, and since we divide by the force in the damperless system to obtain the transmissibility, thus Tr increases. At large values of U , the transmissibility appears to be acceptable ($Tr < 1$) in a large range of speeds, but this is deceiving, since the amplitudes of motion were judged to be excessive.

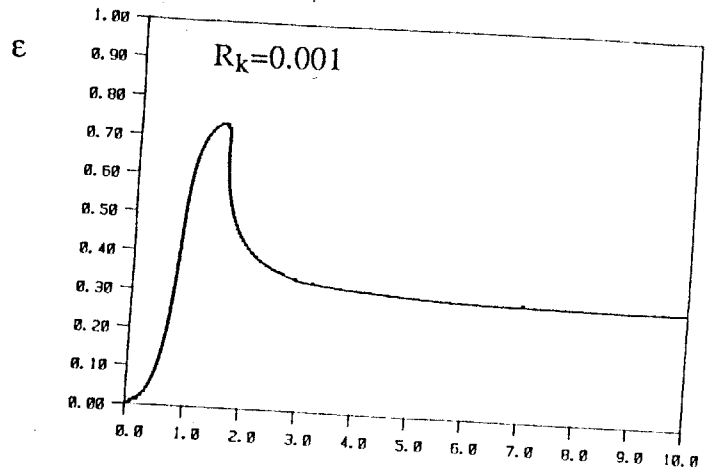
Finally, for the short damper, we investigate the effect of changing the stiffness ratio R_k on the unbalance response of the rotor. Figure 5.16 shows the effect of changing R_k on ϵ . It can be seen that low values of R_k result in the decrease of the magnitude of the jump resonance and the gradual elimination of regions, III and IV, i.e. a damper without a retainer spring, exhibits a superior unbalance response for the parameters used in our generic system. For large values of R_k , the jump resonance becomes more pronounced. The same characteristics are illustrated in Figure 5.17, which shows effect of changing R_k on R^* . Figure 5.18 shows the effect of changing R_k on Tr , from which it can be seen that a softer retainer spring results in better transmissibility characteristics.

5.4.2 Long squeeze film dampers

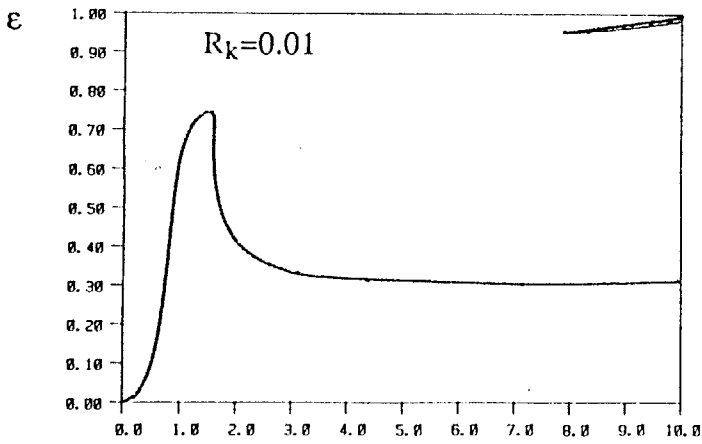
For the long SFDs we chose the same parameters for the datum damper as those of the datum damper of the short SFDs, to be able to compare both system. This is only for



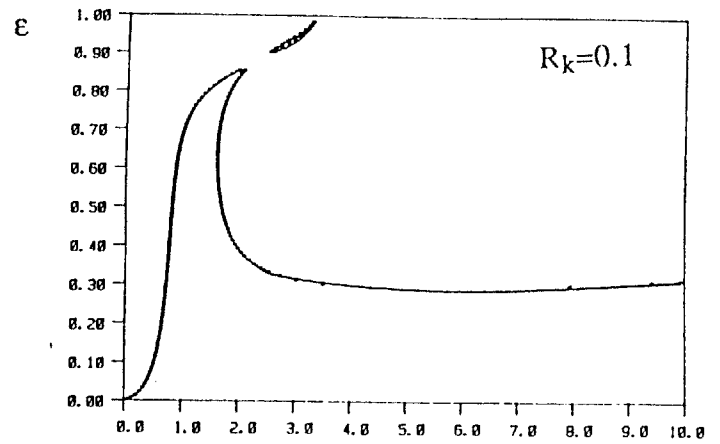
(a)

 Ω^* 

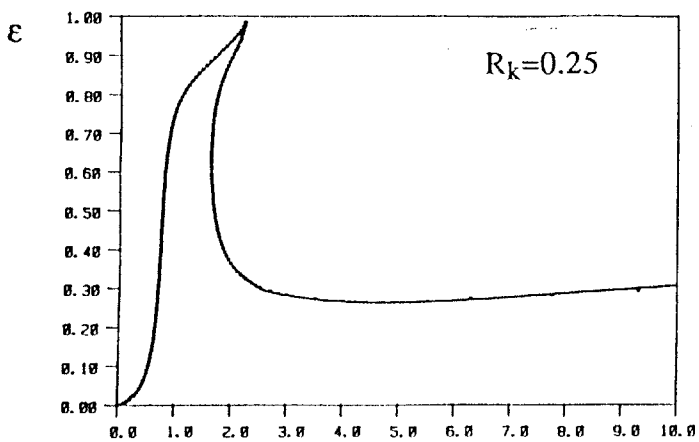
(b)

 Ω^* 

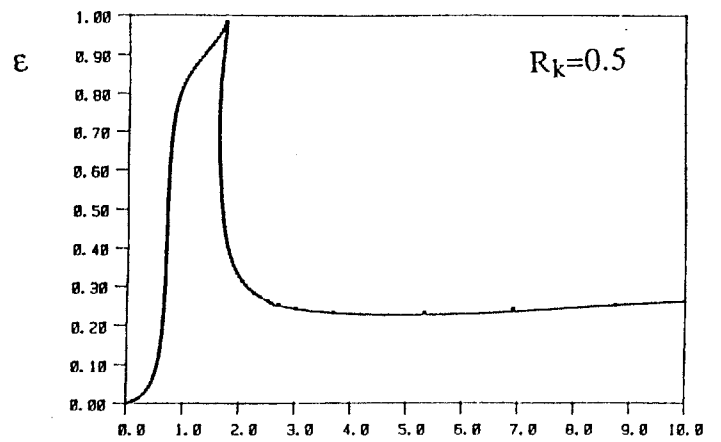
(c)

 Ω^* 

(d)

 Ω^* 

(e)

 Ω^* 

(f)

 Ω^* Figure 5.16 Effect of R_k on unbalance response of generic system, ϵ

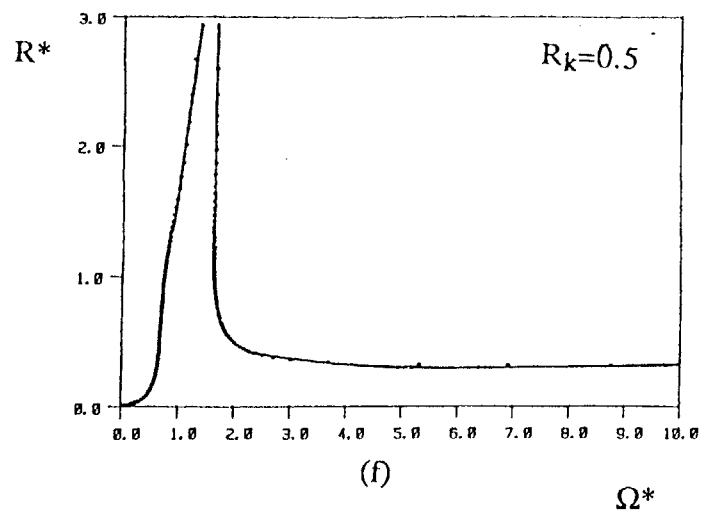
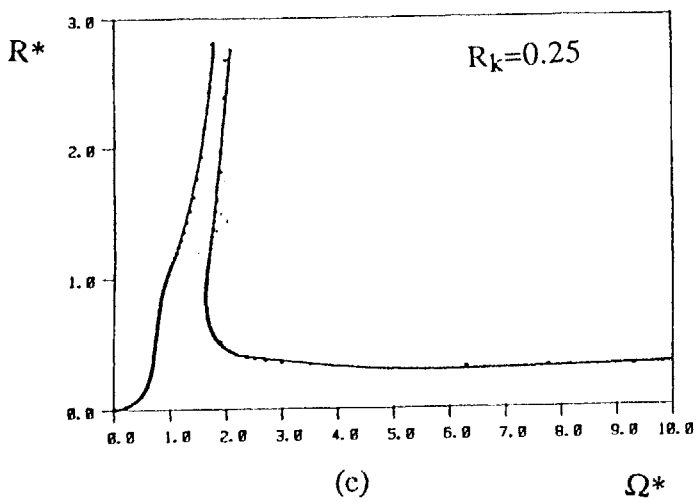
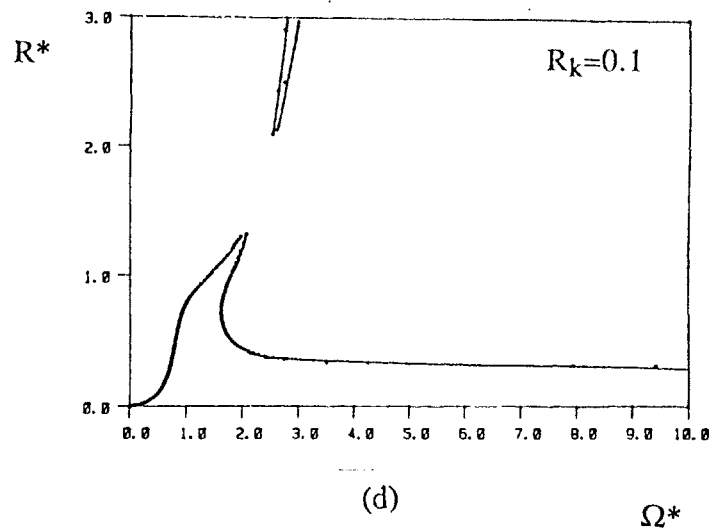
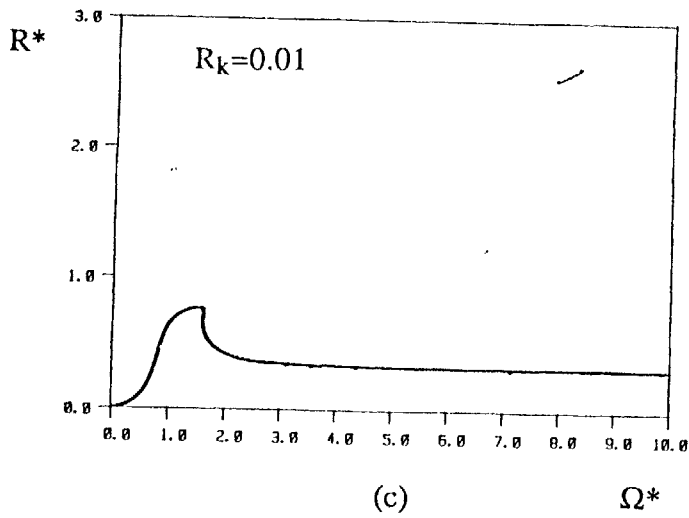
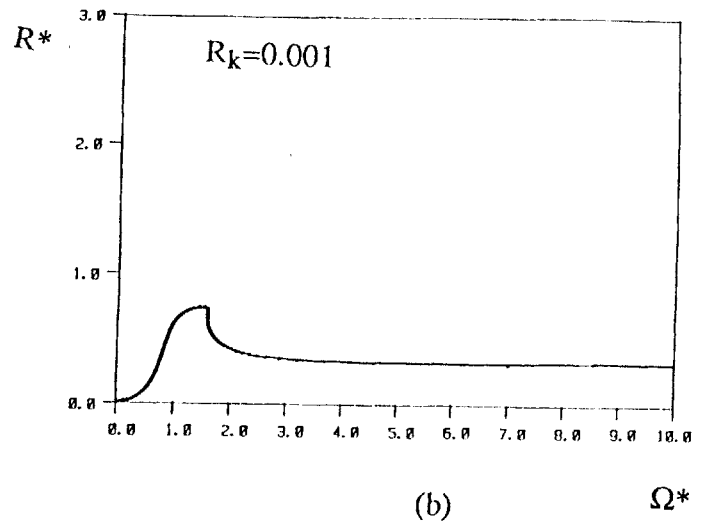
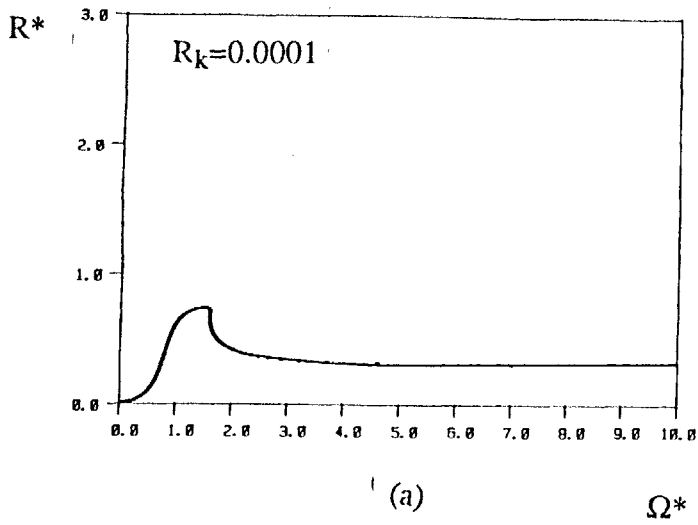


Figure 5.17 Effect of R_k on unbalance response of generic system, R^*

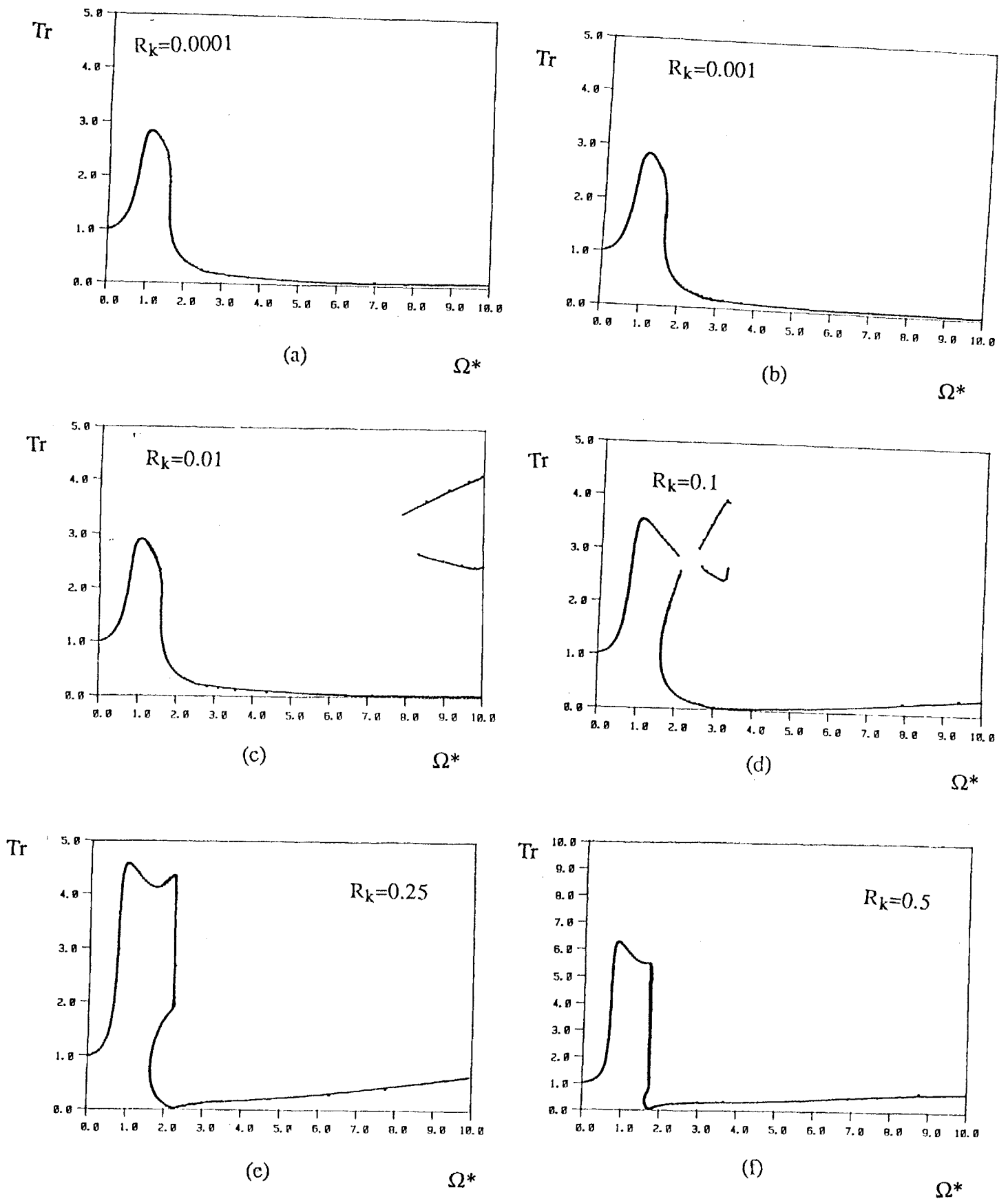
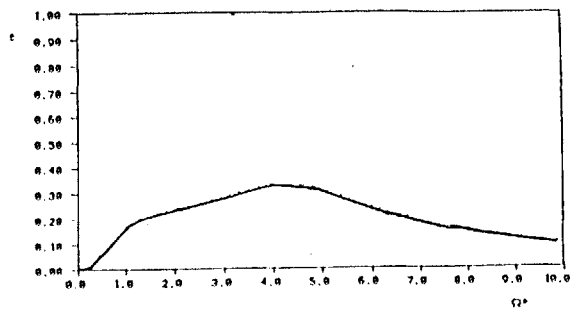


Figure 5.18 Effect of R_k on unbalance response of generic system, Tr

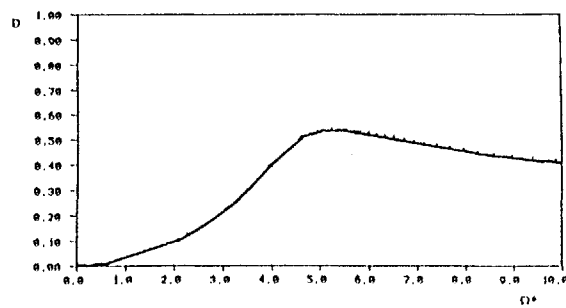
illustration purposes. The unbalance response of the datum system for the long SFD is shown in Figure 5.19. In Figure 5.19 (a) ϵ is shown versus Ω^* , which when compared with Figure 5.4 (a) reveals that for the long damper the first critical is well damped and the second critical occurs at a much lower frequency than for the short damper. The second critical has a larger amplitude than that of the first critical and regions III and IV appear only as a few points at ϵ approximately equal to 1, between the frequencies $\Omega^*=3$ and $\Omega^*=4$, and no jump occurs. Although the second critical appears at a lower frequency, yet it may be concluded that, as far as ϵ is concerned, the unbalance response of the long damper is much better than that of the short damper. Figure 5.19 (b) shows D versus Ω^* , from which it can be seen that, as pointed out earlier, the second mode results in large deflections of the rotor. This second mode is essentially due to fluid inertia, and it affects the unbalance response of the long damper at a much lower speed, as will be illustrated in the following parametric studies. Figures 5.19 (c) and (d) show the angles α and β , respectively, versus Ω^* . Figure 5.19 (e) shows R^* versus Ω^* , and it shows the same characteristics as those for ϵ . Now, Figure 5.19 (f) shows that the transmissibility is large ($Tr > 1$) for the second mode, thus this results in a narrow speed range in which the long SFD would be a good isolator ($Tr < 1$).

Figure 5.20 shows the effect of a full 2π -film on the unbalance response of the datum system. It can be seen, that pressurization results in more damping of the first mode, but the second mode becomes sharper and it moves closer to the first mode. No jump occurs and no regions III and IV. Also, as can be seen from the Tr plot, the vibration isolation capability of the damper ($Tr < 1$ region) is limited to a narrower speed range than that of the datum system.

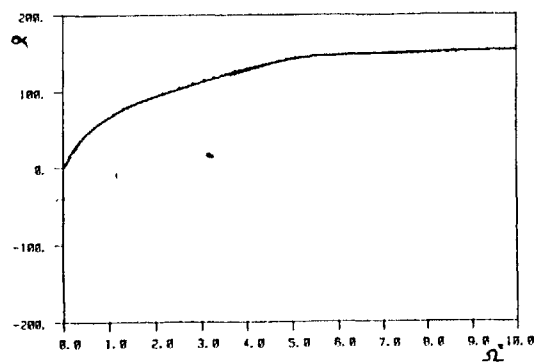
Figures 5.21, 5.22 and 5.23 illustrate the effects of changing the parameter B on the unbalance response of the datum system. Figure 5.21 shows the effect of changing B



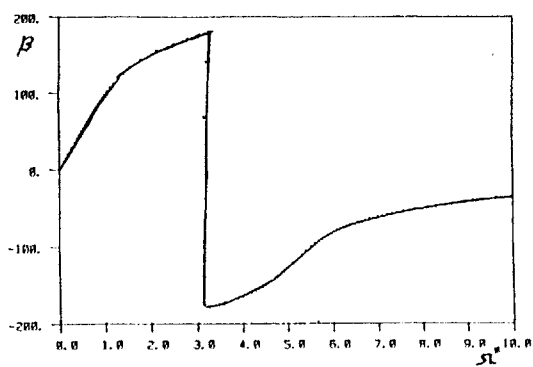
(a)



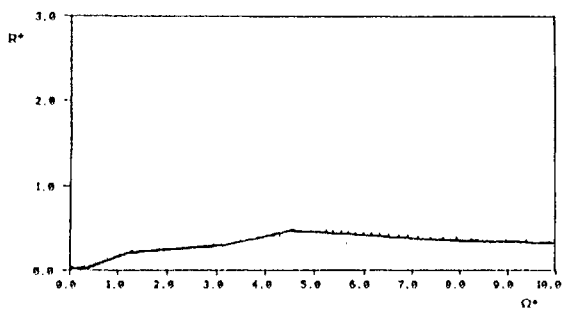
(b)



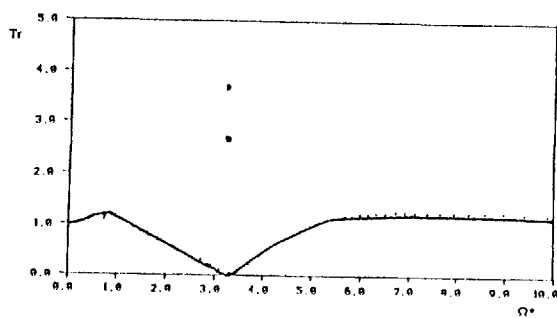
(c)



(d)



(e)



(f)

Figure 5.19 Unbalance response of long damper datum system

2 π -Film

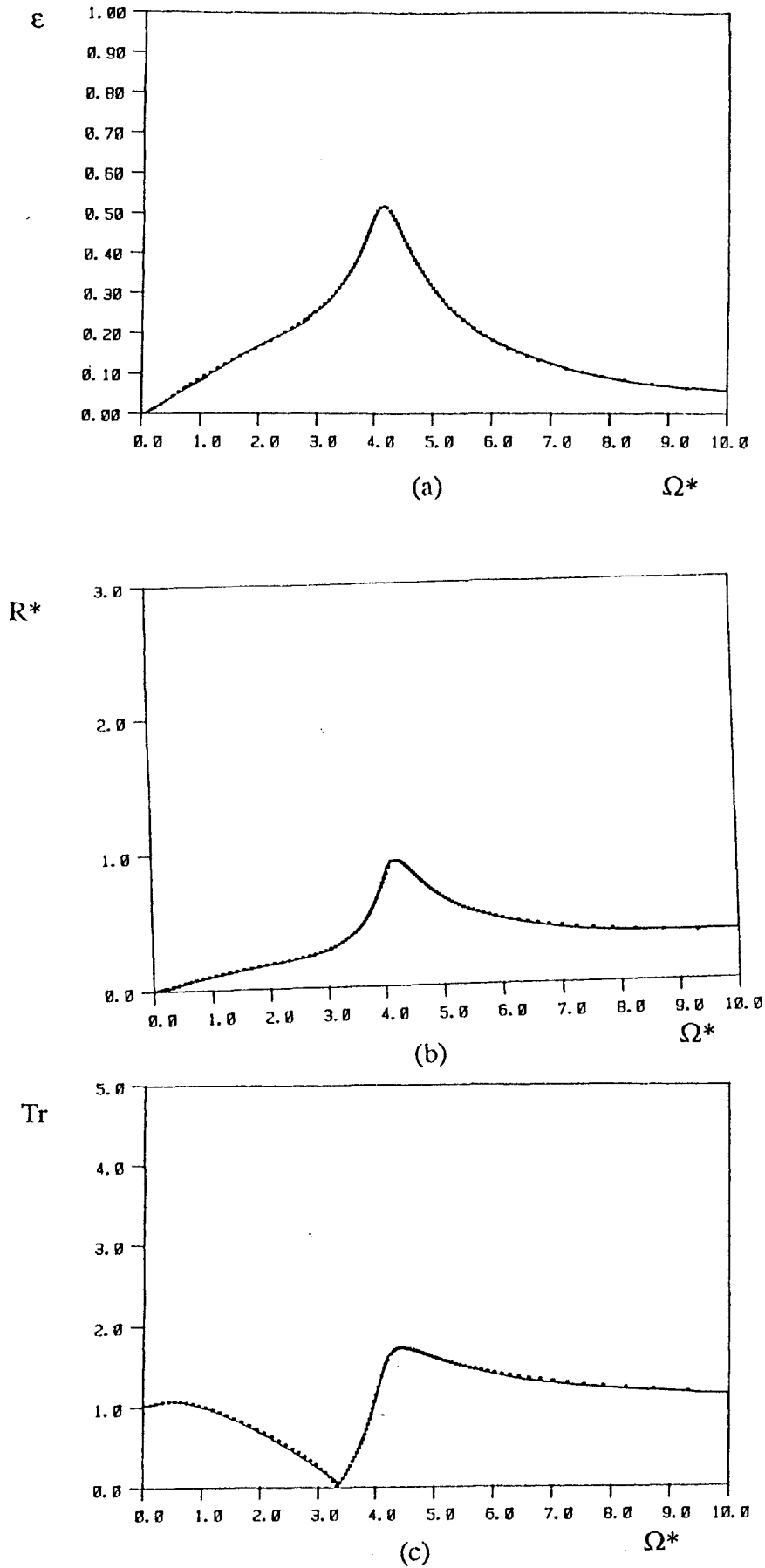


Figure 5.20 Unbalance response of long damper datum system, 2 π -film

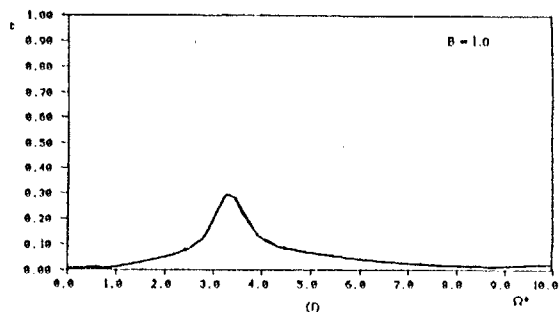
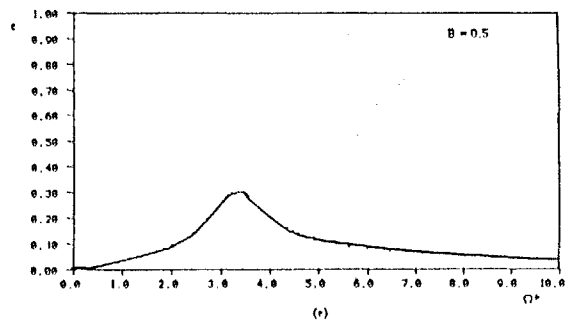
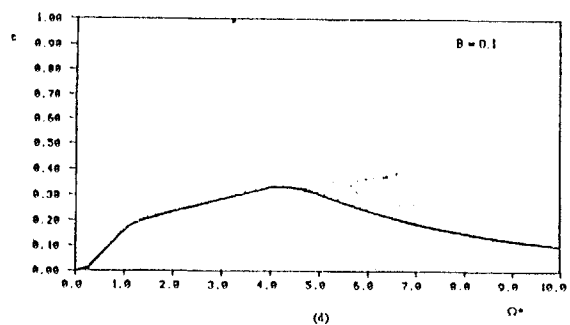
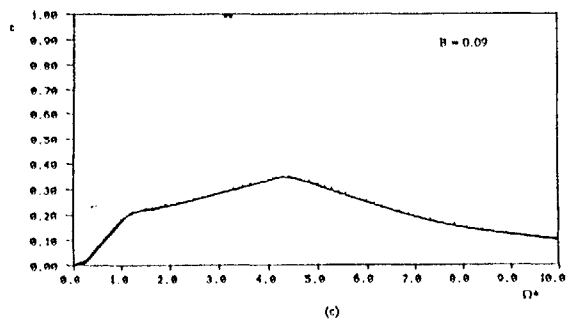
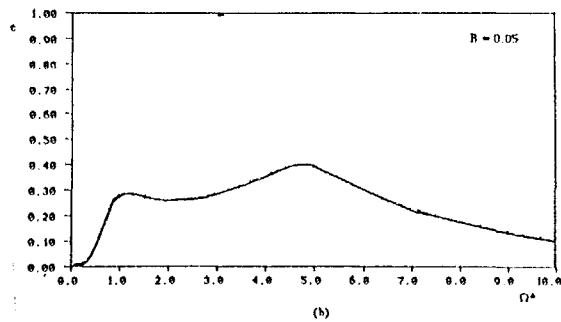
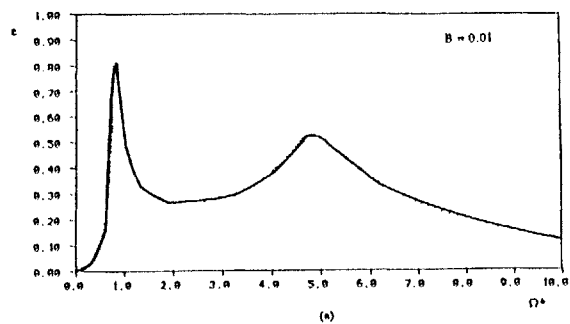


Figure 5.21 Effect of B on unbalance response of long damper datum system, ϵ

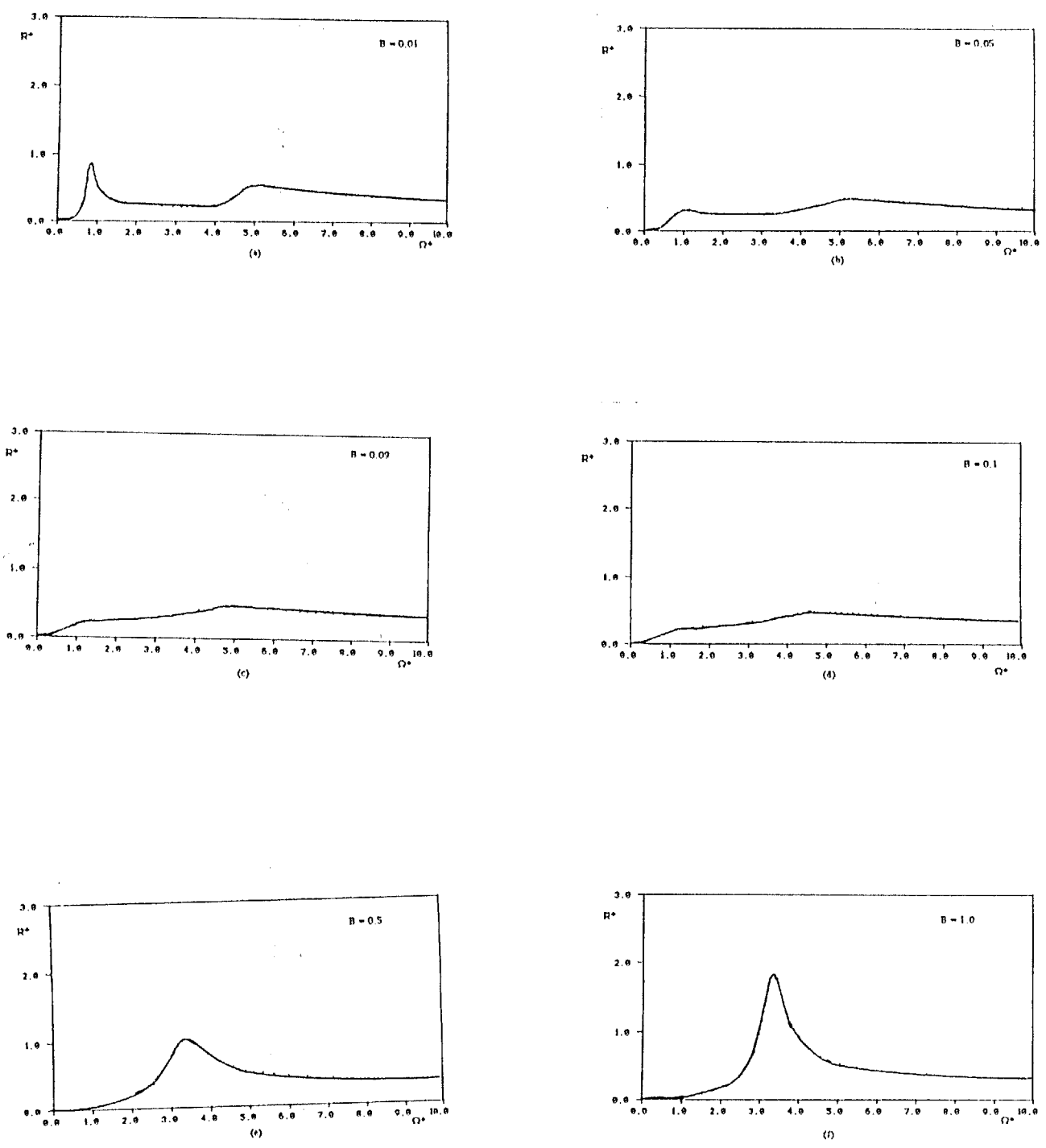


Figure 5.22 Effect of B on unbalance response of long damper datum system, R^*

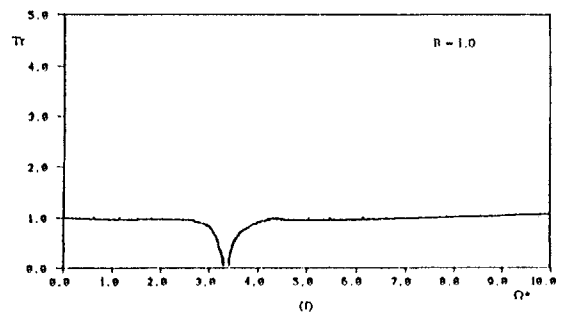
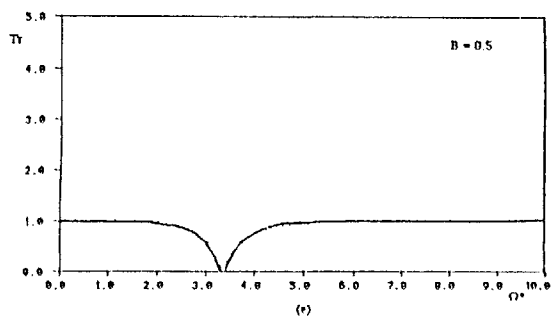
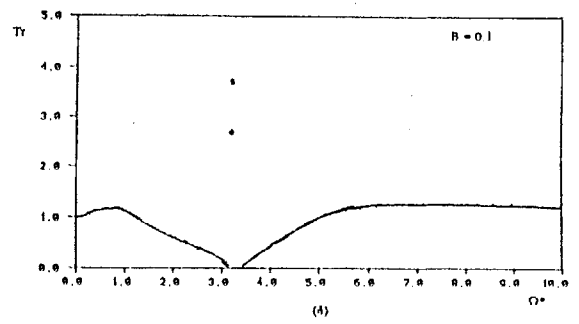
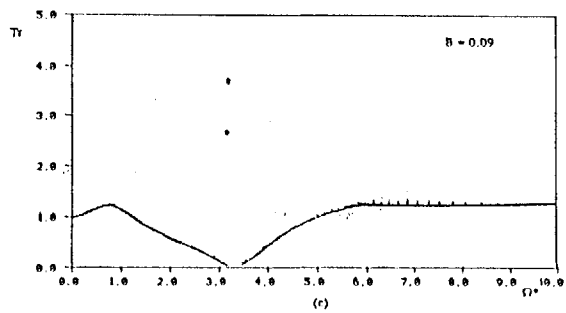
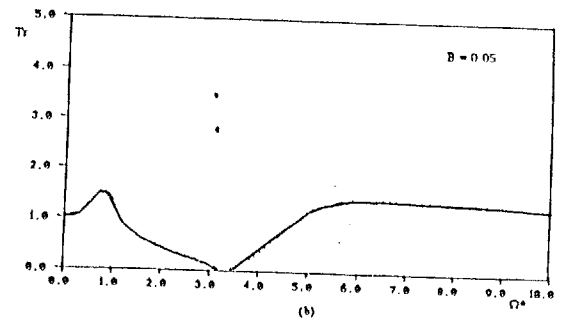
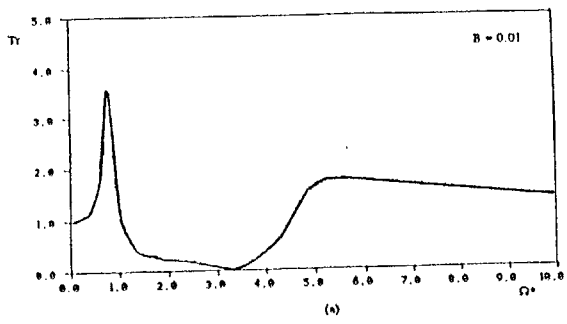


Figure 5.23 Effect of B on unbalance response of long damper datum system, Tr

on ϵ , from which it can be seen that for low values of B the response becomes sharper at resonance. For large values of B , the first mode is suppressed, and only the second mode shows appreciable response. The same characteristics are displayed in Figure 5.22 which shows the effect of changing B on R^* . For large B it is clear that the excited mode is the second mode since it results in large deflections of the rotor, which has been demonstrated to be a characteristic of the second mode. Figure 5.23 shows the effect of changing B on Tr . As B is increased the region of successful vibration isolation ($Tr < 1$) is narrowed. While for low B the force transmitted to the engine frame is larger at the critical speeds. For very large B the damper acts as a hard mount ($Tr = 1$) for most of the speed range.

Figures 5.24, 5.25 and 5.26 show the effects of changing M on the unbalance response of the datum system. The effect of changing M on the eccentricity ratio ϵ is shown on Figure 5.24, from which it can be seen that for very low values of M only one mode is excited and it is well damped. A few points appear near $\epsilon = 1$, which are in regions III and IV. For large values of M the second mode is excited and regions III and IV diminish. For larger M , the second mode exhibits a sharp resonance and regions III and IV disappear. The same characteristics are displayed in Figure 5.25 which shows the effect of changing M on R^* . Figure 5.26 illustrates the effect of changing M on Tr , and it can be seen that for large values of M the region of successful vibration isolation ($Tr < 1$) is narrowed, and the force transmitted to the engine frame near the second critical is large.

The effect of the unbalance U on the unbalance response of the datum system is illustrated in Figures 5.27, 5.28 and 5.29. The effect of changing U on ϵ is shown in Figure 5.27, from which it can be seen that the datum system attenuates both critical speed well for low values of U (the response of the system for $U = 0.01$ is very small and is not shown). For larger values of U the response becomes more pronounced and regions III and IV appear and increase in size. For even larger values of U , regions III and IV unite

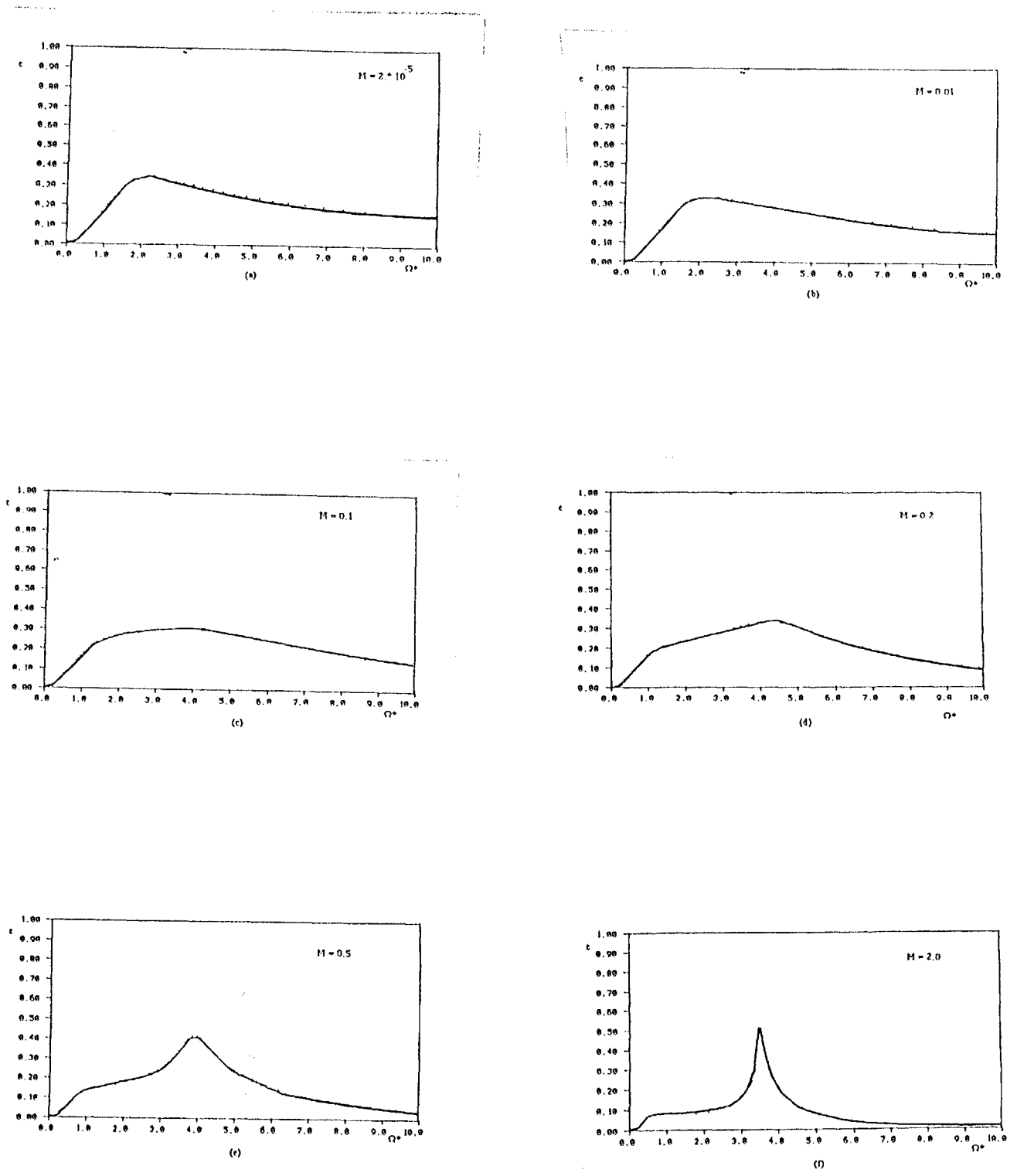


Figure 5.24 Effect of M on unbalance response of long damper datum system, ϵ

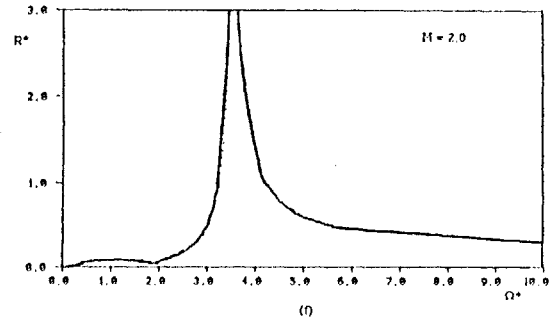
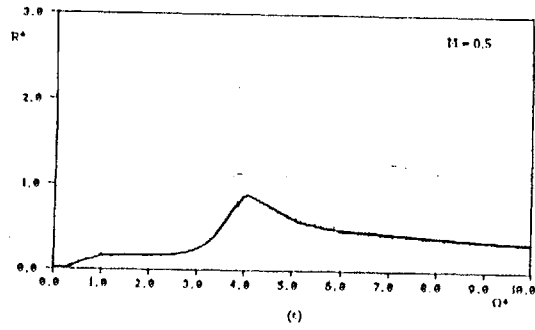
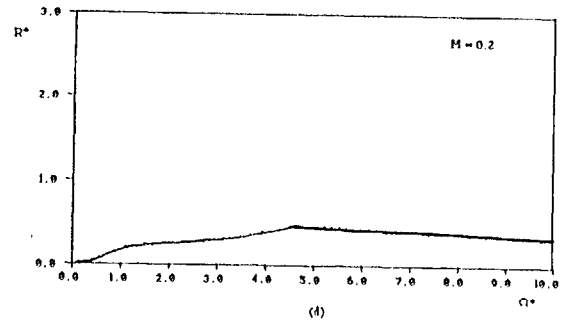
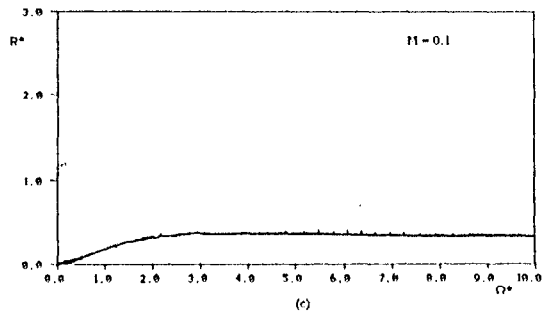
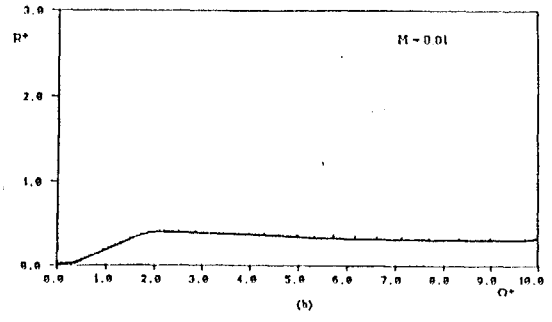
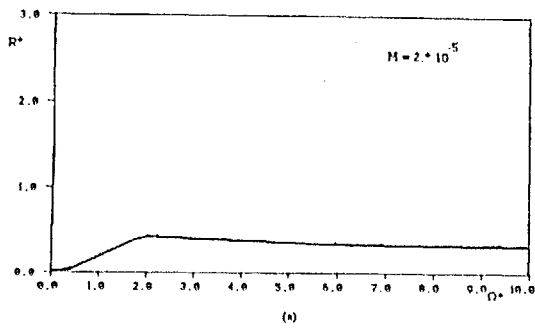


Figure 5.25 Effect of M on unbalance response of long damper datum system, R^*

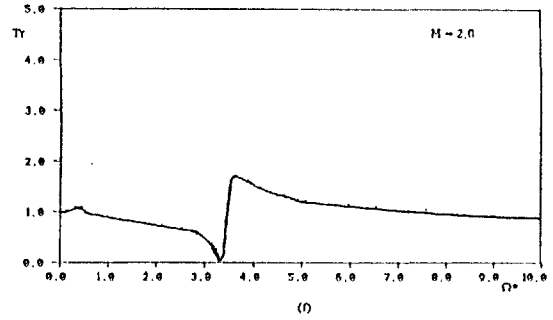
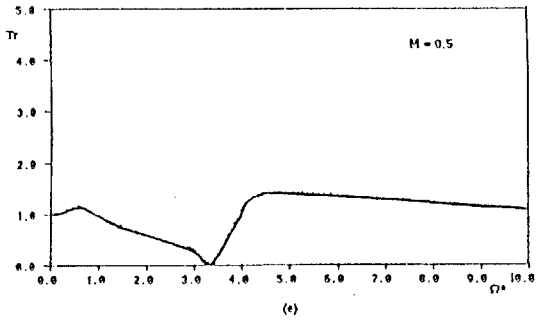
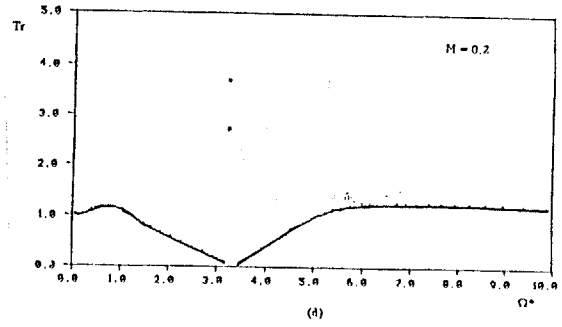
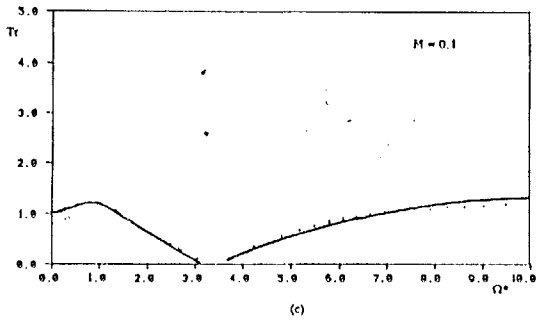
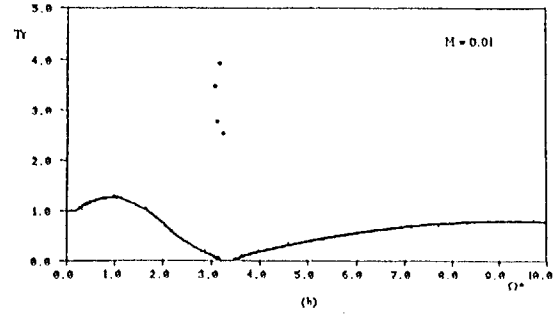
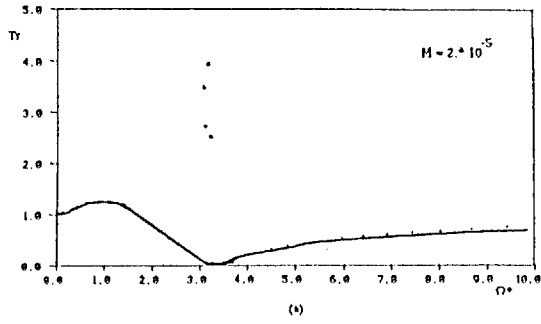


Figure 5. 26 Effect of M on unbalance response of long damper datum system, Tr

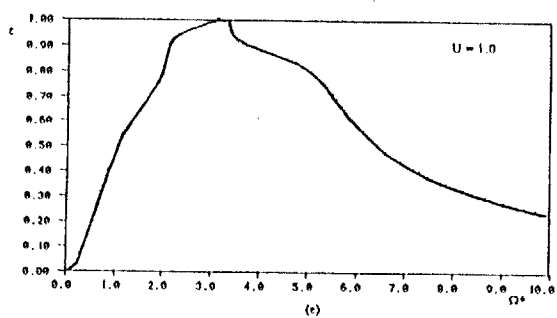
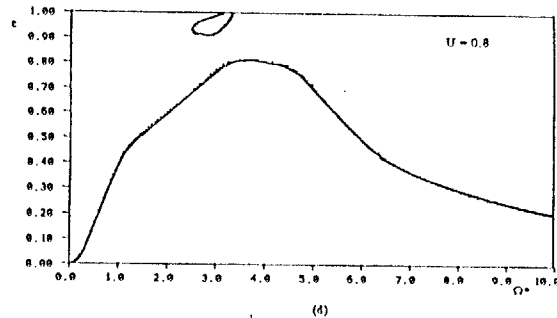
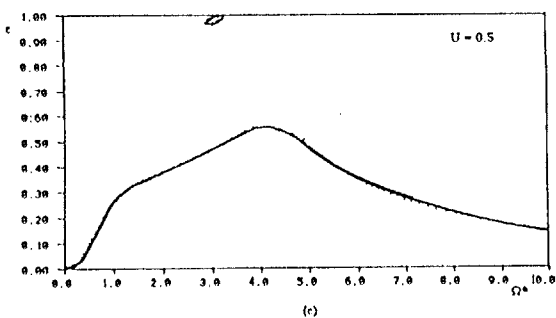
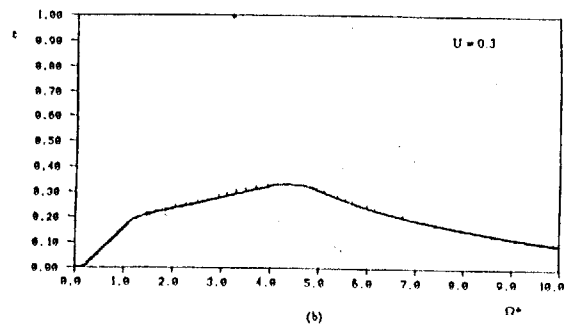
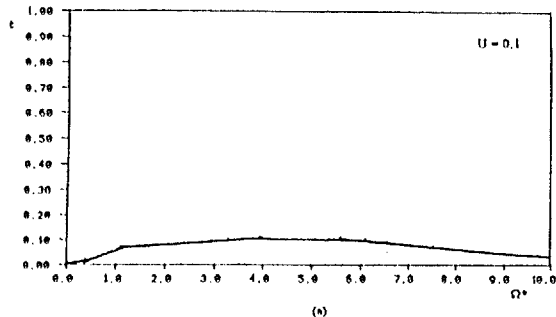


Figure 5.27 Effect of U on unbalance response of long damper datum system, ϵ

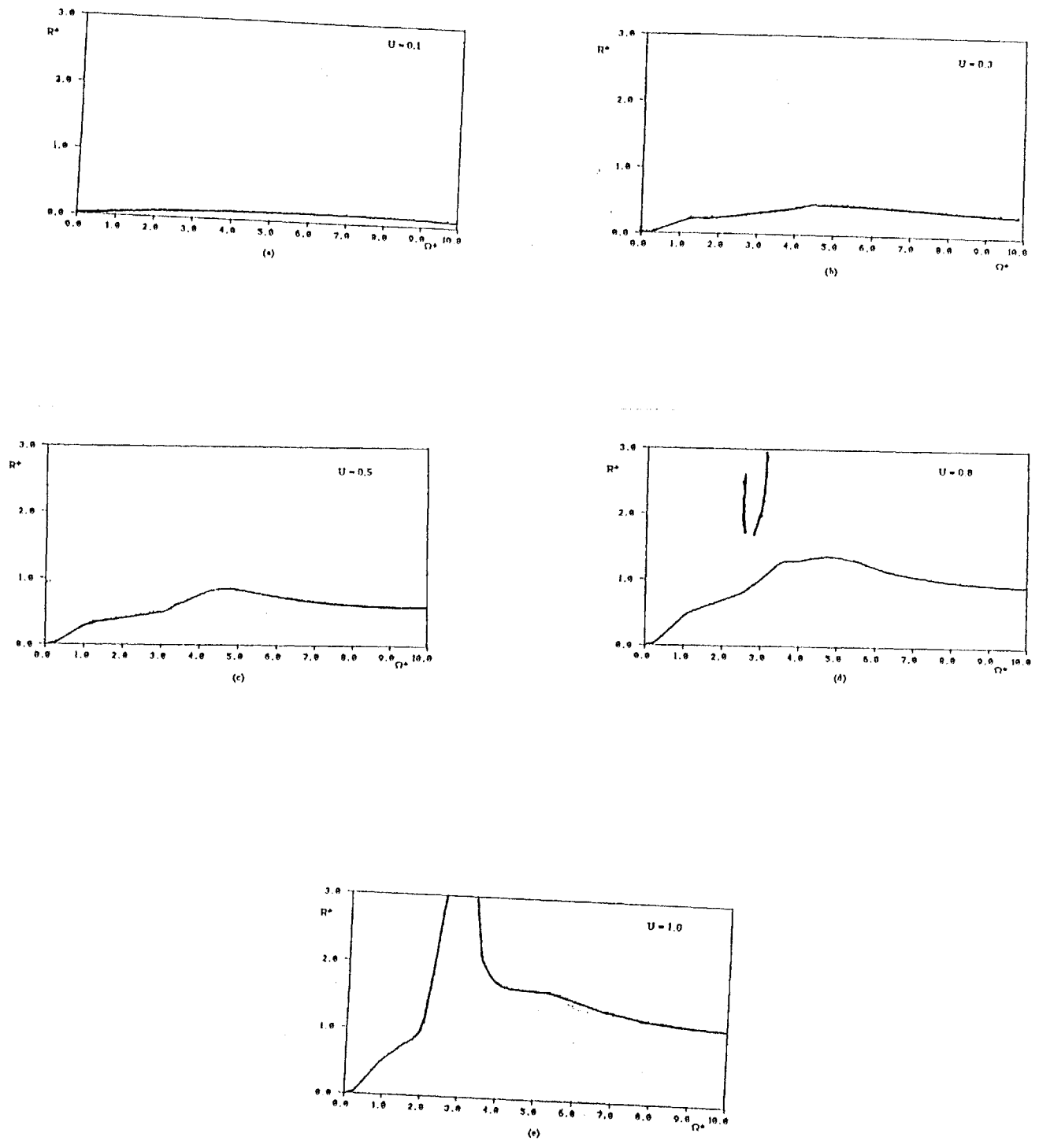


Figure 5.28 Effect of U on unbalance response of long damper datum system, R^*

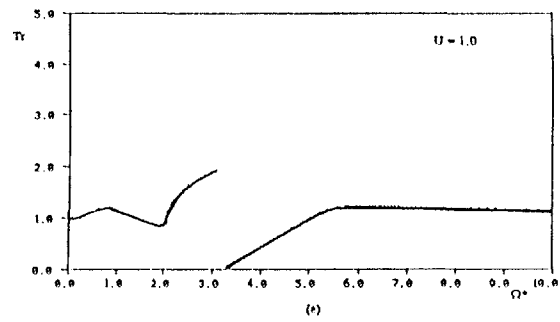
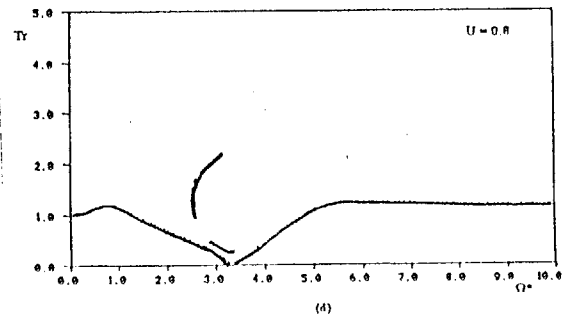
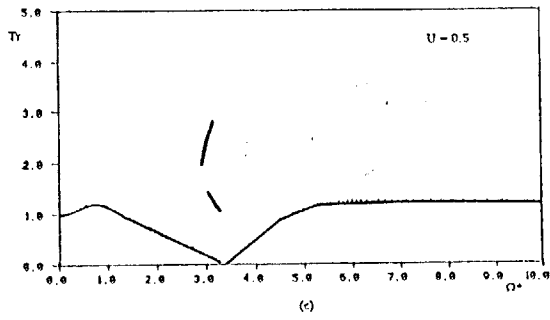
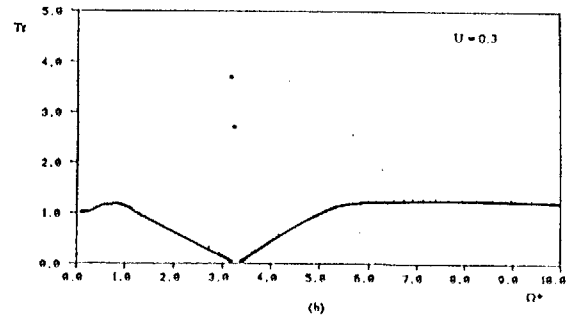
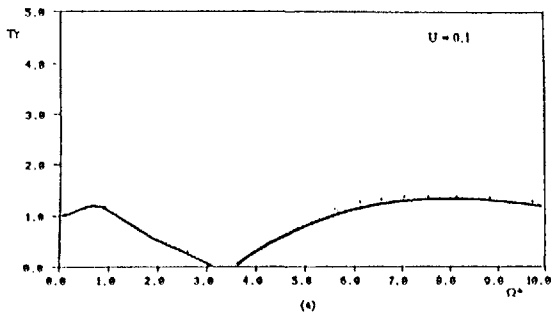


Figure 5.29 Effect of U on unbalance response of long damper datum system, Tr

with regions I and II and a large eccentricity prevails for most of the frequency range. Comparing Figures 5.27 and 5.13 for the short damper, we can see that the long damper is better at attenuating the amplitude of the response. Figure 5.28 shows the effect of changing U on R^* , which exhibits the same characteristics as for ϵ . Figure 5.29 illustrates the effect of changing U on Tr , and it can be seen that except for regions III and IV, the vibration isolation capability of the damper is not affected for most values of U . At large values for U the system exhibits a small region of successful vibration isolation.

Figures 5.30, 5.31 and 5.32 illustrate the effects of changing the stiffness ratio R_k on the unbalance response of the datum system. The effect of changing R_k on ϵ is illustrated in Figure 5.30, from which it can be seen that low values of R_k (i.e. no retainer spring) lead to the elimination of the second resonance from the speed range under consideration. Large values of R_k lead to the appearance of regions III and IV. Also the second mode occurs at a much lower speed, and it exhibits a sharp resonance. The same general results are illustrated in Figure 5.31 which shows the effect of changing R_k on R^* . Figure 5.32 shows the effect of changing R_k on Tr . Here also it can be seen that low values of R_k result in a large region of good vibration isolation ($Tr < 1$). For large R_k the region of good vibration isolation diminishes.

5.5 Conclusions

The following may be concluded from this chapter:

- 1- Using the technique described in section 5.3 in obtaining the steady state unbalance response results in considerable savings of computer time and avoids the trial and error procedures in regions of multiple steady states.

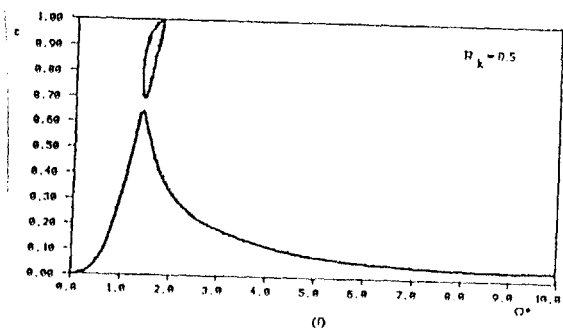
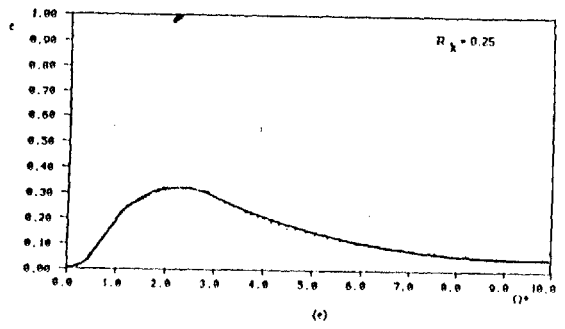
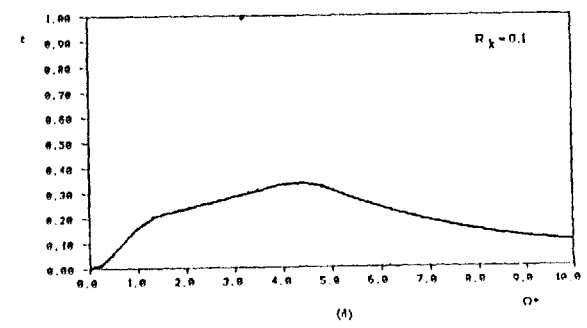
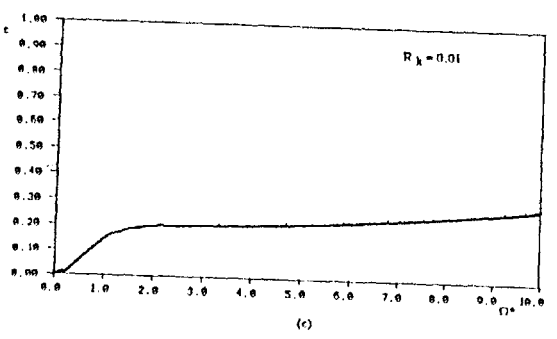
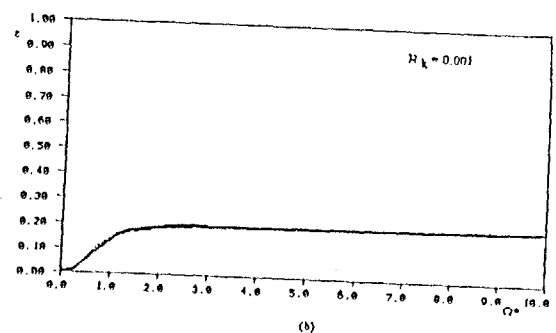
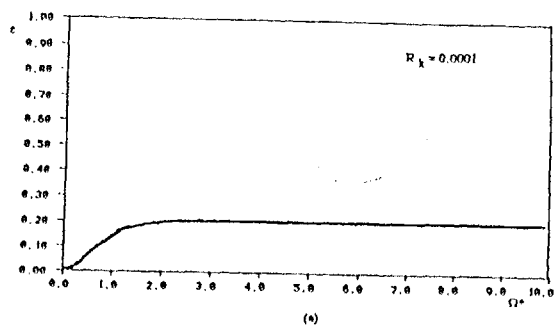


Figure 5.30 Effect of R_k on unbalance response of long damper datum system, ϵ

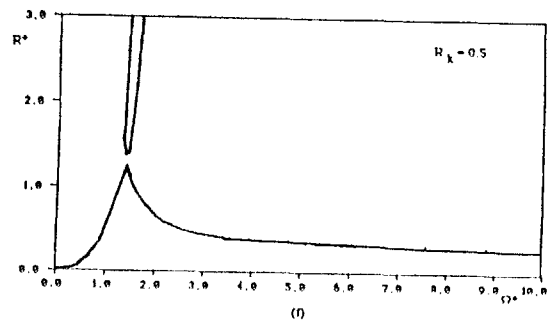
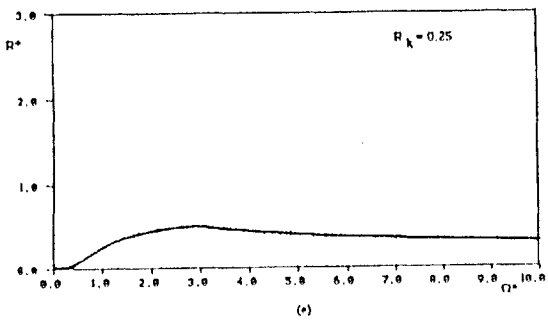
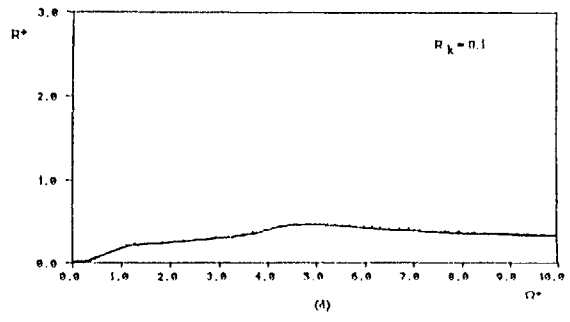
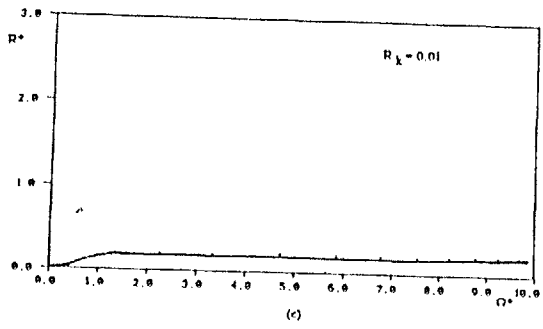
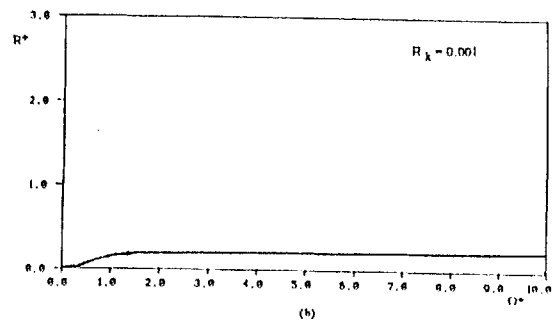
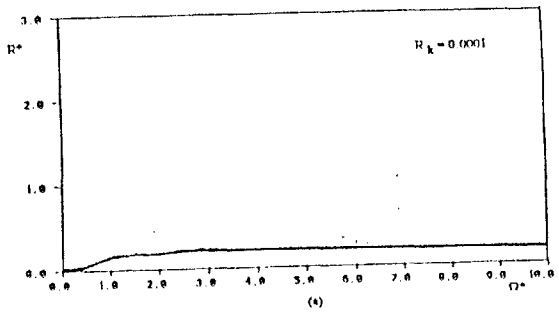


Figure 5.31 Effect of R_k on unbalance response of long damper datum system, R^*

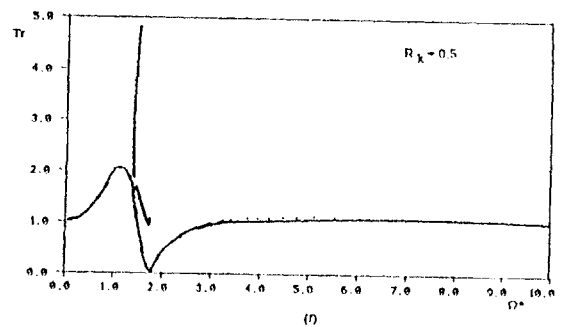
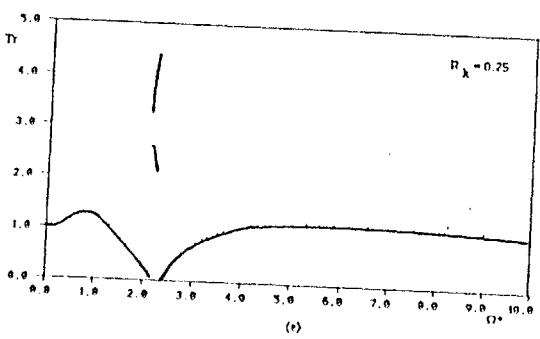
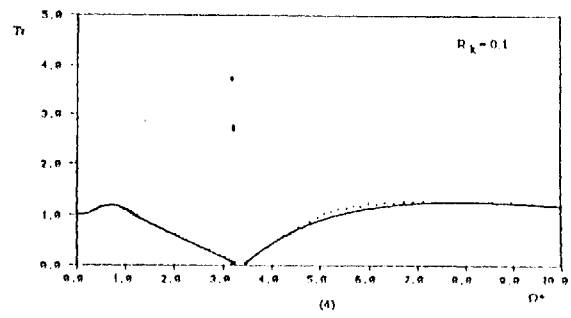
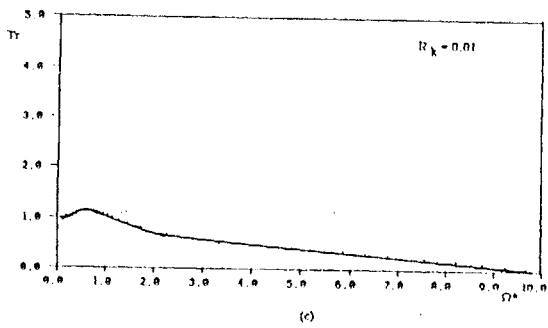
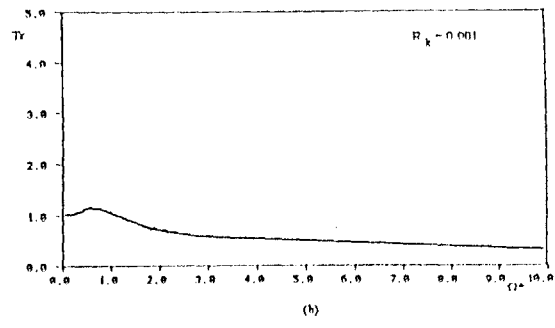
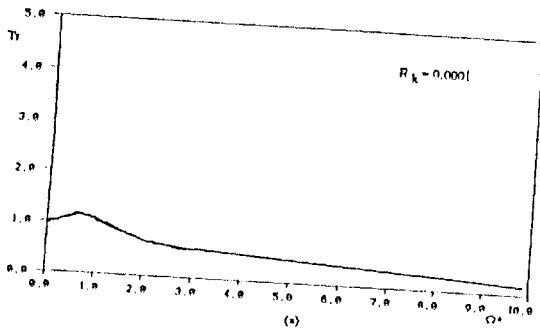


Figure 5.32 Effect of R_k on unbalance response of long damper datum system, Tr

2- The requirements of good vibration isolation ($Tr < 1$) and attenuation of amplitude of response may conflict. In this case a compromise has to be made. In general the short squeeze film damper exhibits better vibration isolation capabilities, while the long squeeze film damper is better at attenuating the amplitude of the whirl.

3- The long squeeze film damper did not exhibit the jump resonance within the range of parameters studied here.

4- Fluid inertia introduces a second mode to the response of the Jeffcott rotor. This mode is well damped for short squeeze film dampers, but may exhibit a sharp resonance for the long squeeze film damper.

5- Fluid inertia tends to decrease the possibility of jump resonance for the first mode in short squeeze film dampers. For long dampers fluid inertia tends to decrease the amplitude of response of the first mode.

6- Fluid inertia results in a decrease of the useful range of vibration isolation ($Tr < 1$) for both short and long dampers.

7- For both the short and long dampers, a system with no retainer spring (or a soft retainer spring) exhibits better steady state unbalance response and vibration isolation capability than that with a retainer spring. This may not be the whole story since a system with no retainer spring would probably exhibit worse transient response than a system with a retainer spring.

8- The increase of the bearing parameter B results in better attenuation of vibration and worsens the vibration isolation capabilities of the damper, while a small B results in worse attenuation of amplitude of vibration and better vibration isolation.

9- An uncavitated damper results in better overall performance of the damper, although the second mode due to fluid inertia is excited at a lower speed.

Chapter 6

Conclusions

The dynamics of rotors incorporating squeeze film dampers was studied in this thesis. The main emphasis is on modelling fluid inertia forces in squeeze film dampers (SFDs), and their effect on the dynamics of a Jeffcott rotor.

6.1 Review of thesis contents

The thesis starts by reviewing the pertinent literature that indicates that the nonlinear effects produced because of the squeeze film damper can have a significant effect on the dynamics of rotors incorporating SFDs. It was also indicated that fluid inertia may be an important factor in determining the dynamics of the rotor.

The damping forces that are produced in a squeeze film damper are derived in chapter 2. Reynolds equation is first derived and both the short and long bearing approximations are used to obtain the pressure equation in SFDs. The damping forces are then obtained by integrating the pressure. For cavitated dampers the π -film theory was used. The nonlinear characteristics of the damper are illustrated by the damping coefficients which are nonlinearly dependent on position for a 2π -film, and on position and velocity, in general, for a cavitated damper.

To determine the fluid inertia forces, the kinetic coenergy method is introduced. It is based on the assumption that the velocity profiles of the oil film do not change much due to fluid inertia. Thus the kinetic coenergy can be determined and Lagrange's equations of

motion are used to determine the inertia forces from the kinetic coenergy. For systems with fluid particles crossing the control surface, the forces determined by Lagrange's equations have to be supplemented to account for the kinetic energy leaving the control volume.

In chapter 3, the kinetic coenergy method is applied to two simplified squeezing flows, namely, the Poiseuille flow due to squeezing motion, and the direct squeeze flow. This is both to better understand the mechanics of squeezing flows and to illustrate the validity of the kinetic coenergy method. It is shown that in the Poiseuille flow case, the fluid inertia force predicted by the kinetic coenergy method is the limit as Reynolds number goes to zero, of the fluid inertia force predicted by the solution of the differential equations governing the flow. It is also shown to be a good approximation for Reynolds number in the range of usual application of SFDs. For the squeeze flow case an additional term is predicted in the inertia force obtained by the kinetic coenergy method. It is shown that this additional term is due to convective acceleration, by an approximate solution of the partial differential equations governing the flow. This approximate method is based on the assumption of the velocity profiles to be those of the inertialess solution, and the momentum equations are integrated across the film.

The kinetic coenergy method is applied to both the short and long squeeze film dampers, in chapter 4. The inertia coefficients of the dampers are presented and are shown to be nonlinear functions of the amplitude of the journal orbit. The fluid inertia forces are then obtained by using Lagrange's equations. For the short squeeze film dampers and cavitated long squeeze film dampers, Lagrange's equations are supplemented to account for the kinetic energy that leaves the control volume. It is also shown that the fluid inertia forces predicted by the solution of the Navier-Stokes equations for the case of a small circular-centered whirl, is closely approximated by the fluid inertia forces predicted by the kinetic coenergy method, for Reynolds number in the range of usual application of SFDs.

In Chapter 5, the dynamics of a Jeffcott rotor incorporating SFDs is presented. The equations of motion are derived and it is shown that the steady state unbalance response can be obtained by assuming circular-centered whirling motions. The resulting algebraic equations are manipulated to obtain a polynomial, which is solved numerically to obtain the unbalance response. This is to avoid trial and error in obtaining solutions of the algebraic equations in regions of multiple solutions. Parametric studies of the steady state unbalance response are also performed.

6.2 Conclusions

The following may be concluded from the thesis:

- 1- The kinetic coenergy method is a powerful tool, that predicts the fluid inertia forces acting on a surface, if the velocity profiles can be estimated beforehand. It has been demonstrated that it predicts fluid inertia forces accurately, including both temporal and convective effects, in squeezing flows.

- 2- For flow situations in which the fluid particles cross the control surface encompassing the system, the effect of the kinetic energy lost through the particles leaving the control volume should be considered, and Lagrange's equations should be supplemented to include such an effect. A power balance on the system proved to be fruitful in obtaining the inertia force due to the loss of kinetic energy with the particles leaving the control volume.

- 3- Fluid inertia forces can be important in squeezing flows in cases where the squeeze Reynolds number is approximately equal to 10. At $Re=10$, the fluid inertia force is equal to the viscous force, above $Re=10$ the inertia force is larger than the viscous force.

4- Convective acceleration contributes to the inertia force significantly when the amplitude of motion is large. For small amplitudes of motion ($\epsilon \ll 1$), the inertia forces due to convective acceleration can be neglected.

5- The inertia forces increase as the clearance is decreased even though the actual mass of the fluid film has decreased, as illustrated in the Poiseuille flow case. This is because of the huge velocities and accelerations that the fluid undergoes in smaller clearances.

6- Both the damping and inertia characteristics of squeeze film dampers are in the form of a tensor. This implies that the squeeze film damper is an anisotropic device. Thus because of the tensor inertia characteristics the momentum vector is not in the same direction as the velocity vector.

7- A radial acceleration (\dot{e}^2/e) is predicted to contribute to the inertia forces in a squeeze film damper. This is not a journal acceleration nor a fluid acceleration, but it affects the journal. This acceleration needs to be investigated further.

8- For cavitating short squeeze film dampers, the centrifugal inertia force reverses its direction at large eccentricities due to the fluid particles leaving the damper.

9- The fluid inertia forces predicted by the kinetic coenergy method are in excellent agreement with the solution of the Navier-Stokes equations for a small circular-centered whirl.

10- Using the technique described in section 5.3 in obtaining the steady state unbalance response results in considerable savings of computer time and avoids the trial and error procedures in regions of multiple steady states.

11- The requirements of good vibration isolation ($Tr < 1$) and attenuation of amplitude of response may conflict. In this case a compromise has to be made. In general the short squeeze film damper exhibits better vibration isolation capabilities, while the long squeeze film damper is better at attenuating the amplitude of the whirl.

12- The long squeeze film damper did not exhibit the jump resonance within the range of parameters studied here.

13- Fluid inertia introduces a second mode to the response of the Jeffcott rotor. This mode is well damped for short squeeze film dampers, but may exhibit a sharp resonance for the long squeeze film damper.

14- Fluid inertia tends to decrease the possibility of jump resonance for the first mode in short squeeze film dampers. For long dampers fluid inertia tends to decrease the amplitude of response of the first mode.

15- Fluid inertia results in a decrease of the useful range of vibration isolation ($Tr < 1$) for both short and long dampers.

16- For both the short and long dampers, a system with no retainer spring (or a soft retainer spring) exhibits better steady state unbalance response and vibration isolation capability than that with a retainer spring. This may not be the whole story since a system with no retainer spring would probably exhibit worse transient response than a system with a retainer spring.

17- The increase of the bearing parameter B results in better attenuation of vibration and worsens the vibration isolation capabilities of the damper, while a small B results in worse attenuation of amplitude of vibration and better vibration isolation.

18- An uncavitated damper results in better overall performance of the damper, although the second mode due to fluid inertia is excited at a lower speed.

6.3 Suggestions for future research

A model of squeeze film dampers that includes fluid inertia effects was presented in this thesis. This model can be incorporated in several ways to enhance our understanding of squeeze film dampers and their effects on the dynamics of rotors. Some suggestions of possible areas of investigation follow:

1- A design procedure for multi-mass flexible rotors incorporating squeeze film dampers needs to be developed. One possible route would be to determine the critical speeds of the rotor system that are within the operating speed range and then determining the modal mass and modal stiffness corresponding to these undamped modes. Using these data and the program UNBRES developed here, a squeeze film damper may be designed to obtain the required response for each mode. An optimization technique may be employed to select the design that meets the required specifications.

2- In determining the dynamics of the Jeffcott rotor in chapter 5, we assumed circular centered whirl, which is an idealization. In the real world, the rotor would be unsymmetrical and would not be centered, thus an analysis of the dynamics of a rotor whose journals execute non-centered, and non-circular whirl is called for. The technique of equivalent linearization [11] should prove to be rewarding in determining the forces in

the squeeze film dampers in this case. This technique also can be employed in programs that determine the dynamics of rotating machinery, which are usually programs based on linear analysis (transfer matrix method, component mode synthesis method,...etc.)

3- Numerical and experimental investigation of the fluid inertia forces in squeeze film dampers, both to verify the model presented here and to investigate the (\ddot{e}^2/e) acceleration predicted in chapter 4. A numerical solution of the simplified Navier-Stokes equations (2.32-2.34) would be necessary.

4- Further investigation of cavitation in squeeze film damper is necessary. A more accurate model of cavitation and the extent of the oil film is essential in determining the forces in squeeze film dampers.

5- Investigation of the nonsynchronous orbits that may occur in squeeze film dampers. This has been observed experimentally [37,77] and should be investigated to determine the possibility of subsynchronous resonances. A possible technique would be to use a Fourier series expansion of the forces in squeeze film dampers, and keeping the components that are of interest. Using orthogonality of Fourier coefficients the subsynchronous motions can be investigated.

6- A long term project would be to develop a nonlinear program that would determine the dynamics and stability of multi-mass flexible rotors that incorporate squeeze film dampers and other nonlinear effects like clearances, rub between rotor and stator, seals,...etc.

Bibliography

- [1] Alderson, R.G., "Instability of an Intershaft Squeeze Film Damper in a Two-Spool Rotor Dynamics Simulator", Rotordynamic Instability Problems in High-Performance Turbomachinery, NASA Conference Publication 2443, 1986, pp. 315-323.
- [2] Allaire, P.E., L.E. Barrett, and E.J. Gunter, "Variational Method for Finite Length Squeeze Film Damper Dynamics With Applications", Wear, Vol. 42, No. 1, 1977, pp. 9-22.
- [3] Barrett, L.E., P.E. Allaire, and E.J. Gunter, "The Dynamic Analysis of Journal Bearings Using a Finite Length Correction for Short Bearing Theory", Topics in Fluid Film Bearing and Rotor Bearing System Design and Optimization, ASME, New York, 1978.
- [4] Booker, J.F., "A Table of the Journal-Bearing Integral", Journal of Basic Engineering, Trans. ASME, June 1965, pp. 533-535.
- [5] Botman, M., "Experiments on Oil-Film Dampers for Turbomachinery", Journal of Engineering for Power, Trans. ASME, Vol. 98, No. 3, July 1976, pp. 393-400.
- [6] Botman, M. and M.A. Samaha, "Experiments on the Dynamic Behavior of a Supercritical Rotor", ASME paper 81-DET-59, 1981.
- [7] Burrows, C.R., M.N. Sahinkaya, and N.C. Kucuk, "Modelling of Oil-Film Forces in Squeeze Film Bearings", Journal of Tribology, Trans. ASME, Vol. 108, 1986 pp. 262-269.
- [8] Burrows, C.R., M.N. Sahinkaya, and N.C. Kucuk, "A New Model to Predict the Behaviour of Cavitated Squeeze Film Bearings", Proc. R. Soc. Lond, Series A, Vol. 411, 1987, pp. 445-466.
- [9] Burrows, C.R., M.N. Sahinkaya, N.C. Kucuk, and M. L. Tong, " In Situ Estimation of Dynamic Characteristics of an Uncavitated Squeeze-Film Damper", Journal of Tribology, Trans. ASME, Vol. 110, No. 1, 1988, pp. 162-166.
- [10] Cameron, A., Basic Lubrication Theory, Third Edition, Ellis Horwood Ltd. Publishers, England, 1981.
- [11] Chen, S., and S. Liu, "Equivalent Linearization of a Squeeze Film Damper", Journal of Vibrations, Acoustics, Stress and Reliability in Design, Trans. ASME, October 1986.
- [12] Childs, D., H. Moes, and H. Van Leeuwen, "Journal Bearing Impedance Descriptions for Rotor Dynamics Applications", Journal of Lubrication Technology, Trans. ASME, Vol. 99, No. 2, 1977, p. 198.

- [13] Constantinescu, V.N., "On the Influence of Inertia Forces in Turbulent and Laminar Self-Acting Films", *Journal of Lubrication Technology*, Trans. ASME, Vol. 92, No. 3 July 1970, pp. 473-479.
- [14] Constantinescu, V.N., and S. Galetuse, "On the Possibilities of Improving the Accuracy of the Evaluation of Inertia Forces in Laminar and Turbulent films", *Journal of Lubrication Technology*, Trans. ASME, January 1974, pp. 69-79.
- [15] Cooper, S., "Preliminary Investigation of Oil Films for the Control of Vibration", *Lubrication and Wear Convention*, I.Mech.E., 1963, pp. 305-315.
- [16] Courage, J.B., "Experimental Study of an Intershaft Squeeze Film Bearing", *Second International Conference on Vibrations in Rotating Machinery*, I.Mech.E., 1980, pp. 375-380.
- [17] Coyne, J. C., and H.G. Elrod, "Conditions for the Rupture of a Lubrication Film, Part 1: Theoretical Model", *Journal of Lubrication Technology*, Trans. ASME, Vol. 92, July 1970, pp. 156-168.
- [18] Coyne, J.C., and H.G. Elrod, "Conditions for the Rupture of a Lubrication Film, Part 2: New Boundary Conditions for Reynolds Equation", *Journal of Lubrication Technology*, Trans. ASME, Vol. 93, Jan. 1971, pp. 451-456.
- [19] Crandall. S.H., D.C. Karnopp, E.F. Kurtz and D.C. Pridmore-Brown, *Dynamics of Mechanical and Electromechanical Systems*, McGraw-Hill, New York , 1968.
- [20] Cunningham, R.E., D.P. Fleming, and E.J. Gunter, "Design of a Squeeze Film Damper for a Multimass Flexible Rotor", *Journal of Engineering for Industry*, Trans. ASME, Nov. 1975, pp. 1383-1389.
- [21] Dogan, M., and R. Holmes, "Squeeze-Film Damping of Rotor-Dynamic Systems" *Shock and Vibration Digest*, Vol. 15, No. 9, Sept. 1983, pp. 3-8.
- [22] Ellis, J., J.B. Roberts and A. Hosseini Sisnaji, "A Comparison of Identification Methods for Estimating Squeeze-Film Damper Coefficients". *Journal of Tribology*, Trans. ASME, Vol. 110, No. 1, January 1988, pp. 119-127.
- [23] El-Shafei, A., "A New Design of Intershaft Squeeze Film Dampers", *Proceedings Vibration Institute*, 1988, pp. 15-23.
- [24] Feder, E., P.N. Bansal, and A. Blanco, "Investigation of Squeeze Film Damper Forces Produced by Circular Centered Orbits", *Journal of Engineering for Power*, Trans. ASME, Vol. 100, 1978, pp. 15-21.
- [25] Greenhill, L.M., and H.D. Nelson, "Iterative Determination of Squeeze Film Damper Eccentricity for Flexible Rotor Systems", *Journal of Mechanical Design*, Trans. ASME, Vol. 104, No. 2, 1982, pp. 334-338.
- [26] Grimm, R.J., "Squeezing Flows of Newtonian Liquid Films - An Analysis Including Fluid Inertia", *Appl. Sci. Res.*, Vol. 32, July 1976, pp. 149-166.
- [27] Guang, M. and X. Zhong-Qing, "Investigation on Steady State Response and its Nonlinear Characteristics of Flexible Rotor Squeeze Film Damper System", ASME paper 85-GT-141, 1985.

- [28] Gunter, E.J., "Influence of Flexibly Mounted Rolling Element Bearings on Rotor Response: Part 1- Linear Analysis", *Journal of Lubrication Technology*, Trans. ASME, Vol. 92. No. 1, Jan. 1970, pp. 59-75.
- [29] Gunter, E.J., L.E. Barrett, and P.E. Allaire, "Design of Nonlinear Squeeze Film Dampers for Aircraft Engines", *Journal of Lubrication Technology*, Trans. ASME, Vol. 99, No. 1, 1977, pp. 57-64.
- [30] Gunter, E.J., D.F. Li and L.E. Barrett. "Unbalance Response of a Two Spool Gas Turbine Engine with Squeeze Film Bearings", ASME paper 81-GT-219, Presented at the Gas Turbine Conference & Products Show, March 9-12, 1981.
- [31] Hahn, E.J., "An Energy Approach to Linearizing Squeeze Film Damper Forces", *Proc. I.Mech.E.*, Vol. 199, No. C1, 1985, pp. 57-63.
- [32] Hashish, E., T.S. Sankar, and M.O.M. Osman, "Finite Journal Bearing With Nonlinear Stiffness and Damping - Part 1: Improved Mathematical Models", *Journal of Mechanical Design*, Trans. ASME, Vol. 104, April 1982, pp. 397-405.
- [33] Hashish, E., T.S. Sankar, and M.O.M. Osman, "Finite Journal Bearing With Nonlinear Stiffness and Damping - Part 2: Stability Analysis", ASME paper 81-DET-52, 1981.
- [34] Hibner, D.H., P.N. Bansal, and D.F. Buono, "Analysis and Experimental Investigation of the Stability of Intershaft Squeeze Film Dampers - Part 2: Control of Instability", *Journal of Mechanical Design*, Trans. ASME, Vol. 100. No. 3, July 1978, pp. 558-562.
- [35] Hibner, D.H., R.G. Kirk, and D.F. Buono, "Analytical and Experimental Investigation of the Stability of Intershaft Squeeze Film Dampers - Part 1: Demonstration of Instability", *Journal of Engineering for Power*, Trans. ASME, Vol. 99, No. 1, Jan. 1977, pp. 47-52.
- [36] Holmes, R., "The Non-Linear Performance of Squeeze-Film Bearings", *Journal of Mechanical Engineering Science*, *I.Mech.E.*, Vol. 14, No. 1, 1972, pp. 74-77.
- [37] Holmes, R., "The Control of Engine Vibration Using Squeeze-Film Dampers", *Journal of Engineering for Power*, Trans. ASME, Vol. 105, July 1983, pp. 525-529.
- [38] Holmes, R., and M. Dogan, "Investigation of a Rotor Bearing Assembly Incorporating a Squeeze-Film Damper Bearing", *Journal of Mechanical Engineering Science*, *I.Mech.E.*, Vol. 24, No.3, 1982, pp. 129-137.
- [39] Holmes, R., and M. Dogan, "The Performance of a Sealed Squeeze-Film Bearing in a Flexible Support Structure", *Proc. I. Mech. E.*, Vol. 199, No. C1, 1985.
- [40] Humes, B., and R. Holmes, "The Role of Subatmospheric Film Pressures in the Vibration Performance of Squeeze-Film Bearings", *Journal of Mechanical Engineering Science*, *I.Mech.E.*, Vol. 20, No. 5, 1978, pp. 283-289.

- [41] Ishizawa, S., "The Unsteady Laminar Flow Between Two Parallel Discs With Arbitrary Varying Gap Width", *Bulletin of JSME*, Vol. 9, No. 35, 1966, pp. 533-550.
- [42] Jones, A.F., and S.D.R. Wilson, "On the Failure of Lubrication Theory in Squeezing Flows", *Journal of Lubrication Technology*, *Trans. ASME*, Vol. 97, 1975, pp. 101-104.
- [43] Lamb, H., Hydrodynamics, 6th Edition, Cambridge University Press, 1932, Dover reprint.
- [44] Li, Q., and J.F. Hamilton, "Investigation of the Transient Response of A Dual-Rotor System With Intershaft Squeeze Film Damper", *Journal of Engineering for Gas Turbine and Power*, *Trans. ASME*, Vol. 108, No. 4, Oct. 1986, pp. 613-618.
- [45] Li, Q., L. Yan, and J.F. Hamilton, "Investigation of The Steady-State Response of a Dual-Rotor System With Intershaft Squeeze Film Damper", *Journal of Engineering for Gas Turbine and Power*, *Trans. ASME*, Vol. 108, No. 4, Oct. 1986, pp. 605-612.
- [46] Li, X., and D.L. Taylor, "Perturbation Solutions for Eccentric Operation of Squeeze Film Damper Systems", *Journal of Engineering for Gas Turbines and Power*, *Trans. ASME*, Vol. 108, No.4, Oct. 1986, pp. 619-623.
- [47] Lund, J.W. , "Modal Response of a Flexible Rotor in Fluid-Film Bearings", ASME paper 73-DET-98, 1973.
- [48] Lund, J.W., "Stability and Damped Critical Speeds of a Flexible Rotor in Fluid-Film Bearings", *Journal of Engineering for Industry*, *Trans. ASME*, May 1974, pp. 509-517.
- [49] Lund, J.W., "Review of the Concept of Dynamic Coefficients for Fluid Film Journal Bearings", ASME paper 86-Trib-48, 1986.
- [50] Lund, J.W., A.J. Smalley, J.A. Tecza, and J.F. Walton, "Squeeze-Film Damper Technology: Part 1 - Prediction of Finite Length Damper Performance", ASME paper 83-GT-247, 1983.
- [51] Marmol, R.A., and J.M. Vance, "Squeeze Film Damper Characteristics for Gas Turbine Engines", *Journal of Mechanical Design*, *Trans. ASME*, Vol. 100, 1978, pp. 139-146.
- [52] Mclean, L.J., and E.J. Hahn, "Unbalance Behavior of Squeeze Film Damped Multi-Mass Flexible Rotor Bearing Systems", *Journal of Lubrication Technology*, *Trans. ASME*, 1983, pp. 22-28.
- [53] McLean, L.J, and E.J. Hahn, "Stability of Squeeze Film Damped Multi-Mass Flexible Rotor Bearing Systems", *Journal of Tribology*, *Trans. ASME*, 1985, pp. 402-410.
- [54] Meirovitch, L., Methods of Analytical Dynamics, McGraw-Hill, New York, 1970.
- [55] Milne-Thomsen, L.M., Theoretical Hydrodynamics, 2nd edition, Macmillan Co., New York, 1949.

- [56] Modest, M.F., and J.A. Tichy, "Squeeze Film Flow in Arbitrarily Shaped Journal Bearings Subject to Oscillations", *Journal of Lubrication Technology*, Trans. ASME, Vol. 100, July 1978, pp. 323-329.
- [57] Mohan, S., and E.J. Hahn, "Design of Squeeze Film Damper Supports for Rigid Rotors", *Journal of Engineering for Industry*, Trans. ASME., August 1974, pp. 976-982.
- [58] Pan, C.H.T., and J. Tonnesen, "Eccentric Operation of the Squeeze-Film Damper", *Journal of Lubrication Technology*, Trans. ASME, July 1978, pp. 369-377.
- [59] Parkins, D.W., and R. May-Miller, "Cavitation in an Oscillatory Oil Squeeze Film", *Journal of Tribology*, Trans. ASME, Vol. 106, July 1984, p. 360.
- [60] Parkins, D.W., and W.T. Stanley, "Characteristics of an Oil Squeeze Film", *Journal of Lubrication Technology*, Trans. ASME, Oct. 1982, p. 497.
- [61] Parkins, D.W., and J.H. Woollam, "Behavior of an Oscillating Oil Squeeze Film", ASME paper 85-Trib-32, 1985.
- [62] Pinkus, O., and B. Sternlicht, Theory of Hydrodynamic Lubrication, McGraw-Hill, New York, 1961.
- [63] *Proceedings of the Conference on the Stability and Dynamic Response of Rotors with Squeeze-Film Bearings*, University of Virginia, Charlottesville, May 8-10, 1979, U. S. Army Research Office, Research Triangle Park, North Carolina.
- [64] Rabinowitz, M.D., and E.J. Hahn "Stability of Squeeze Film Damper Supported Flexible Rotors", *Journal of Engineering for Power*, Trans. ASME, Vol. 99, No. 4, 1977, pp. 545-551.
- [65] Rabinowitz, M.D., and E.J. Hahn, "Steady State Performance of Squeeze Film Damper Supported Flexible Rotors", *Journal of Engineering for Power*, Trans. ASME, Vol. 99, No. 4, 1977, pp. 552-558.
- [66] Rabinowitz, M.D., and E.J. Hahn, "Optimal Design of Squeeze Film Supports for Flexible Rotors", *Journal of Engineering for Power*, Trans. ASME, 1983, pp. 487-494.
- [67] Rabinowitz, M.D., and E.J. Hahn, "Experimental Evaluation of Squeeze Film Supported Flexible Rotors", *Journal of Engineering for Power*, Trans. ASME, 1983, pp. 495-503.
- [68] Ramli, M.D., J. Ellis, and J.B. Roberts, "On the Computation of Inertial Coefficients in Squeeze-Film Bearings", *Proc. I.Mech.E.*, Vol. 201, No. C2, 1987, pp. 125-131.
- [69] Ramli, M.D., J.B. Roberts, and J. Ellis, "Determination of Squeeze Film Dynamic Coefficients from Experimental Transient Data", *Journal of Tribology*, Trans. ASME, Vol. 109, No. 1, January 1987, pp. 155-163.

- [70] Reinhardt, E., and J.W. Lund, "The Influence of Fluid Inertia on the Dynamic Properties of Journal Bearings", *Journal of Lubrication Technology*, Trans. ASME, Vol. 97, No. 2, 1975, pp.159-167.
- [71] San Andrés, L.A. and J.M. Vance, "Effects of Fluid Inertia and Turbulence on the Force Coefficients for Squeeze Film Dampers", *Journal of Engineering for Gas Turbine and Power*, Trans. ASME, Vol. 108, No. 2, April 1986, pp. 332-339.
- [72] San Andrés, L.A. and J.M. Vance, "Effects of Fluid Inertia on Finite-Length Squeeze-Film Dampers", ASLE preprint 86 - TC - 4D - 1, 1986.
- [73] San Andrés, L.A. and J.M. Vance, "Force Coefficients for Open-Ended Squeeze-Film Dampers Executing Small-Amplitude Motions About an Off-Center Equilibrium Position", ASLE preprint 86 - AM - 3A - 2, 1986.
- [74] San Andrés, L.A. and J.M. Vance, "Effect of Fluid Inertia on Squeeze-Film Damper Forces for Small-Amplitude Circular-Centered Motions", ASLE preprint 86 - AM - 3A - 3, 1986.
- [75] San Andrés, L.A. and J.M. Vance, "Experimental Measurement of the Dynamic Pressure Distribution in a Squeeze-Film Bearing Damper Executing Circular-Centered Orbits", ASLE preprint 86 - TC - 4D - 2, 1986.
- [76] San Andrés, L.A. and J.M. Vance, "Effect of Fluid Inertia on the Performance of Squeeze Film Damper Supported Rotors", *Journal of Engineering for Gas Turbine and Power*, Trans. ASME, Vol. 110, No. 1, January 1988, p. 51.
- [77] Sharma, R.K., and M. Botman, "An Experimental Study of the Steady-State Response of Oil-Film Dampers", ASME paper 77-DET- 33, 1977.
- [78] Simandiri, S., and E.J. Hahn, "Effect of Pressurization on the Vibration Isolation Capability of Squeeze Film Bearings", *Journal of Engineering for Industry*, Trans. ASME, 1976, pp. 109-117.
- [79] Smith, D.M., "Dynamic Characteristics of Turbine Journal Bearings", *Lubrication and Wear Convention*, I.Mech.E, 1963, pp. 72-86.
- [80] Smith, D.M., "Journal Bearing Dynamic Characteristics - Effect of Inertia of Lubricant", *Proc. I.Mech.E.*, 1964-1965, Vol. 179, pp. 37-44.
- [81] Storace, A., and S.J. Cline, "NASA-General Electric Energy Efficient Engine High Load Squeeze Film Damper-System Analysis and Test Results", AIAA paper 84-1217, AIAA/SAE/ASME 20th Joint Propulsion Conference, 1984.
- [82] Szeri, A.Z., ed., Tribology : Friction, Lubrication and Wear, Hemisphere publishing, 1980.
- [83] Szeri, A.Z., "Some Extensions of the Lubrication Theory of Osborne Reynolds", ASME paper 86-Trib-47, 1986.
- [84] Szeri, A.Z., A.A. Raimondi, and A. Giron-Durate, "Linear Force Coefficients of Squeeze Film Dampers", *Journal of Lubrication Technology*, Trans. ASME, 1983, pp. 326-334.

- [85] Taylor, D.L., and B.R.K. Kumar, "Nonlinear Response of Short Squeeze Film Dampers", *Journal of Lubrication Technology*, Trans. ASME, Vol. 102, January 1980, pp. 51-58.
- [86] Taylor, D.L., and B.R.K. Kumar, "Closed Form Steady State Solution for the Unbalance Response of a Rigid Rotor in Squeeze Film Damper", *Journal of Engineering for Power*, Trans. ASME, Vol. 105, No. 3, 1983, pp. 551-559.
- [87] Tecza, J.A., J.C. Giordano, E.S. Zorzi, and S.K. Drake, "Squeeze Film Damper Technology : Part 2 - Experimental Verification Using a Controlled Orbit Test Rig", ASME paper 83 - GT - 248, 1983.
- [88] Terrill, R.M., "The Flow Between Two Parallel Circular Disks, One of Which is Subject to a Normal Sinusoidal Oscillation", *Journal of Lubrication Technology*, Trans. ASME, Vol. 91, No. 1, January 1969, pp. 126-131.
- [89] Thomsen, K.K., and H. Andersen, "Experimental Investigation of a Simple Squeeze Film Damper", *Journal of Engineering for Industry*, Trans. ASME, May 1974, pp. 427-430.
- [90] Thurgood, D.A., "Dynamics of High Speed Rotative Assemblies", Second International Conference on Vibrations in Rotating Machinery, I.Mech.E., 1980, paper C 309/80, pp. 389-393.
- [91] Tichy, J.A., "Effects of Fluid Inertia and Viscoelasticity on Squeeze-Film Bearing Forces" Trans. ASLE, Vol. 25, No. 1, pp. 125-132.
- [92] Tichy, J.A., "The Effect of Fluid Inertia in Squeeze Film Damper Bearings : A Heuristic and Physical Description", ASME paper 83 - GT - 177, 1983.
- [93] Tichy, J.A., "Effects of Fluid Inertia and Viscoelasticity on the One-Dimensional Squeeze-Film Bearing", Trans. ASLE, Vol. 27, No. 2, pp. 164-167.
- [94] Tichy, J.A., "Measurement of Squeeze Film Bearing Forces to Demonstrate the Effect of Fluid Inertia", ASME paper 84 - GT - 11, 1984.
- [95] Tichy, J.A., and M.F. Modest, "Squeeze Film Flow Between Arbitrary Two-Dimensional Surfaces Subject to Normal Oscillations.", *Journal of Lubrication Technology*, Trans. ASME, Vol. 100, 1978, pp. 316-322.
- [96] Tichy, J.A., and W.O. Winer, "Inertial Considerations in Parallel Circular Squeeze Film Bearings", *Journal of Lubrication Technology*, Trans. ASME, Vol. 92, No. 4, 1970, pp. 588-592.
- [97] Tonnesen, J., "Experimental Parametric Study of a Squeeze Film Bearing", *Journal of Lubrication Technology*, Trans. ASME, April 1976, pp. 206-213.
- [98] Vance, J.M., and A.J. Kirton, "Experimental Measurement of the Dynamic Force Response of a Squeeze-Film Bearing Damper", *Journal of Engineering for Industry*, Trans. ASME, November 1975, pp. 1282-1290.

- [99] Walton II, J.F., J.A. Walowit, E.S. Zorzi, J. Schrand, "Experimental Observation of Cavitating Squeeze -Film Dampers", Journal of Tribology, Trans. ASME, Vol. 109, April 1987, pp. 290-295.
- [100] Warner, P.C., "Static and Dynamic Properties of Partial Journal Bearings", Journal of Basic Engineering, Trans. ASME, June 1963, pp. 247-257.
- [101] White, D.C., "The Dynamics of a Rigid Rotor Supported on Squeeze Film Bearings", Conference on Vibrations in Rotating Machinery, Proc. I.Mech.E., 1972, pp. 213-229.
- [102] Shames, I., Mechanics of Fluids, McGraw-Hill, New York, 1962.

APPENDIX

LISTING OF PROGRAM UNBRES

C PROGRAM UNBRES TO OBTAIN THE UNBALANCE RESPONSE OF A
C FLEXIBLE ROTOR MOUNTED ON A SQUEEZE FILM DAMPER,
C INCLUDING INERTIA COEFFICIENTS, USING THE IMSL ROUTINE
C ZPOLR

C-----

```
DIMENSION A(9),D(2,380),C(2,380)
```

```
DIMENSION TR(380),RS(380)
```

```
COMPLEX Z(8)
```

```
REAL MTT,M,M12,M22,MTT1
```

```
OPEN(FILE='ALY.DAT',UNIT=3,STATUS='OLD')
```

```
READ(3,*)RK,SK,B,U,M,CD,L,L1
```

```
CLOSE(UNIT=3)
```

```
NDEG=8
```

```
OPEN(FILE='UNBRES.DAT',UNIT=4,STATUS='OLD')
```

```
WRITE(4,*)RK,SK,B,U,M,CD,L,L1
```

PI=3.141592654

C1=CD**2-2.*SK

I=1

DO 10 J=1,99

E=FLOAT(J)/100.

IF(L1.EQ.1)THEN

CRT=2.*E/((1.-E**2)**2)

CTT=PI/(2.*(1.-E**2)*SQRT(1.-E**2))

MTT=PI*(1.-SQRT(1.-E**2))/(10.*E**2)

M22=-27.*(4.+2.*ALOG(ABS((1.-E)/(1.+E)))/E)/(140.*E)

M12=-27.*PI*(2.-(2.-E**2)/SQRT(1.-E**2))/(140.*E**2)

EDM=.1*PI*(1./SQRT(1.-E**2)-2.*(1.-SQRT(1.-E**2))/E**2)

IF(L.EQ.2)THEN

CRT=0.

M22=2.*M22

M12=0.

MTT=2.*MTT

CTT=2.*CTT

EDM=2.*EDM

END IF

MTT=MTT+0.5*EDM-M12

GOTO 5

END IF

IF(L1.EQ.2)THEN

CRT=24.*E/((2.+E**2)*(1.-E**2))

CTT=12.*PI/((2.+E**2)*SQRT(1.-E**2))

MTT1=(5.*E**2-2.)+4.*(1.-E**2)**1.5/(2.+E**2)

MTT=MTT1*1.2*PI/(E**2*(2.+E**2))

M22=((3.*E/(2.+E**2)-1.)**3/(1.-E)**2)

M22=54.*(M22+((3.*E/(2.+E**2)+1.)**3/(1.+E)**2))/35.

A1=((3.*E/(2.+E**2)-1.)**2/(1.-E))

M22=M22+.6*(A1-((3.*E/(2.+E**2)+1.)**2/(1.+E)))

M12=0.

EDM1=-1.2*PI*4.*(1.+E**2)*MTT1/(E*(2.+E**2))**2

EDM2=-12.*(2.+E**2)*SQRT(1.-E**2)-8.*(1.-E**2)**1.5

EDM=1.2*PI*(10.+EDM2/(2.+E**2)**2)/(2.+E**2)+EDM1

IF(L.EQ.2)THEN

CRT=0.

M12=0.

M22=0.

MTT=2.*MTT

CTT=2.*CTT

EDM=2.*EDM

END IF

MTT=MTT+0.5*EDM-M12

GOTO 5

END IF

$$5 \quad A(1)=(M22^{**2}+MTT^{**2})*(M/SK)^{**2}$$

$$A(2)=2.*B*M*(-CRT*MTT+CTT*M22)/(SK^{**2})$$

$$A(3)=(CRT^{**2}+CTT^{**2})*(B/SK)^{**2}-2.*RK*M*MTT/(SK^{**2})$$

$$A(3)=A(3)-2.*M*MTT/SK$$

$$A(3)=A(3)+C1*M^{**2}*(M22^{**2}+MTT^{**2})/(SK^{**2})$$

$$A(4)=2.*RK*B*CRT/(SK^{**2})+2.*B*CRT/SK$$

$$A(4)=A(4)+2.*B*M*C1*(CTT*M22-CRT*MTT)/(SK^{**2})$$

$$A(5)=1.-(U/E)^{**2}+2.*M*MTT+2.*RK/SK+M^{**2}*(M22^{**2}+MTT^{**2})$$

$$A(5)=A(5)+C1*(B^{**2}*(CRT^{**2}+CTT^{**2})-2.*RK*M*MTT)/(SK^{**2})$$

$$A(5)=A(5)+(RK/SK)^{**2}-2.*M*CD^{**2}*MTT/SK$$

$$A(6)=2.*B*(M*(-CRT*MTT+CTT*M22)-CRT+C1*RK*CRT)/(SK^{**2})$$

$$A(6)=A(6)+2.*(M*M22*CD+B*CRT*CD^{**2}/SK)$$

$$A(7)=B^{**2}*(CRT^{**2}+CTT^{**2})-2.*RK*(M*MTT+1.-C1*RK)/(SK^{**2})$$

$$A(7)=A(7)+CD^{**2}*(1.+2.*RK/SK)+2.*B*CTT*CD$$

$$A(8)=2.*RK*B*CRT$$

$$A(9)=RK^{**2}$$

CALL ZPOLR(A,NDEG,Z,IER)

C OBTAIN ROOTS OF INTEREST

DO 20 K=1,8

IF(ABS(AIMAG(Z(K))).GT.1.E-4)GOTO 20

IF(REAL(Z(K)).LT.0.)GOTO 20

OM=REAL(Z(K))

D(1,I)=OM

D(2,I)=E

I=I+1

20 CONTINUE

10 CONTINUE

C ORDER THE DATA

DO 30 K=1,I-1

Y=1.E+5

DO 40 J=1,I-1

IF((D(1,J).EQ.0.0).AND.(D(2,J).EQ.0.0))GOTO 40

IF(D(1,J).LT.Y)THEN

Y=D(1,J)

IJ=J

```

        END IF
40    CONTINUE
        C(1,K)=Y
        C(2,K)=D(2,IJ)
        D(1,IJ)=1.E+6
30    CONTINUE

C    FIND DEFLECTION,ALFA,BETA,TRANSMISSIBILITY,RUNOUT

        DO 100 II=1,I-1

        OM=C(1,II)
        E=C(2,II)

        IF(L1.EQ.1)THEN
            CRT=2.*E/((1.-E**2)**2)
            CTT=PI/(2.*(1.-E**2)*SQRT(1.-E**2))
            MTT=PI*(1.-SQRT(1.-E**2))/(10.*E**2)
            M22=-27.*(4.+2.*ALOG(ABS((1.-E)/(1.+E)))/E)/(140.*E)
            M12=-27.*PI*(2.-(2.-E**2)/SQRT(1.-E**2))/(140.*E**2)
            EDM=.1*PI*(1./SQRT(1.-E**2)-2.*(1.-SQRT(1.-E**2))/E**2)

        IF(L.EQ.2)THEN
            CRT=0.
            M22=2.*M22
            M12=0.
            MTT=2.*MTT

```

```

      CTT=2.*CTT
      EDM=2.*EDM

END IF

MTT=MTT+0.5*EDM-M12

GOTO 55

END IF

IF(L1.EQ.2)THEN

  CRT=24.*E/((2.+E**2)*(1.-E**2))

  CTT=12.*PI/((2.+E**2)*SQRT(1.-E**2))

  MTT1=(5.*E**2-2.)+4.*(1.-E**2)**1.5/(2.+E**2)

  MTT=MTT1*1.2*PI/(E**2*(2.+E**2))

  M22=((3.*E/(2.+E**2)-1.))**3/(1.-E)**2

  M22=54.*(M22+((3.*E/(2.+E**2)+1.))**3/(1.+E)**2)/35.

  A1=((3.*E/(2.+E**2)-1.))**2/(1.-E)

  M22=M22+0.6*(A1-((3.*E/(2.+E**2)+1.))**2/(1.+E))

  M12=0.

  EDM1=-1.2*PI*4.*(1.+E**2)*MTT1/(E*(2.+E**2))**2

  EDM2=-12.*(2.+E**2)*SQRT(1.-E**2)-8.*(1.-E**2)**1.5

  EDM=1.2*PI*(10.+EDM2/(2.+E**2)**2)/(2.+E**2)+EDM1

IF(L.EQ.2)THEN

  CRT=0.

  M12=0.

  M22=0.

  MTT=2.*MTT

  CTT=2.*CTT

```

```

        EDM=2.*EDM
    END IF
    MTT=MTT+0.5*EDM-M12
    GOTO 55
END IF

55  D(1,II)=OM

    F=(SK-OM**2)**2+(CD*OM)**2
    G1=B*CTT*OM+M*M22*OM**2
    G=RK+B*CRT*OM-M*MTT*OM**2
    H=RK**2+2.*RK*B*CRT*OM+OM**2*(B**2*(CTT**2+CRT**2)-
2.*M*RK*MTT)
    H=H+2.*M*B*(CTT*M22-
CRT*MTT)*OM**3+M**2*(MTT**2+M22**2)*OM**4

    ALPHA=ATAN2(G1,G)
    AF=ALPHA*180./PI

    IF(H.LT.0.)THEN
        WRITE(5,*)OM,E,H
        D(2,II)=0.
        GOTO 15
    END IF

    D(2,II)=E*SQRT(H)/SK

15  G2=(SK-OM**2)*D(2,II)*SIN(ALPHA)+CD*OM*D(2,II)*COS(ALPHA)

```


$G3=(SK-OM^{**2})*D(2,II)*COS(ALPHA)-CD*OM*D(2,II)*SIN(ALPHA)$

$G22=G2+CD*OM*E$

$G33=G3-E*OM^{**2}$

$BT=ATAN2(G22,G33)*180./PI$

$FT=E*SQRT(G^{**2}+G1^{**2})$

$FT1=SK*U*OM^{**2}/(SQRT(F))$

$TR(II)=ABS(FT/FT1)$

$RS(II)=SQRT(E^{**2}+D(2,II)^{**2}+2.*E*D(2,II)*COS(ALPHA))$

WRITE(4,*)C(1,II),C(2,II),D(2,II),AF,BT

100 CONTINUE

CLOSE(UNIT=4)

WRITE(5,101)

101 FORMAT(' DO YOU WANT EPSILON ? (1=Y,2=N)')

READ(5,*)N1

IF(N1.EQ.2)GOTO 110

CALL AXES(C,I-1,1,'OMEGA','EPS.','UNBAL. RESP.',2)

CALL PLTDAT(C,I-1,1)

CALL PTQUERY(N)

```

IF(N.EQ.0)GOTO 110

CALL PTOPEM
CALL PTSCLE(C,I-1,' ',' ',2)
CALL PTPLOT(C,I-1,7,1,0)
CALL PTCLSE

110 WRITE(5,102)
102 FORMAT(' DO YOU WANT D ? (1=Y,2=N) ')
READ(5,*)N1

IF(N1.EQ.2)GOTO 120

CALL AXES(D,I-1,1,'OMEGA','D','UNBAL. RESP.',2)
CALL PLTDAT(D,I-1,1)
CALL PTQUERY(N)
IF(N.EQ.0)GOTO 120

CALL PTOPEM
CALL PTSCLE(D,I-1,' ',' ',2)
CALL PTPLOT(D,I-1,7,1,0)
CALL PTCLSE

120 WRITE(5,105)
105 FORMAT(' DO YOU WANT TRANSMISSIBILITY ? (1=Y,2=N) ')
READ(5,*)N1

```

```

IF(N1.EQ.2)GOTO 150

DO 65 K=1,I-1
D(2,K)=TR(K)
65 CONTINUE

CALL AXES(D,I-1,1,'OMEGA','TR','UNBAL. RESP.',2)
CALL PLTDAT(D,I-1,1)
CALL PTQUERY(N)
IF(N.EQ.0)GOTO 150

CALL PTOPEN
CALL PTSCLC(D,I-1,' ',' ','2)
CALL PTPLOT(D,I-1,7,1,0)
CALL PTCLSE

150 WRITE(5,106)
106 FORMAT(' DO YOU WANT R ? (1=Y,2=N) ')
READ(5,*)N1

IF(N1.EQ.2)GOTO 160

DO 66 K=1,I-1
D(2,K)=RS(K)
66 CONTINUE

CALL AXES(D,I-1,1,'OMEGA','R','UNBAL. RESP.',2)

```

CALL PLTDAT(D,I-1,1)

CALL PTQUERY(N)

IF(N.EQ.0)GOTO 160

CALL PTOPEN

CALL PTSCLE(D,I-1,' ',' ',2)

CALL PTPLOT(D,I-1,7,1,0)

CALL PTCLSE

160 CALL PQUERY

CALL EXIT

STOP

END